STRUCTURAL MODELING TECHNIQUES FOR CONCRETE SLAB AND GIRDER BRIDGES

by

E. V. Leyendecker

and

J. E. Breen

Research Report Number 94-1

Research Project Number 3-5-66-94

Structural Model Study of Concrete Slab and Girder Spans

Conducted for

The Texas Highway Department

In Cooperation with the
U. S. Department of Transportation
Federal Highway Administration
Bureau of Public Roads

by

CENTER FOR HIGHWAY RESEARCH
THE UNIVERSITY OF TEXAS AT AUSTIN

August 1968

The opinions, findings, and conclusions expressed in this publication are those of the authors and not necessarily those of the Bureau of Public Roads.

P R E F A C E

This report is the first in a series which will summarize a detailed investigation of the behavior of pan-formed concrete slab and girder bridge systems which are widely used by the Texas Highway Department. This report treats the detailed techniques developed for the utilization of reduced scale models in the study and also reports on the degree of correlation between the model tests and full scale prototype testing. Subsequent reports will treat the techniques employed and results obtained in the field testing and the general behavior and recommendations based thereon from the main model test series.

This work is a part of Research Contract 3-5-66-94 entitled "Structural Model Study of Concrete Slab and Girder Spans." The studies described herein were conducted as a part of the overall research program at The University of Texas Center for Highway Research, under the administrative direction of Dean John J. McKetta. The work was sponsored jointly by the Texas Highway Department and the Bureau of Public Roads under an agreement between The University of Texas at Austin and the Texas Highway Department.

Liaison with the Texas Highway Department was maintained through the contact representative, Mr. B. R. Winn; Mr. I. C. Daniel was the contact representative for the Bureau of Public Roads. Particular thanks are due all of these contact representatives as well as Mr. H. D. Butler, Design Engineer, and Mr. C. D. Hanley, Mr. E. L. Hardeman, and Mr. J. Garrett of District 9 of the Texas Highway Department, who were of invaluable assistance during the field testing phase of the project. A special acknowledgment must be made of the excellent cooperation of the R. T. Farr Co., the bridge subcontractor for the field test specimen.

This study was directed by John E. Breen, Associate Professor of Civil Engineering. The model study phase was supervised by E. V. Leyendecker and the field study phase by T. A. Armstrong, both Research Engineers, Center for Highway Research.

A B S T R A C T

Detailed procedures for fabricating, instrumenting, and loading approximately 1/6-scale reinforced microconcrete "direct models" of a typical pan-formed concrete slab and girder bridge system are presented. The methods rely on achievement of a high degree of material similarity between prototype and model to permit observation of realistic behavior at service load, moderate overload, and ultimate load levels.

The report describes techniques utilized in a reasonably successful study and provides comparisons between model and prototype behavior. The techniques used resulted in models in which the observed load distribution exhibited a high degree of correlation with the prototype field test observations. In addition, the ultimate loads of reduced (statically determinate) sections were in close agreement with accepted ultimate strength theory.

Use of similar "direct model" techniques in future investigations is recommended.

C O N T E N T S

CHAPTER		Page
I.	INTRODUCTION	1
	1.1 General	1
	1.2 Prototype Bridge System	4
	1.3 Object and Scope of Investigation	11
	1.4 Program of Research	12
	1.5 Objective of This Report	14
II.	FUNDAMENTAL SIMILITUDE CONSIDERATIONS	15
	2.1 Introduction	15
	2.2 Indirect Models	16
	2.3 Direct Models	17
	2.4 Model Selection	17
	2.5 Scale Relations	18
	2.5.1 Materials	18
	2.5.2 Loads	18
	2.6 Scale Factor Selection	21
III.	MODEL TECHNOLOGY	24
	3.1 Introduction	24
	3.2 Materials	25
	3.2.1 Microconcrete	25
	3.2.2 Reinforcement	31
	3.3 Forms	35
	3.4 Fabrication	39
	3.5 Instrumentation	47
	3.5.1 Load Control	47
	3.5.2 Structural Response	47
	3.6 Loading	52
	3.6.1 Gravity Loads	52
	3.6.2 Live Loads	55
IV.	RELIABILITY	60
	4.1 Introduction	60
	4.2 Comparison at Service Load Levels	60
	4.3 Ultimate Strength Reliability	70

CHAPTER Page

V. CONCLUSIONS AND RECOMMENDATIONS 73

5.1 Conclusions 73
5.2 Recommendations 74

5.2.1 Microconcrete 74

BIBLIOGRAPHY 75

APPENDIX A PROTOTYPE BRIDGE PLANS 77

L I S T O F T A B L E S A N D F I G U R E S

TABLE

		Page
1.1	Summary of Model Tests	3

FIGURE

1.1	Typical CG Series Span, CG-0-35-40 (0° skew shown)	5
1.2	Prototype Reinforcement and Pan Forms	7
1.3	Pan Arrangements for Standard Skews	8
1.4	Pan Form Support Details	9
1.5	Bearing Support Details	10
2.1	General Stress-Strain Curve	19
2.2	Estimated Cost Variation with Scale of a Reinforced Concrete Bridge Model	23
3.1	Prototype Aggregate Gradation	26
3.2	Model Aggregate Gradation	28
3.3	Stress-Strain Curves for Microconcrete and Prototype Concrete	30
3.4	Typical Stress-Strain Curves Before and After Stress Relief Annealing	33
3.5	Crack Patterns Using Smooth and Deformed No. 2 Bars	34
3.6	Typical Stress-Strain Curves for Main Flexural Reinforcement	36
3.7	Pan Form Shaping Operations	38
3.8	Model Pan Form Details	40
3.9	Substructure Steel and Casting	41

FIGURE Page

3.10 Girder Cages 42

3.11 Support Conditions 44

3.12 Method of Installing Dead Load Wires 45

3.13 Models Ready for Casting 46

3.14 Pancake Type Load Cell 48

3.15 Strain Gage Installation 50

3.16 Reaction Measurements 50

3.17 Grid System 51

3.18 Gravity Load Compensation 53

3.19 Comparison of Desired and Actual Dead Load Moment Diagrams 54

3.20 Live Load System 56

3.21 Relation between Full-Size and Model AASHO H20-S16 Truck 57

3.22 Single Wheel, Single Axle, and Single AASHO Truck 59

4.1 Comparison of AASHO H20 Design Vehicle and Vehicle Used for Tests 62

4.2 Strain Data for One Truck on Exterior Girders 63

4.3 Strain Data for One Truck on Interior Girders 64

4.4 Strain Data for Two Trucks Spaced Apart 65

4.5 Strain Data for Two Trucks Spaced Close Together 66

4.6 Strain Data for Three Trucks 67

4.7 Summary of Model and Prototype Data with Regression Analysis 68

4.8 Cross Section and Properties for MSG Series 71

4.9 Behavior of Beams MSG-1 and MSG-2 72

FIGURE Page

A.1 Steel Forms for 40'-0" Slab and Girder Spans, ... Sheet 1 of 2 78

A.2 Steel Forms for 40'-0" Slab and Girder Spans, ... Sheet 2 of 2 79

A.3 Texas Highway Department Plan Sheet, CG-0-35-40 80

A.4 Texas Highway Department Plan Sheet, BCG-0-35-40 81

A.5 Texas Highway Department Plan Sheet, BCG-0-35-40 (45°'00') 82

A.6 Texas Highway Department Plan Sheet, CG-0-33-40 83

A.7 Texas Highway Department Plan Sheet, BCG-0-33-40 (26°-34') 84

N O T A T I O N

$A_{s_{SG-2}}$ = area of tension reinforcement in Model SG-2

$A_{s_{SG-3}}$ = area of tension reinforcement in Model SG-3

d_1, d_2 = truck axle spacing

ϵ = strain

ϵ_m = model strain

ϵ_p = prototype strain

E_c = modulus of elasticity of concrete

f = stress

f_m = model stress

f_p = prototype stress

f_s = tensile stress in reinforcement

f_y = yield strength of reinforcement

f_u = ultimate strength of reinforcement

f'_c = compressive strength of concrete

$\sqrt{f'_c}$ = square root of compressive strength of concrete in psi

i_m = arbitrary point on the model material stress-strain curve

i_p = arbitrary point on the prototype material stress-strain curve

ℓ_m = length dimension on model

ℓ_p = length dimension on prototype

L = span length

M	=	moment
P	=	concentrated load
S_ϵ	=	strain scale factor, $S_\epsilon = \epsilon_p/\epsilon_m$
S_f	=	stress scale factor, $S_f = f_p/f_m$
S_ℓ	=	geometrical scale factor, $S_\ell = \ell_p/\ell_m$
SWG	=	steel wire gage
w	=	weight of concrete, lb/cu.ft
W	=	total weight in tons of an AASHO truck

C H A P T E R I

INTRODUCTION

1.1 General

This report on structural modeling techniques is the first in a series of reports on a research program entitled "Structural Model Study of Concrete Slab and Girder Bridges." This report is limited to consideration of the model techniques and credibility developed in the investigation.

In the analysis of the behavior of complex structures, the structural engineer has traditionally utilized a mathematical model for obtaining an understanding, or at least an insight, into the response of the structure to given sets of loadings. Due to the wide acceptance of the elastic theory of analysis, the mathematical models developed tended to be linear, elastic formulations of the problems. As designers realized that the complexity of the problems was outstripping the methods of analysis available, a system of techniques for using linear, elastic, small-scale physical models of the prototype structure as analogue computers was developed. Usually the models were carefully fabricated from linear, elastic materials such as plastics or light gage metals. Care was taken in loading to keep stresses within the proportional limits. Under these conditions, the results of studies using structural models tended to confirm the results of elastic analyses. With the increased capability for handling large systems of simultaneous equations due to the advent of high speed digital computers, there was a decline in interest in the utilization of the elastic structural model except in a few areas such as shell buckling.

However, developments in structural engineering in the past two decades have pointed out a growing awareness of some serious limitations

of present methods of analysis. The development of plastic design concepts in structural steel, ultimate strength design concepts in reinforced concrete, as well as nonlinear analysis concepts, have created a demand for further observation of actual structural behavior to permit the accurate construction of new types of mathematical models for design tools. Further observations will be required to correctly assess the limits of applicability of the design techniques developed.

Needless to say, it would be impractical, and in some cases almost impossible, to gather all the required data from tests (including load tests to destruction) of prototype structures. To meet the needs for data describing basic cross-sectional capacities, tests have been run on individual structural members. In most cases, the tests have been performed on reduced-scale structural models of the members manufactured from the same type materials as would be used in the prototype. Reduced-scale structural model tests of individual structural members have become a very accepted basis for structural research.

With the development of more accurate models for predicting both the response of a member to a load stimulus and the ultimate capacity of member cross sections, this study focuses attention on the adequacy of methods of structural analysis to predict load distributions and overall structural behavior of actual structures subject to realistic loading. In particular, since most reinforced concrete structures are subject to localized cracking and inelastic stress distributions, the adequacy of linear methods of structural analysis must be examined. Since in beam and slab type structures the moments developed in the slabs are quite sensitive to beam deflections and the load distributed to the beams is quite sensitive to slab stiffness, changes in flexural stiffness due to cracking or inelastic effects could greatly modify the results of conventional methods of analysis.

Concurrent with the growing awareness of a need to reexamine design methods for complex structures, has been the development of a system of "direct" structural model testing which emphasizes basic agreement between prototype and model physical characteristics. This

is a welcome supplement to the indirect model which was simply an analogue computer representing the assumptions of the analysis rather than the properties of the structure. While many utilizations of structural models have been made in Europe (notably at the Cement and Concrete Association in England, the Technische Hochschule in Munich, the Portuguese National Civil Engineering Laboratory at Lisbon, and the Instituto Sperimentale Modelli e Strutture at Bergamo, Italy), a significant series of model studies of multipanel reinforced concrete slab structures has recently been completed in the United States. A series of two-way slabs, flat slabs, and flat plates were observed under service loads, moderate overloads, and ultimate loads. In conjunction with the main test program, which centered about nine panel systems supported on twelve columns, a series of models of the 60 ft. by 60 ft. prototype structures was made in three separate laboratories. All models were reinforced microconcrete structures in which great care was utilized to obtain all of the important material characteristics of the prototype materials. A wide range of scale factors was utilized with an extremely fine agreement in results as shown in the following table:

TABLE 1.1. SUMMARY OF MODEL TESTS

Laboratory	Scale	Ratio		Ultimate Load
		Flat	Plate	Ultimate Load of 1/4 Scale Model Flat Slab
PCA[1]	3/4	1.02		
U. of Ill.[2]	1/4	1.00		1.00
	1/16			0.98
M.I.T.[3]	1/28	1.07 (Average of 3 Models Variance ±7%)		

The excellent agreement between models of substantially different scales was summarized by Guralnick[1*] as follows:

*Superscript numbers refer to references in Bibliography.

> The striking similarity of structural performance, both qualitative and quantitative, between model and test structure appears to offer impressive support for the increased use of structural model testing as a tool in reinforced concrete research and design.

It is noteworthy to note that the failure in all of the flat plate models was identical, i.e., punching through of an interior column. Other failures in the slab model series were due to deficiencies in columns, and to torsion in spandrel beams. These factors were overlooked in the mathematical models for design. A great advantage of the detailed structural model is the ability to observe design omissions and detailing errors as well as design inconsistencies.

All of these points have been realized in this reinforced microconcrete model study of concrete slab and girder bridge systems conducted in the Civil Engineering Structural Research Laboratory at the Balcones Research Center of The University of Texas. Extensive developmental work has been completed to gain experience and confidence in microconcrete model techniques. Programs of investigation of material characteristics have developed microconcretes with typical values of f'_c and E_c as found in practice, as well as test equipment and methods suitable for reduced scale testing. Methods of fabrication have been developed for reinforcement cages and dimensional tolerances have been controlled to ensure repeatability. Complete loading and instrumentation systems have been developed to permit simulation and measurement of actual behavior at both service and ultimate loads. It is felt that a significant insight has been obtained regarding the fundamental behavior of reinforced concrete pan-formed slab and girder systems which will result in a more accurate design procedure.

1.2 Prototype Bridge System

The basic structural system investigated was the Texas Highway Department's widely used pan-formed slab and girder bridge system known as the CG Series. The basic structure is a monolithically cast pan-formed slab and girder unit as shown in Fig. 1.1. It is designed as a simply supported span with a nominal span length of 40 ft.-0 in. for a

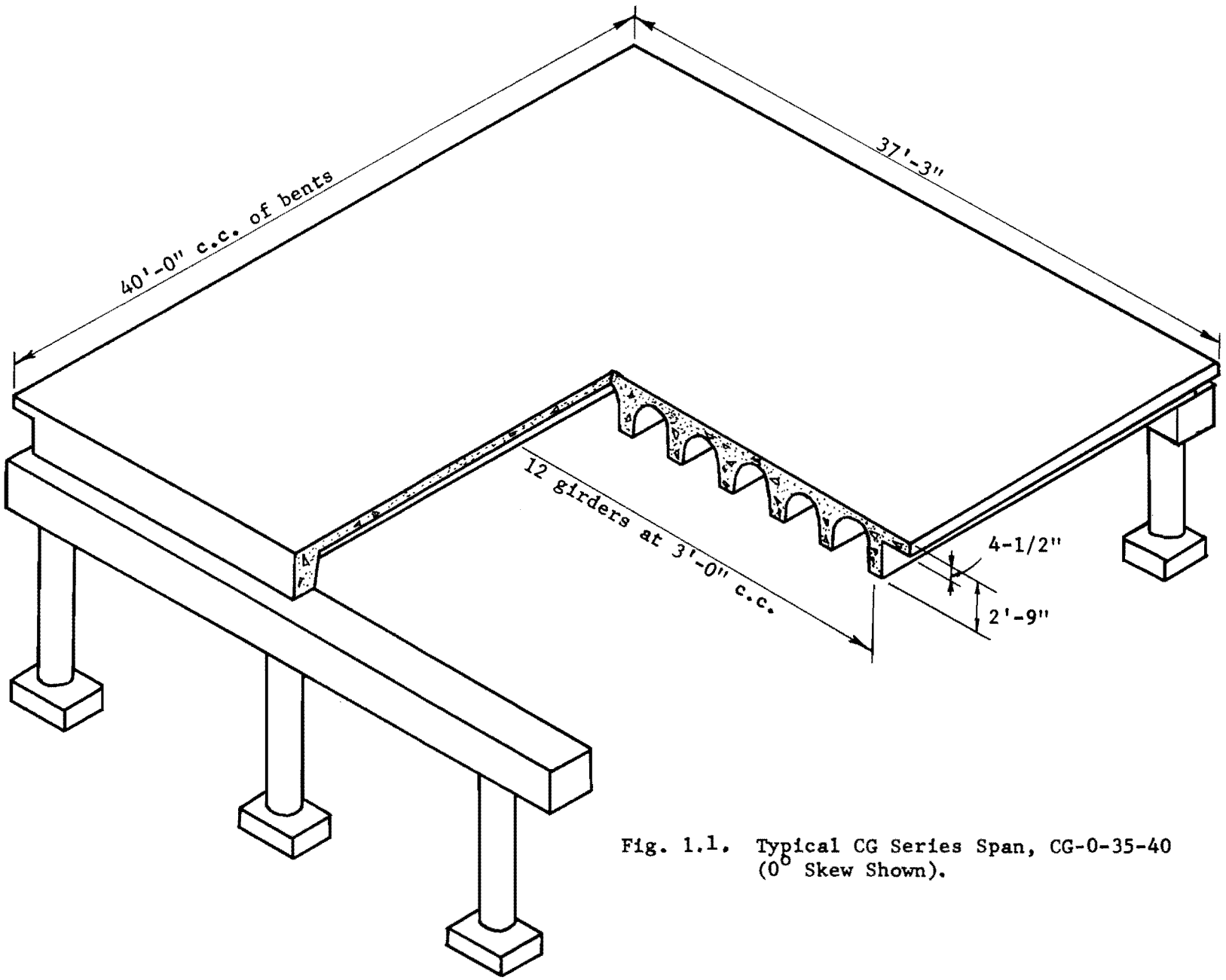

Fig. 1.1. Typical CG Series Span, CG-0-35-40 (0^{0} Skew Shown).

right angle bridge. Standard designs are available for skew spans varying from 0° to 45° with the angle of skew being the angle between the axis of the bent cap and a line perpendicular to the flow of traffic.

Figure 1.1 shows the transverse cross section to be comprised of a series of semicircular arch units. This shape is obtained by casting on a series of standard semicircular pan forms. Detailed plans for these forms are given in Figs. A.1 and A.2 in Appendix A of this report. Typical girder and slab reinforcement, as well as a general view of the pan forms, are shown in Fig. 1.2.

The roadway width can be varied in three-foot increments by adding or subtracting the three-foot pan form units. The skew angle may be varied by sliding pans relative to one another until the desired skew is obtained. Skew angles are controlled by having a uniform hole spacing on the bottom connecting angles on each pan. Skew variations are obtained by slipping the pans one or more holes relative to the adjacent pans. Standard details are available for a one, two, three, or four-hole skew corresponding to skew angles as shown in Fig. 1.3. An increasing skew angle also slightly increases the span length. This is partially due to the greater width of the bent cap when measured on a skewed line. In addition, there is a need to increase the clear distance between bents to accommodate the standard straight end pans. The increase in clear distance is also indicated in Fig. 1.3(c).

Major economic benefits are realized by the design of the pan forms as structural units supported from the bent caps without interior falsework during construction. Pan support details vary according to the angle of skew, but basically the pans are supported from clips bolted to the faces of the bent caps. Typical pan supports are shown in Fig. 1.4 for a 26°-34' skew. The triangular gap between the pan form and bent cap is usually formed with a piece of plywood.

The end diaphragms are cast directly on asphalt board lying on the top surface of the bent cap. The asphalt board is shown in place on the expansion end support in Fig. 1.4. Details for both supports are shown in Fig. 1.5.

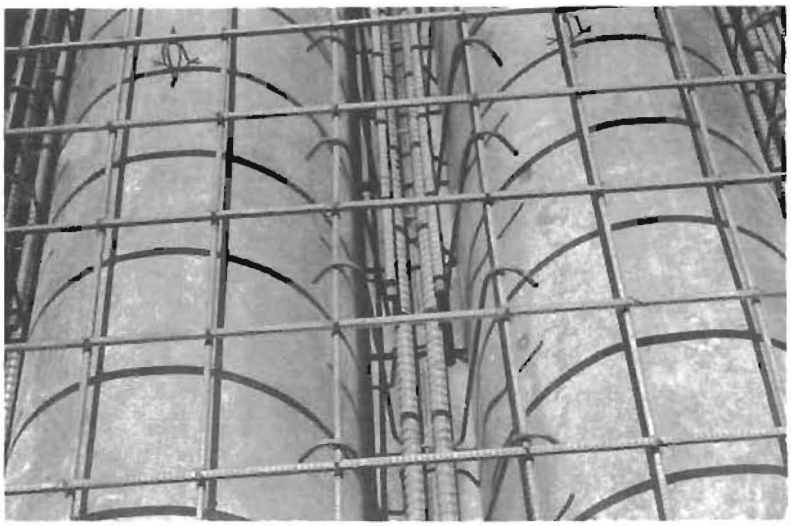

(a) Girder Steel.

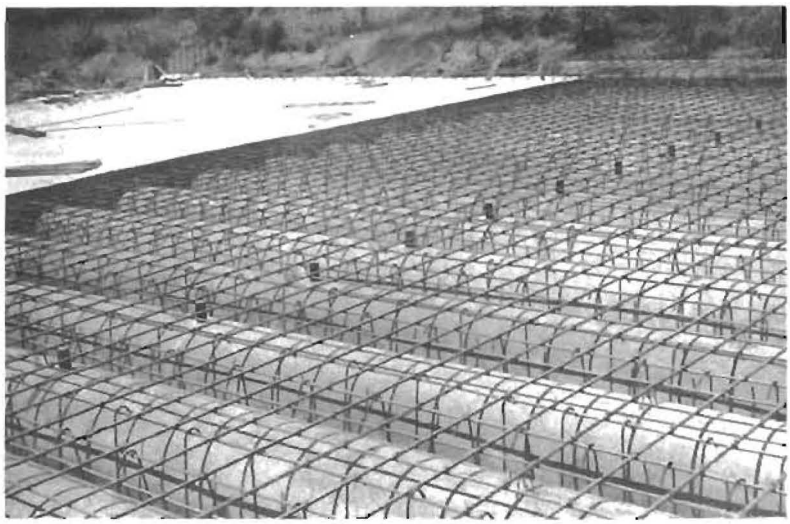

(b) Slab Steel and View of Pan Forms.

Fig. 1.2. Prototype Reinforcement and Pan Forms.

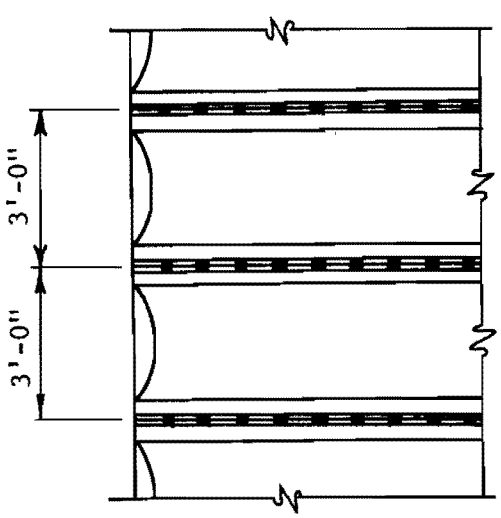

(a) Normal.

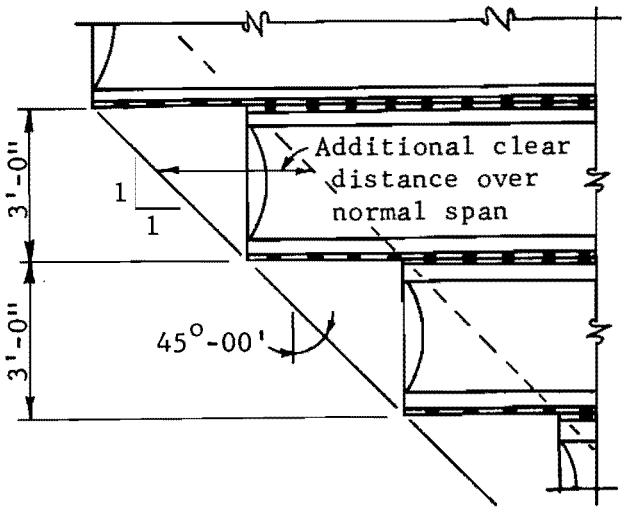

About 1/2" from and parallel to face of bent cap. Typical for all spans.

(c) Four Hole Skew.

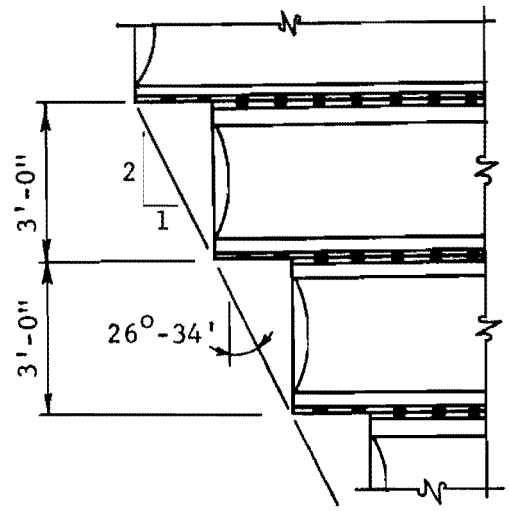

(b) Two Hole Skew.

Not Shown

One Hole Skew
Three Hole Skew

Skew Angle	No. of holes Skew	Bevel	Span Length C.to C. of bents
Normal	None	None	40'-0"
14°-02'	1	1:4	40'-10"
26°-34'	2	1:2	41'-9"
36°-52'	3	3:4	42'-9"
45°-00'	4	1:1	43'-10"

Fig. 1.3. Pan Arrangement for Standard Skews.

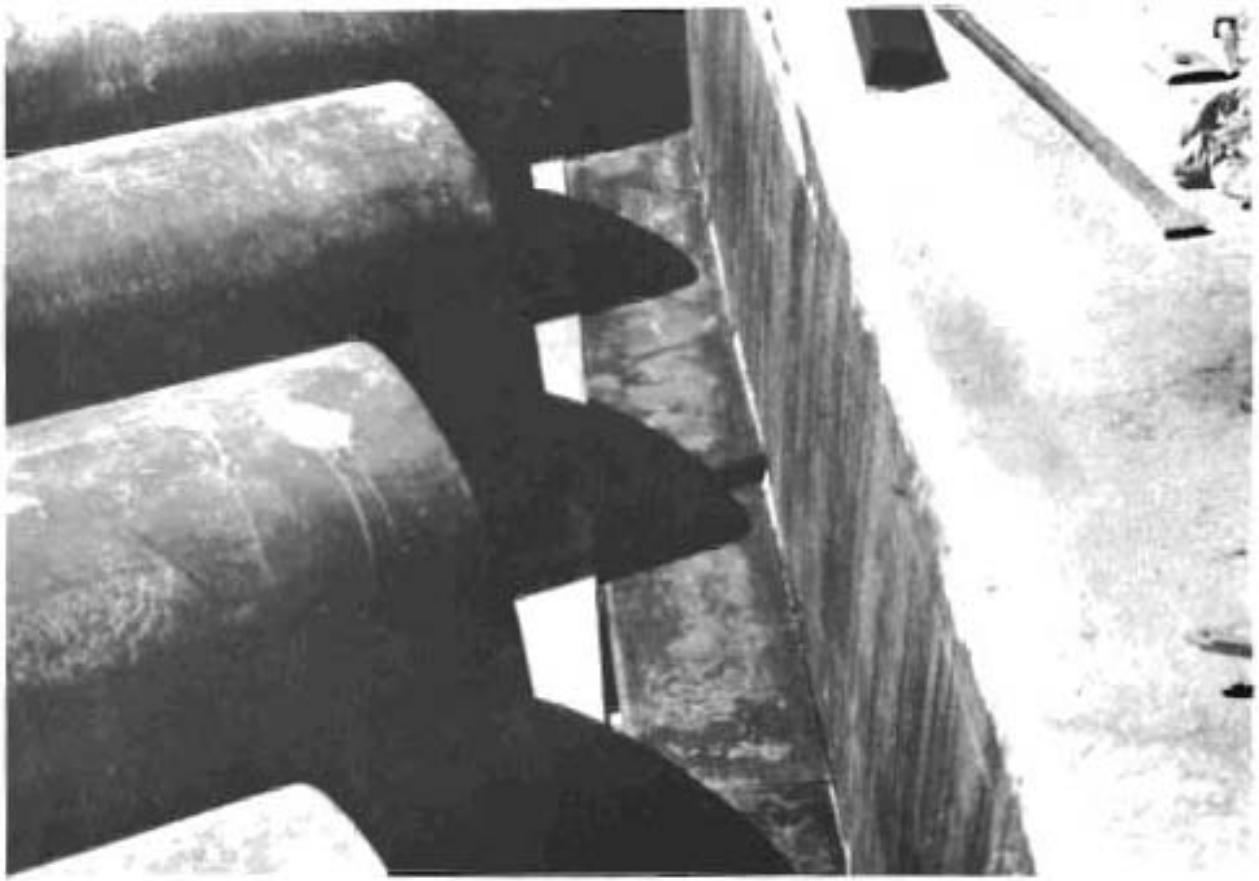

Fig. 1.4. Pan Form Support Details.

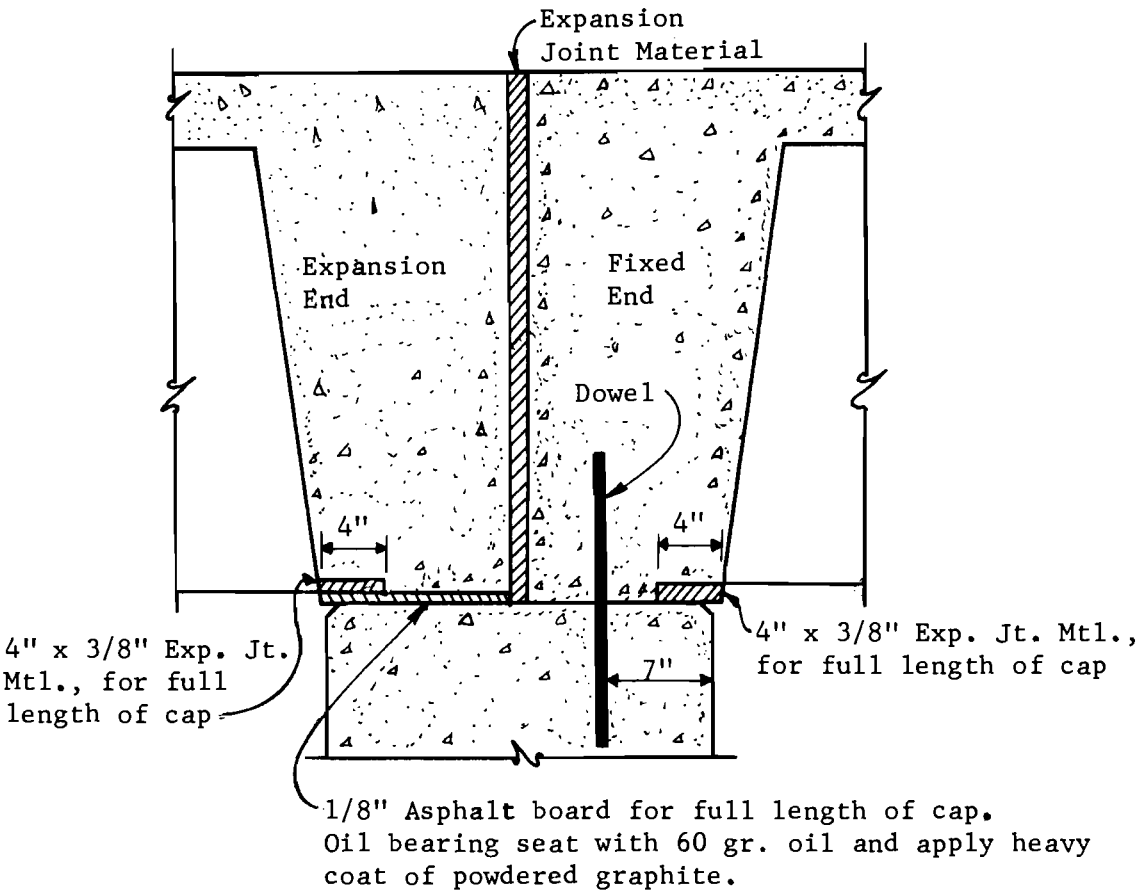

Fig. 1.5. Bearing Support Details.

The basic concrete cross section is used for several typical loadings (i.e., H15, H20, and H20-S16 AASHO* trucks). Flexural capacity is varied by changing the quantity of flexural reinforcement provided. Shear capacity is varied by changing the stirrup size and spacing.

1.3 Object and Scope of Investigation

A detailed investigation was carried out on the CG series of pan form slab and girder bridges, using approximately 1/6-scale "direct models" of the bridges (including substructure); these model tests were supplemented by full-size field testing, as well as analytical procedures. The overall objectives of the investigation are as follows:

(a) To investigate the behavior at service loads, moderate overloads, and at ultimate loads of typical pan-formed concrete slab and girder bridge spans, using reinforced microconcrete structural models.

(b) To confirm the observed behavior at service loads by full-scale testing of a prototype structure.

(c) To evaluate the effectiveness of the end diaphragms in participating with the bent caps to carry slab loads.

(d) To make recommendations regarding the adequacy of present design provisions based on these test results.

Objective (a) included an evaluation of "load distribution" patterns to the girders at various load levels. This was particularly desirable since the curved cross section of the structure implies a higher transverse rigidity than encountered in the usual slab and girder bridges having constant thickness slabs. This transverse rigidity caused some doubt over the accuracy of the usual AASHO slab and girder design procedures when applied to this type of bridge.

The desirability of testing at various levels of loading (some of which would cause cracking in the prototype) warranted the use of

---

*American Association of State Highway Officials.

more complex microconcrete test specimens rather than an elastic test specimen.

1.4 Program of Research

The following criteria were adopted to meet the objectives of the investigation:

(a) Model materials must have properties closely resembling the prototype materials. While it is possible to utilize the mathematical theory of similitude to interpret and correlate the behavior of linear models with different material properties in the model and the prototype, no such procedure is valid in ultimate strength models. Since the failure mechanism in the prototype materials is not completely understood, it is felt essential to strive to utilize model materials with physical properties as identical as possible to those of the prototype to minimize variation in failure criteria.

(b) Boundary conditions must match the prototype as faithfully as possible. To carry this out it was considered essential to model a typical substructure unit in order to include typical support deflection and rotation effects. It was also felt necessary to include dead load effects from adjacent spans on these supports as well as typical joint details. While the span is idealized as having "simple supports," the actual support details, as shown in Fig. 1.5, prevent both translation and rotation at one end and, hence, the span is "partially fixed." These support details were carefully modeled to assess this effect.

(c) Wherever possible independent checks of statically determinate subsystems must be utilized for verification of accuracy. Since inclusion of true boundary conditions makes theoretical analysis extremely difficult, all loading and measuring systems were verified in tests on simply supported members with known behavior. In addition, backup check measurement systems were provided where possible. These precautions developed confidence in the techniques utilized with the indeterminate slab and girder system.

The overall study consisted of the following principal test specimens:

(a) Model SG-1.--This is a 1/5.5-scale model of a 0^{o} skew, 40 ft. span, CG Series bridge. Details are shown on the Texas Highway Department Plan Sheet CG-0-35-40 (Fig. A.3) in Appendix A. The model was cast in place on a model of the substructure design for the prototype span. Substructure details are shown on the Texas Highway Department Plan Sheet BCG-0-35-40 (Fig. A.4) in Appendix A.

(b) Model SG-2.--This is a 1/5.5-scale model of a 45^{o} skew, 43 ft. - 10 in. span. Details are shown in Figs. A.3 and A.5.

(c) Model SG-3.--This model duplicates SG-2 in all respects except for the main flexural reinforcement, where high strength steel (f_y = 60 ksi and f_s = 24 ksi) was substituted for intermediate grade steel (f_y = 40 ksi and f_s = 20 ksi). The area of steel provided was changed so that the total tensile force at allowable steel stress was maintained constant (i.e., $A_{s_{SG3}} = \frac{20}{24} A_{s_{SG2}}$). The model was cast in place on the same substructure used for Model SG-2.

(d) Model SG-4.--This is a 1/5.5-scale model of a 26^{o}-34' skew, 41 ft. - 9 in. span. Details are shown on the Texas Highway Department Plan Sheet CG-0-33-40 (Fig. A.6) in Appendix A. The model was cast in place on a model of the substructure designed for the prototype span. Substructure details are shown on Texas Highway Department Plan Sheet BCG-0-33-40 (26^{o}-34') — (Fig. A.7) in Appendix A.

Model SG-4 (including substructure) is the reduced scale model of the full-size prototype bridge CG-1 which was tested at service load levels.

(e) Prototype CG-1.--This is a full-size prototype bridge of a 26^{o}-34' skew, 41 ft. - 9 in. span, with the same details shown in Figs. A.6 and A.7 for Model SG-4. The bridge was a part of a Farm-to-Market road near Belton, Texas.

Secondary tests were run on several models, as follows:

(a) Shear Tests.--Model SG-2 was loaded for maximum moment and then reloaded with a maximum shear loading in order to determine which was most critical for design.

(b) Punching Tests.--Punching tests to determine shear resistance to individual wheel loads were performed on an undamaged portion of the slab of model SG-3 after the bridge span had failed in flexure.

(c) Bent Cap Tests.--The substructure for Model SG-4 was tested by loading the cap of one bent with a series of concentrated loads which were increased until failure occurred. The remaining bent was then loaded to failure by applying the same load configuration through the end diaphragms to determine the stiffening effect of these diaphragms.

Models SG-1, SG-2, SG-3, and SG-4, along with their auxiliary shear and punching tests, were tested in order to meet objective (a) in Section 1.3. Model SG-4 and Prototype CG-1 were tested in order to meet objective (b) in Section 1.3. The bent cap tests were performed in order to meet objective (c). Collectively, the results from all tests were designed to meet objective (d).

1.5 Objective of This Report

The objective of this report is to introduce the overall test programs and to document, in detail, the procedures used to construct and test the reinforced concrete structural models used in this investigation. An evaluation of the models used is presented in relation to present theories as well as by direct comparison with results from a prototype structure.

C H A P T E R I I

FUNDAMENTAL SIMILITUDE CONSIDERATIONS

2.1 Introduction

Usage of structural models has increased during the last twenty years although most of the required principles have been widely known since the early part of this century. The initial surge of recent interest in the use of structural models came as engineers were challenged with the analysis of varied complex forms such as doubly curved thin shell roofs and dams, complex irregular building frames, and unusual slab systems. In many cases the analytical solutions for these structures were too complex for hand computation, even when restricted to linear elastic idealization. With the advent of high speed digital computers and with the refinement of matrix solutions and development of finite element methods of analysis, the more powerful computer analyses have begun to replace the linear models in many applications. In very recent years, improved material and instrumentation capabilities have resulted in development of accurate models which are not restricted to linear elastic behavior. With the aid of such models, considerable advances in the understanding of actual structural behavior are available, and, in turn, this heightened understanding allowing more realistic design procedures.

Thus, two very different types of structural models are available, i.e., "indirect models" or "direct models." These models have very different ranges of application and represent very different model technologies as outlined in subsequent sections.

2.2 Indirect Models

The indirect model is essentially an analogue computer for solution of idealized structural systems. The indirect model is usually fabricated from linearly elastic materials and is loaded so that stresses do not reach the proportional limit. Under these load conditions such models tend to confirm the results of mathematical analyses based on linear elastic assumptions.

The "indirect model" may not represent the prototype cross sections to a linear scale, but rather represent to an arbitrary scale such section properties as axial or flexural stiffnesses. This distorted scaling is accurate only if the complete relationships of variables on structural behavior are known in advance. This may be the case, for example, with flexure in a typical two-dimensional building frame. If, however, effects such as shear or torsion are not known, then the "indirect model" must be reproduced to a linear scale. This would be the case for a slab and girder bridge where the girders may have torsional properties that cannot be neglected.

The "indirect model" is loaded by subjecting it to arbitrary forces or displacements. The resulting measured deformations may be used to construct influence lines for variables such as force, shear, moment, or deflection for the prototype structure. Various load conditions may be investigated by using the measured influence lines and the principle of superposition. However, as with the principle of superposition, the indirect model is limited strictly to investigations of linear elastic behavior.

Since it was evident from the outset that the present study had to consider structural behavior in both the uncracked and cracked section range, and since the fundamental relationships between factors such as flexural and torsional stiffness were unknown, the indirect model could not be used in this study.

2.3 Direct Models

The direct model is essentially an analogue computer for solution of the actual structural system with a minimum of "idealized" boundary conditions. The direct model emphasizes the agreement between prototype and model physical characteristics and boundary conditions. As such it does not satisfy erroneous analytical assumptions, which distort the true nature of the structure.

The ideal direct model is a true-to-scale model in which all details are linearly reproduced, although practicality requires that this type of model sometimes be simplified to omit minor details that should not significantly affect the structural behavior. The direct model may be used to measure stresses, forces, moments, or displacements, due to a particular loading. The direct model is extremely valuable in that it may be used to document elastic, inelastic, and ultimate load behavior. This use over the full range of loadings is extremely useful in determining the range of applicability of elastic theories for a structure constructed from an inelastic material such as reinforced concrete.

Another major benefit of the direct model is that the efficiency of details such as connections may be evaluated. Often structural capacities are governed by details or types of behavior which are ignored in the analytical idealizations but show up in realistic direct models.

2.4 Model Selection

The "direct model" constructed of reinforced microconcrete was selected for use in this study because it was the only type of model which would permit documentation of elastic, inelastic, and ultimate load behavior.

A type of reduced scale concrete referred to as microconcrete* was selected as a primary modeling material because its mechanical

---

*Discussed in more detail in Section 3.2.1.

properties are virtually identical with those of the concrete used in the prototype full-size structures. Concrete substitutes[4] such as gypsum plasters were avoided, due to the pronounced variation in brittle failure criteria. Since the failure criteria for the prototype concrete are not well understood, it was felt that model materials should be as close as possible to the prototype materials in all mechanical characteristics. Although many such substitutes have been advocated because of their rapid setting time, this is not a critical factor in a study involving a rather extensive loading program. With the use of high early strength (Type III) cements, only one week is required for curing. The attachment of instrumentation and application of loading systems often requires more time than this, so rapid curing is not a critical factor.

2.5 Scale Relations

2.5.1 Materials.--A generalized stress-strain curve illustrating idealized relations between the prototype and model materials is shown in Fig. 2.1. The factors S_f and S_ϵ are referred to as the stress and strain scale factors, respectively. The geometrical scale factor, S_ℓ, relates the model and prototype dimensions (model length = $1/S_\ell$ x prototype length). Microconcrete may be designed with a resultant stress-strain diagram equal to that of the prototype, hence $S_f = S_\epsilon$ = unity. With proper selection of model reinforcement, the same statement can apply to the reinforcing steel.

Where shear and torsional stresses may be important as well as with significant plate behavior, it is essential that Poisson's ratio for the model and prototype materials be equal. This requirement is readily achieved where the model materials are essentially the same as the prototype materials.[5]

2.5.2 Loads.[6]--Once the material scaling factors, S_f and S_ϵ, and the geometrical scale factor, S_ℓ, have been determined, the model and prototype loads may be related as follows:

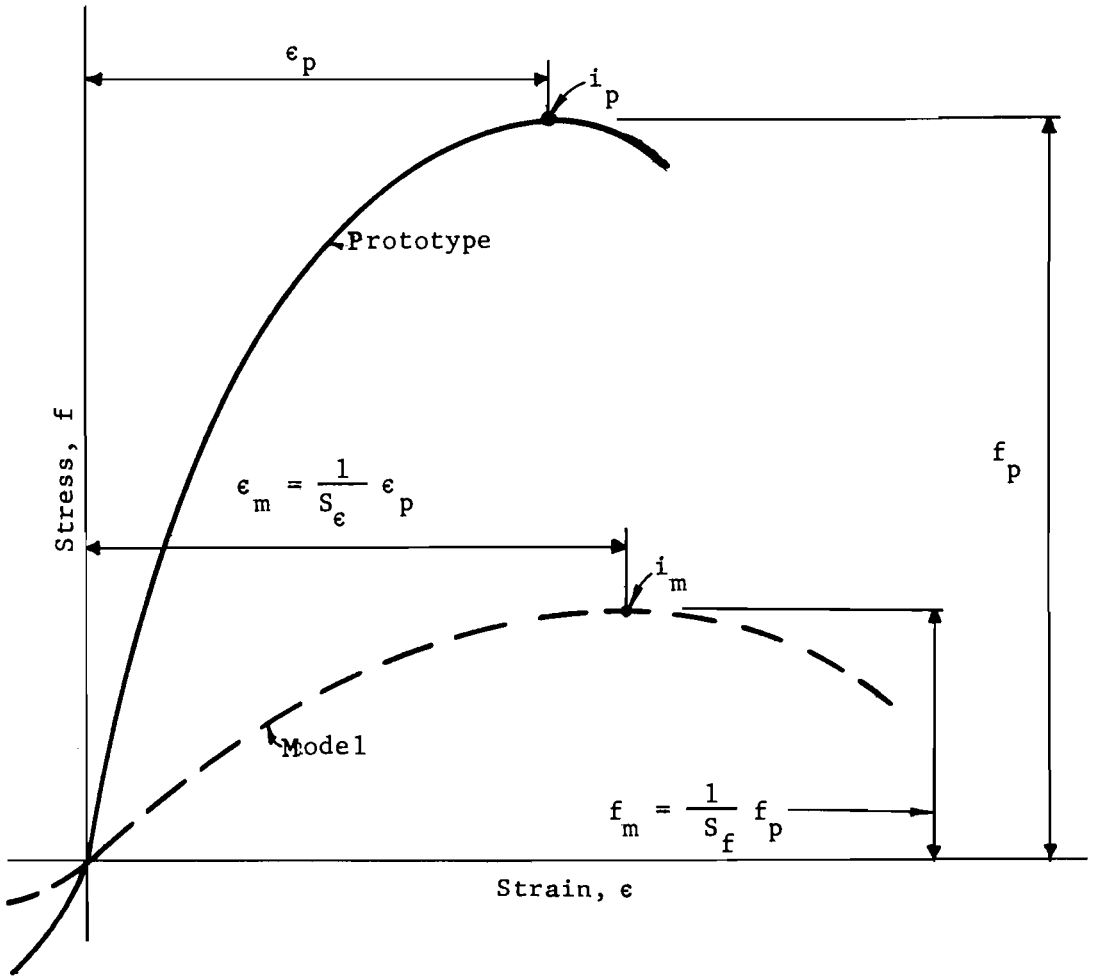

Fig. 2.1. General Stress-Strain Curve.

1. Loads distributed over an area

   Model load per unit area = $1/S_f$ x prototype load per unit area

2. Loads distributed over a length

   Model load per unit length = $1/S_f$ x $1/S_\ell$ x prototype load per unit length

3. Concentrated loads

   $$\text{Model load} = \frac{1}{S_f} \times \left(\frac{1}{S_\ell}\right)^2 \times \text{prototype load}$$

4. Gravity loads

   $$\text{Model density} = \frac{S_\ell}{S_f} \times \text{prototype density}$$

If the above requirements are met, then the model deflections = $\frac{1}{S_\epsilon} \times \frac{1}{S_\ell}$ x prototype deflection.

The "direct model" chosen utilizes the same material properties as the prototype, hence $S_\epsilon = S_f = 1$. Thus, the prototype and model loads are related only by the geometrical scaling factor. In this case the load relations become:

1. Loads distributed over an area

   Model load per unit area = prototype load per unit area

2. Loads distributed over a length

   Model load per unit length = $\frac{1}{S_\ell}$ x prototype load per unit length

3. Concentrated loads

   $$\text{Model load} = \left(\frac{1}{S_\ell}\right)^2 \times \text{prototype load}$$

4. Gravity loads

   Model density = S_ℓ x prototype density

If the above requirements are met, then the measured strain in the model is equal to the prototype strain and the model deflections are $\frac{1}{S_\ell}$ times the prototype deflections.

The unrealistic requirement for substantially increased model density may be overcome by the application of external loads as discussed in a later section.

2.6 Scale Factor Selection

The geometric scale factor, $S_\ell = \frac{\ell p}{\ell m}$, is determined by economics, available materials, fabrication methods, and testing procedures. Frequently the major considerations are other than economic. Very small scales ($1/S_\ell \ll 1$) may be utilized with the "indirect model" technique, due to the relative ease of fabrication and loading. The scale may often be set merely by the thickness of materials available. The selection of a scale factor for a "direct model" is often more complex. The similitude requirements make careful material selection a necessity; hence, for reinforced concrete models the availability of wire sizes with the proper stress-strain characteristics may "fix" the scale factor. The amount of joint and section detail that can faithfully be reproduced in a model also limits the scale used.

At the beginning of this project, a study was made of the factors affecting the fabrication and loading costs for these models. The requirement of obtaining information over the full range of loading (elastic, inelastic, and ultimate) dictated the use of "direct (micro-concrete) models." Because of the nature of the prototype loadings, a versatile loading system had to be developed to allow the placement of wheel, axle, single truck, or multiple truck loads in any position on the bridge with relative ease. As typical in bridges, the gravity (dead) load formed a substantial part of the total design load on the structure. In order to account for density scaling (model density = S_ℓ x prototype density) an auxiliary loading system was used to maintain full gravity load on the models.

Detailed studies were made of both fabrication and loading system costs for a number of scale factors. The costs of reusable items such as forms and loading frames were amortized over five models. The results of these studies are shown in Fig. 2.2. Loading costs decrease rapidly with the geometric scale, since concentrated loadings such as trucks are reduced as $(1/S_\ell)^2$; hence, smaller loading frames may be used. For very small scales the costs level out, since very small loads may be applied by dead weights, although these must be accurately calibrated. Fabrication costs (which include the cost of attaching strain gages on the reinforcement) increase at the smallest scales, due to the difficulty in fabricating small, complex cages to close tolerances. The total combined cost of fabrication and loading indicates a minimum cost at about 1/8 scale. There is very little difference in costs in the range of 1/5 to 1/10 scales when compared to the cost of full-size testing (15 to 17% of prototype).

Previous experience at the Civil Engineering Structures Research Laboratory at The University of Texas at Austin has indicated that a scale of 1/8 is about a lower limit for very complex structural models. In this study the main reinforcing steel in the prototype was a No. 11 bar; the availability of deformed No. 2 bars was a major consideration in the selection of the scale as $1/S_\ell = 2/11 = 1/5.5$.

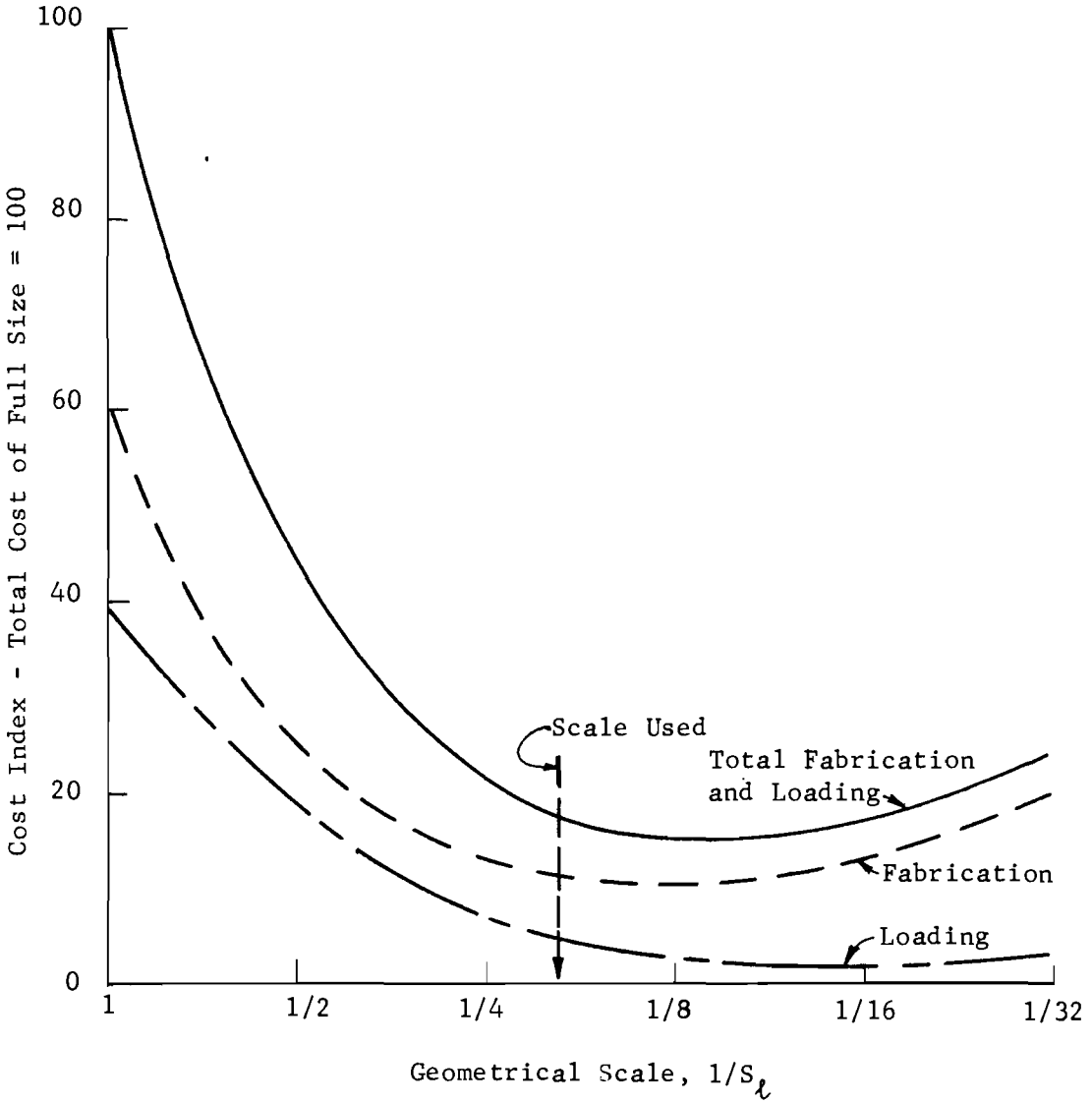

Fig. 2.2. Estimated Cost Variance with Scale of a Reinforced Concrete Bridge Model.

C H A P T E R I I I

MODEL TECHNOLOGY

3.1 Introduction

The basic goal in the direct modeling process is to obtain a realistic approximation of the behavior of the prototype over a complete spectrum of loads from dead load through service loads until collapse loads. In order to accomplish this, the following are necessary:

(a) The model must reflect the "as built" characteristics of the prototype and not the idealizations of an analytical mathematical model.

(b) Materials used must meet similitude requirements so that $S_f = S_\epsilon = 1$.

(c) Fabrication techniques should closely approximate details such as spacing, connections, and tolerances.

(d) Boundary conditions should match field conditions and not analytic idealizations (i.e., supports may be actually restrained although the analysis may assume simple supports).

(e) Instrumentation must be sensitive to the range of structural response anticipated.

(f) Loading systems must be reasonably representative of prototype loadings and must be flexible enough to perform accurately over the wide range of loading from service to ultimate load levels.

(g) The entire testing system must be continuously checked and verified. Preliminary tests should be run with simplified boundary conditions

to assess the potential accuracy of the model. If the techniques are inadequate for statically determinate conditions, they are unwarranted for more complex conditions.

Accumulated years of experience with linear analysis and idealized linear models have inculcated habits and practices which must be avoided in investigations where inelastic behavior is anticipated. Reliance on the principles of superposition can be used only if the principle has been proven at the particular load levels contemplated. The repeal of the law of superposition greatly increases the complexity of loading systems.

3.2 Materials

3.2.1 Microconcrete. The model concrete used in this investigation is referred to as microconcrete. It is designed based on geometric scaling of the prototype aggregate gradation curve. Modification of the scaled curve is usually required around the No. 100 and No. 200 sieve sizes. Smaller particles are impractical as well as undesirable, due to increased water requirements because of the increased surface areas involved.[4] Once the aggregate gradation curve is obtained, the microconcrete is designed on a trial batch basis with several trials usually required to adjust the water-cement ratio. The microconcretes usually appear rather harsh, although they can be placed easily with a vibrator.[5] This procedure, based on scaling the aggregate gradation curve, is probably limited to a scale of 1/10 or 1/12.[5,6,7]

Microconcrete for this study was designed using a typical Texas Highway Department mix design for superstructure concrete as a prototype. The initial step in the design of the microconcrete was selection of a microconcrete aggregate gradation. A prototype combined gradation curve was selected as shown in Fig. 3.1(b) which met requirements for a typical combination of the standard fine and coarse aggregate gradations shown in Fig. 3.1(a).

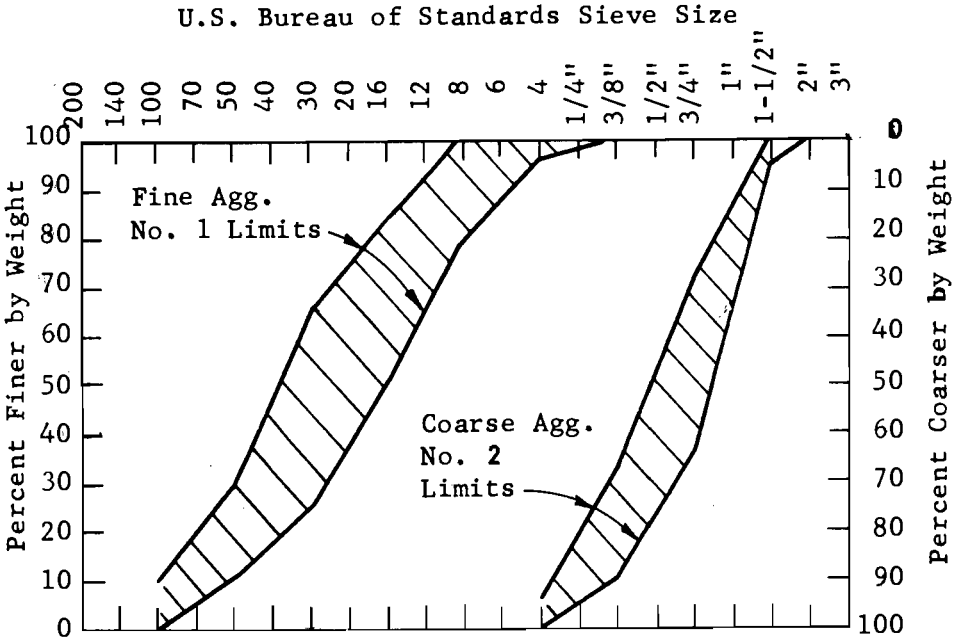

(a) Texas Highway Department Aggregate Gradation.

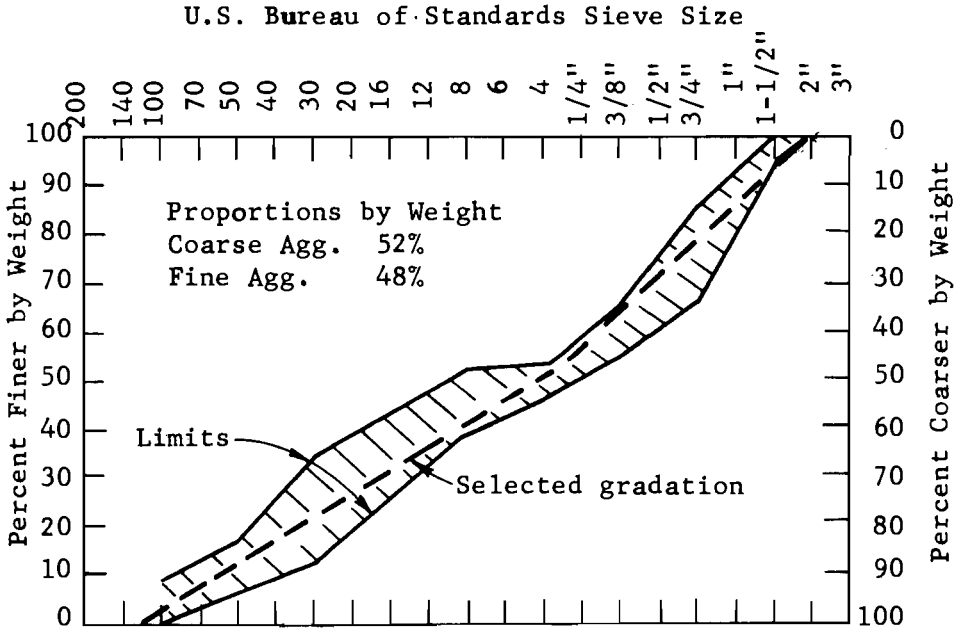

(b) Texas Highway Department Combined Aggregate Gradation.

Fig. 3.1. Prototype Aggregate Gradation.

The selected prototype gradation was then reduced by the geometrical scale factor $S_{\ell} = 5.5$ to obtain the desired gradation for the model as shown in Fig. 3.2(b). Since the scaled gradation curve is difficult and undesirable to model in the very small particle sizes, the scaled gradation was modified by linearly varying the gradation from the desired 50 percent at the No. 20 sieve to 0 percent finer than the No. 200 sieve. This modified gradation line shown in Fig. 3.2(b) is the goal sought in blending the available aggregates whose individual gradation curves are shown in Fig. 3.2(a). The actual model aggregate gradation curve obtained is also shown in Fig. 3.2(b). This model aggregate was obtained using the following combination of aggregates:

TCM 1/8	26%
Ottawa Silica Bond Sand	30%
No. 1 Blast Sand	28%
No. 2 Blast Sand	8%
Colorado River Red Sand	8%

The final gradation obtained is a reasonable approximation of the modified curve desired being deficient only around the No. 100 screen. The model aggregate had a specific gravity of 2.60 and absorption of 0.7 percent which compare closely to the prototype values of 2.62 and 0.5 percent, respectively.

Final mix design was based on a trial batch basis, with the initial trial using the requirements for Texas Highway Department Class A superstructure concrete.[8] This mix proved unworkable and numerous additional trials were made until a workable concrete with stress-strain characteristics quite similar to the prototype concrete were obtained. Because of the lengthy time and multiple batches required for placement of the microconcrete in the model bridge, a Texas Highway Department approved retarding agent "Airsene L" was used to delay initial set and improve workability. The final mix design used was:

Water-cement ratio by weight	0.687
Cement factor (sacks per cu.yd.)	5.0
Aggregate-cement ratio by weight	6.53
Retarding agent (fl.oz. per sack)	6.0

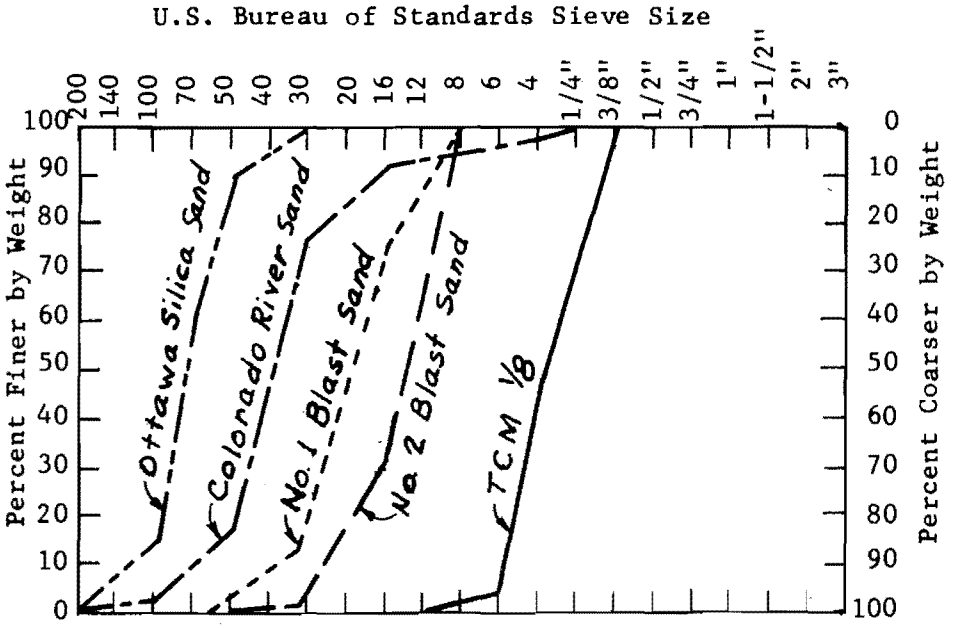

(a) Basic Aggregate Gradation Curves.

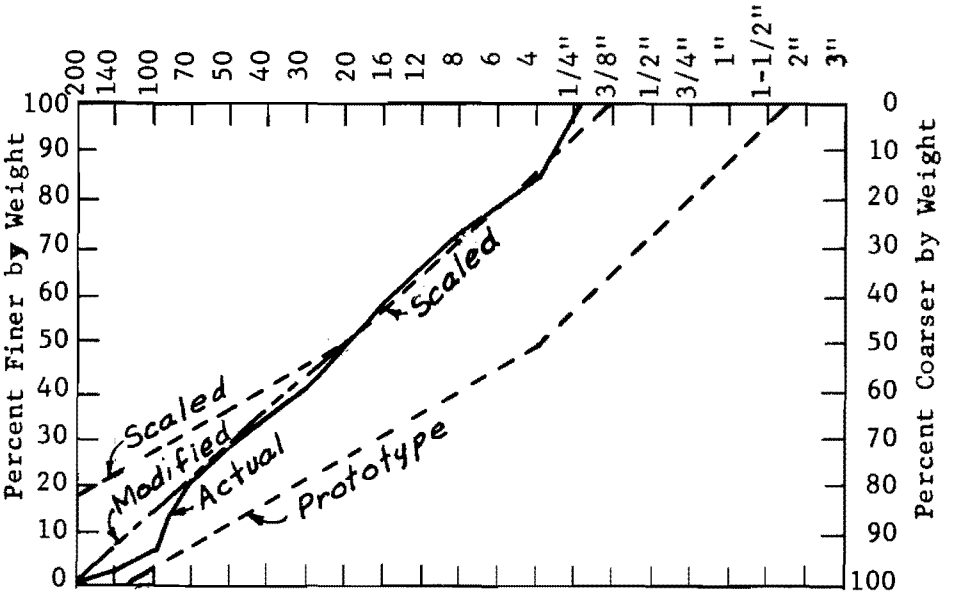

(b) Microconcrete Aggregate Gradation.

Fig. 3.2. Model Aggregate Gradation.

This microconcrete had an air content of 5-3/4 percent and a wet unit weight of 133 lbs. per cu. ft.

Consistency was determined by visual inspection rather than by slump tests. Microconcrete slump tests are not accurate indicators of consistency since microconcrete usually appears harsh and stiff, although it can be easily placed with the aid of a vibrator.

Stress-strain curves for both the microconcrete and the prototype concrete are shown in Fig. 3.3. Strain measurements up to ultimate were obtained by averaging the readings from electrical resistance strain gages placed on diametrically opposite faces of the cylinders. The descending portions of the curves were obtained by measuring the displacement of the testing machine loading head with dial gages. The model cylinder was 3 in. in diameter by 6 in. in height instrumented with 1/4 in. gage length foil strain gages. The prototype cylinder was the standard 6 in. by 12 in. cylinder instrumented with 1/2 in. gage length wire strain gages.

Several curves are shown in Fig. 3.3. The microconcrete of this investigation (shown as a solid curve with data points plotted) had an ultimate strength of 4530 psi while the prototype concrete (shown as a dashed curve with data points plotted) had an ultimate strength of 4700 psi. The other curves (ultimate strengths on the order of 3000 psi) are taken from a study by Aldridge[5] and tend to verify the shape of the stress-strain curves for the prototype and microconcrete.

The moduli of elasticity shown were calculated using the ACI Building Code formula $E_c = 33\, w^{1.5} \sqrt{f'_c}$,[9]

where E_c = modulus of elasticity, psi
w = weight of concrete, lb/cu.ft.
f'_c = compressive strength of concrete, psi

The moduli are 3,410,000 psi and 3,950,000 psi for the microconcrete and prototype concrete respectively. The values closely match the observed values for the secant modulus at 0.45 f'_c and show that the difference between moduli is mostly a function of unit weight. Studies with microconcretes

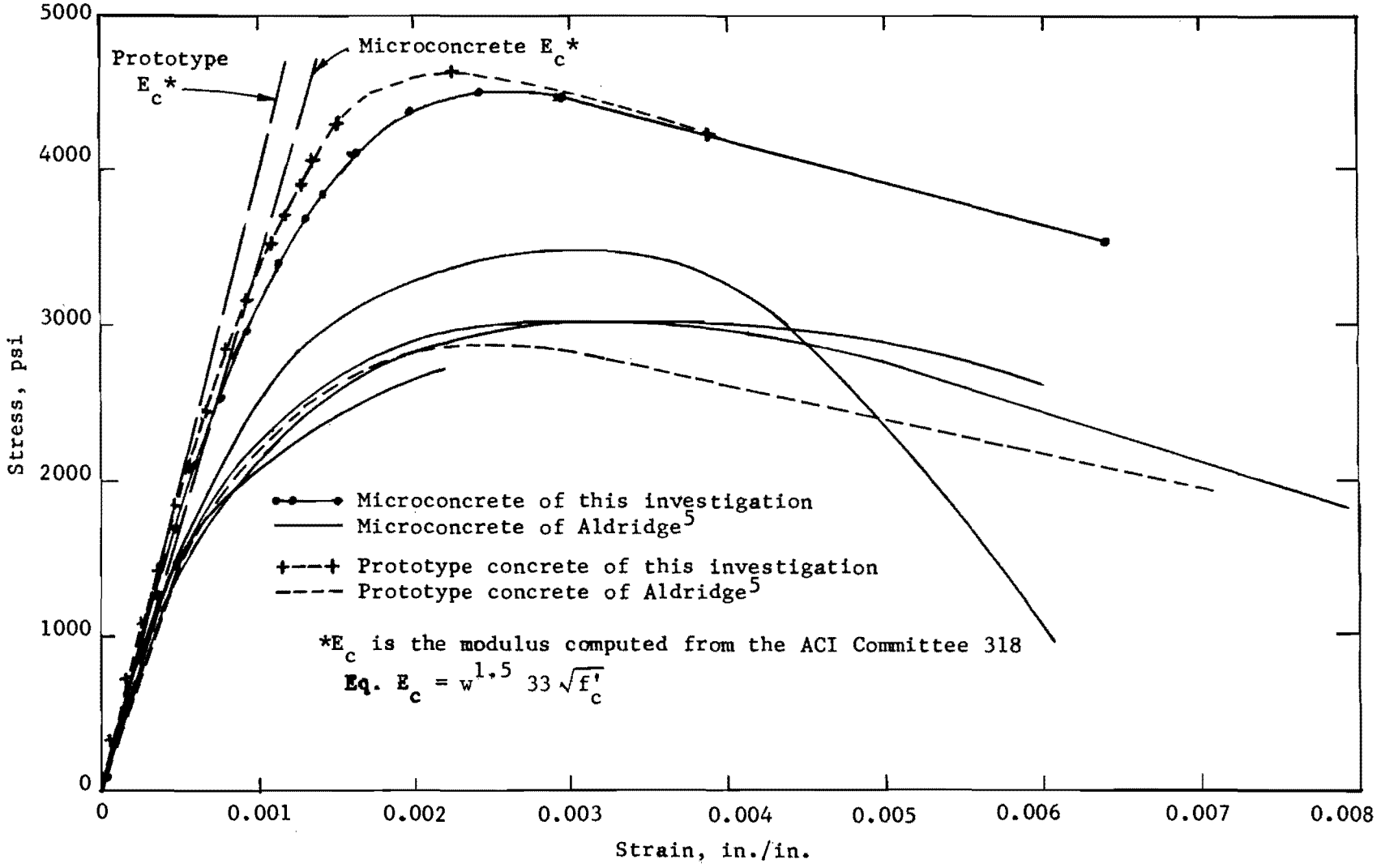

Fig. 3.3. Stress-Strain Curves for Microconcrete and Prototype Concrete.

utilizing nongraded aggregates (sand mortars) indicate very appreciable moduli differences.[4]

Split cylinder tensile strengths were obtained using cylinders from the same batches of microconcrete and prototype concrete used to obtain the compressive stress-strain curves shown in Fig. 3.3. The microconcrete split cylinder strength was 555 psi which is about $0.12\ f'_c$ or $8.3\sqrt{f'_c}$. The prototype concrete split cylinder strength was 480 psi, which is about $0.10\ f'_c$ or $7.0\sqrt{f'_c}$. These values are in good agreement with results found by Aldridge[5] and White.[4] The results indicate a definite increase in split cylinder tensile strength for the microconcrete, although the magnitude of the variation in tensile strength is sufficiently low so that it should not greatly affect strength calculations. The major effect will be somewhat higher crack formation loads in microconcretes.

3.2.2 Reinforcement. Reinforcement properties may be the most critical factor in a model study of a reinforced concrete structure where flexure predominates. It is essential that the steel used in the model and the prototype have virtually identical stress-strain curves, particularly with reference to sharpness of definition of yielding.

At large scales, where commercially available reinforcement may be used, there is usually little difficulty in obtaining the desired stress-strain curves. In the usual small-scale model case, some or all of the reinforcement will be smaller than the minimum (#3) ASTM A305 deformed reinforcement. Steel Wire Gage (SWG) wire is available for use as model reinforcement in this case, but presents several problems. This material is usually stored in coils. Upon purchasing it must be uncoiled, straightened, and cut to length. The usual commercial straightening process strain-hardens the steel. In this state it may be ideal for high-strength reinforcement, although this is not always the case. The wire must be carefully tested and if the stress-strain curve is undesirable the wire may be cold-worked or heat-treated to obtain the desired properties. Round stock and small reinforcement bars may also require altered stress-strain curves and may be treated in a similar fashion.

The SWG wire initially obtained for this project exhibited a "round house" (i.e., no sharply defined yield plateau) stress-strain curve with a high yield point. Heat treatment was used to give the wire a desired "flat top" yield plateau as typical with intermediate grade reinforcement. Typical curves (treated and untreated) for several SWG wire sizes and a No. 2 bar are shown in Fig. 3.4. The heat treatment increases the ductility of the bars by 20 percent to 50 percent, as well as producing a flat yield plateau. Ultimate strengths were reduced by a small amount.

Smooth (nondeformed) SWG wires and No. 2 bars do not function in bond in the same manner as deformed bars, hence their use is limited to studies where bond is not a major factor. The smooth wires used in this investigation were allowed to rust to improve bond properties. After two of the bridge models had been tested, a special supply of No. 2 deformed bars became available. Since No. 2 bars were used as the main flexural reinforcement, it was felt that use of deformed bars would result in a more realistic crack pattern. Two beams, each consisting of two typical interior girders of the bridge model, were cast with the only difference being in the reinforcement used. Smooth No. 2 bars were used in one, while deformed No. 2 bars were used in the other. Crack patterns observed in these tests are shown in Fig. 3.5. The beams were loaded with uniform loads to compensate for dead load scaling and then point loads at midspan were applied and increased until failure. The top beam shown used smooth bars and developed one wide crack at midspan with a few smaller cracks nearby. This is typical of a beam in which the reinforcement possesses poor bond properties. The lower beam was reinforced with deformed flexural reinforcement and has a more realistic cracking pattern, as found in prototype specimens.

White[4] has compared the crack patterns of models reinforced with smooth wires, threaded wires (by means of a die), and deformed wire against the crack patterns of large test specimens reinforced with normal size reinforcement. In every case he found that any roughening of the wire surface, whether by rusting or deformation, improved the cracking similitude of the models. The smooth wires resulted in a small

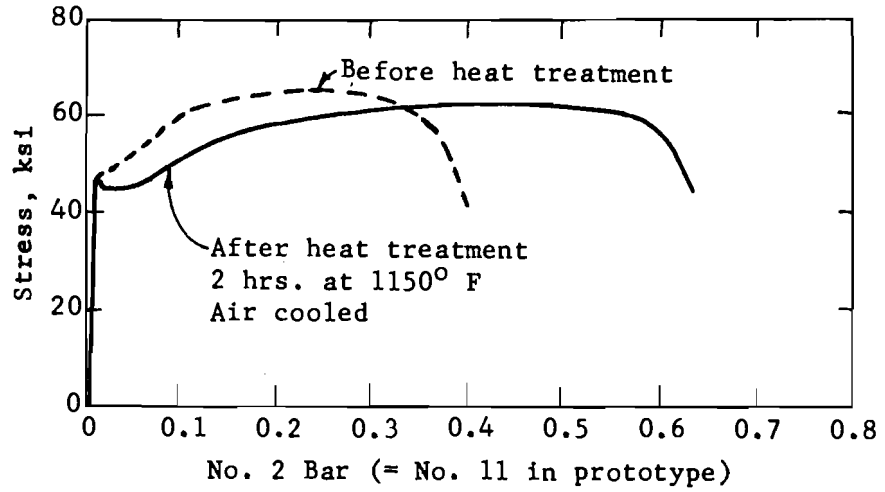

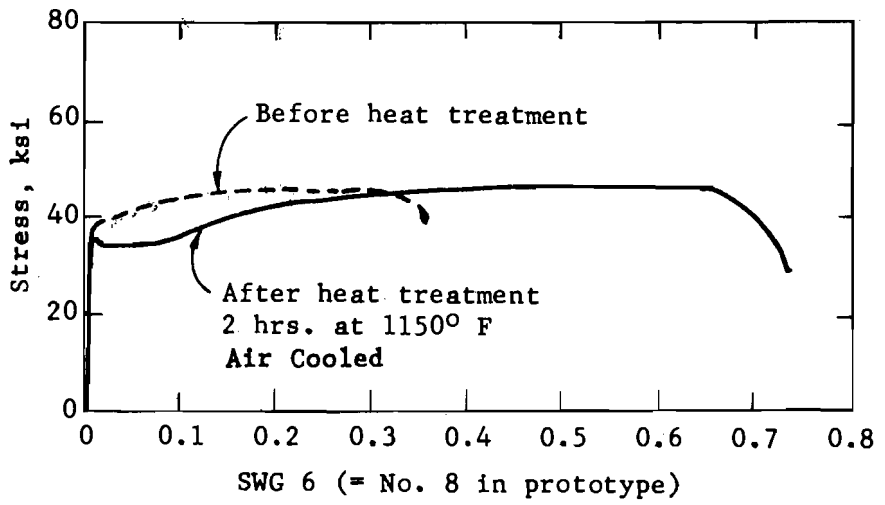

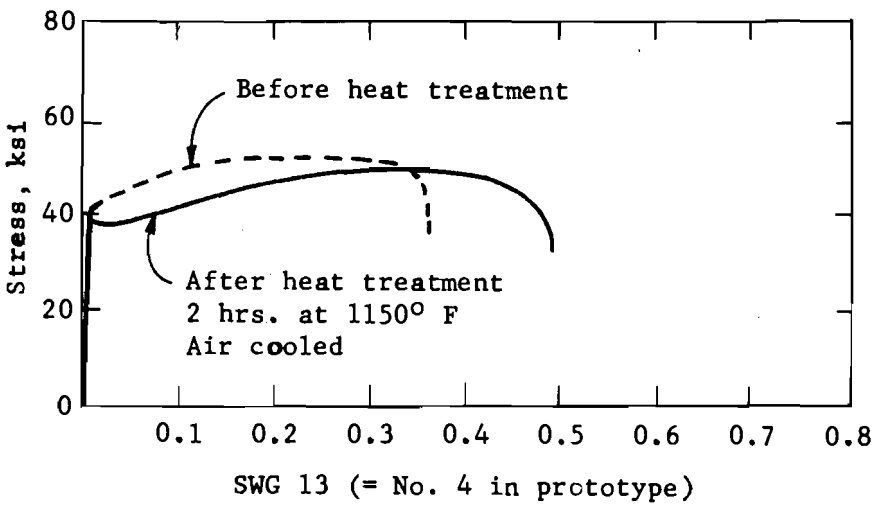

Unit Strain in a 2-in. Gage Length

Fig. 3.4. Typical Stress-Strain Curves before and after Stress Relief Annealing.

Fig. 3.5. Crack Patterns Using Smooth and Deformed No. 2 Bars.

number of cracks and poor agreement in crack spacing with the large test specimens.

Since the two beams shown in Fig. 3.5 followed the trend indicated by White, subsequent bridge models were reinforced with deformed No. 2 bars as the main flexural steel. All reinforcement smaller than No. 2 bars was well-rusted SWG wire.

Typical stress-strain curves for the main reinforcement used in this investigation are shown in Fig. 3.6. The No. 2 deformed bar was used as high strength steel in Model SG-3. As outlined in the Research Program in Section 1.4, Model SG-3 was identical to Model SG-2, except that high strength steel was used in the former and intermediate grade steel was used in the latter. The substitution was made by adjusting the areas so that the total bar force at design stress (24 ksi) for the high strength steel was equivalent to the total bar force at design stress (20 ksi) for the intermediate grade steel. The prototype for SG-2 was reinforced with four No. 11 bars and two No. 5 bars in each girder. With the use of high strength steel this was reduced to four No. 11 bars to provide the same service load moment capacity per girder.

3.3 Forms

In realistic modeling, fabrication tolerances must be reduced in proportion to the scale utilized. This requires careful consideration of forming techniques. While prototype methods and forming materials may frequently be used to advantage with larger scales, they were judged undesirable at approximately 1/6 scale. Instead, Plexiglas forms were used for three basic reasons advanced by Breen:[10]

(1) Its transparency greatly facilitates placement and visual inspection of the reinforcement and subsequently of the microconcrete.

(2) No bond release agent is required as the concrete does not adhere to it. This is particularly important since the use of the form oils is undesirable in the small sections because of the reduced covers.

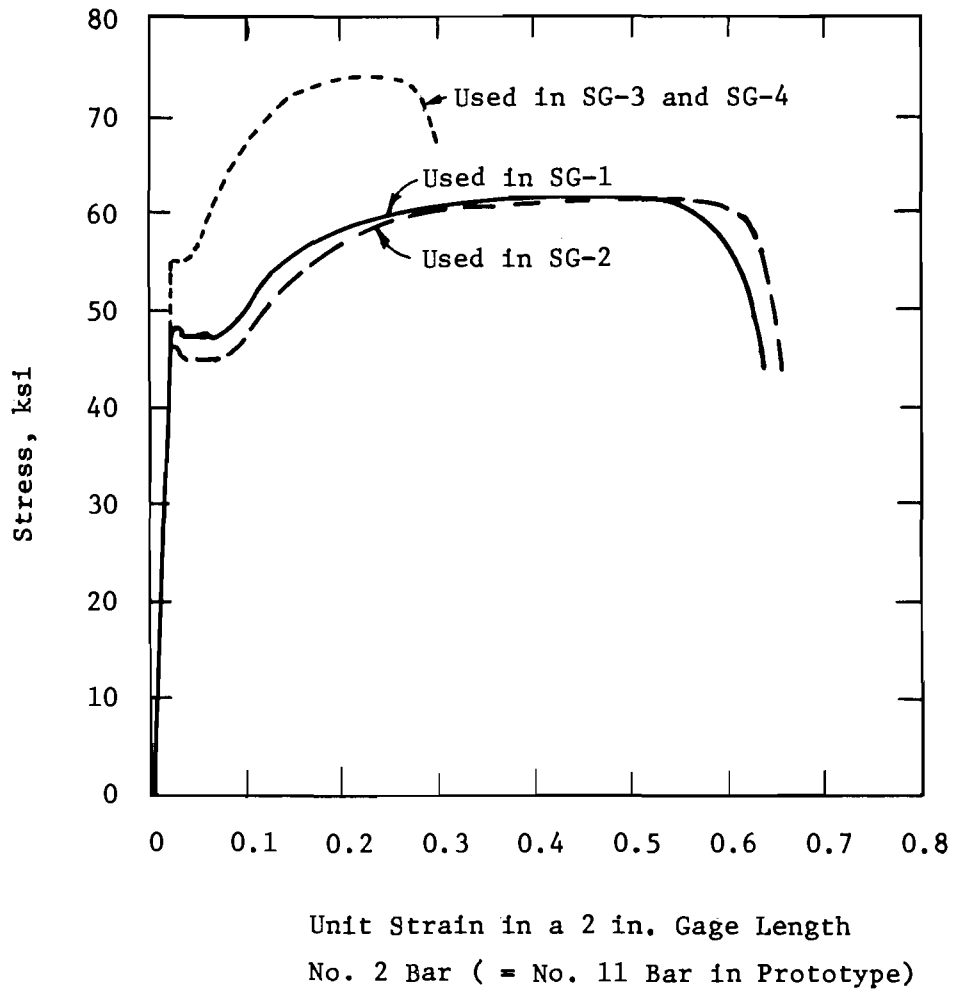

Fig. 3.6. Typical Stress-Strain Curves for Main Flexural Reinforcement.

(3) It does not absorb water from the mixture, and the joints can be adequately sealed so that the premature surface drying noted with wooden forms is eliminated.

The transparent property of the Plexiglas forms greatly facilitated the placement of the large quantities of reinforcement. The capability of visually checking the location and cover on each reinforcement cage as placed cannot be overemphasized. Since it required several days to set formwork and place cages, the use of form oil was impractical as well as undesirable because of the small covers which were on the order of 1/4 in. Furthermore, the curved cross section of the bridge required a form material that could be accurately bent to the correct shape. Well-established techniques were available for molding Plexiglas into the desired shape.

The model pan forms were scaled from the Standard Texas Highway Department Plans shown in Figs. A.1 and A.2 in Appendix A, using the geometric scale factor S_{ℓ}, with minor modifications made by adding more stiffening diaphragms.

The forms were constructed from standard 1/8-in. thick sheets of Plexiglas using a heating process for shaping. A mold was constructed from a steel pipe which had been machined to the proper radius and to which steel plates were attached as indicated in Fig. 3.7. Plexiglas cut to appropriate width was positioned on the mold and held in place with light machine screws. An external heat source (infrared space heaters) was used to bring the Plexiglas to the glass transition temperature, whereupon it would sag under its own weight onto the mold. The heat source was immediately removed and pressure was applied to the Plexiglas to prevent wrinkling while cooling by using a flexible upper mold composed of narrow wooden strips interconnected by thin metal strips. Initial pressure was applied to the wooden mold by hand for several minutes and then gravity load was applied. The Plexiglas was initially rapidly cooled by blowing compressed air through the pipe mold and onto the surface of the material. The Plexiglas was then allowed to slow cool for an additional thirty minutes before removal

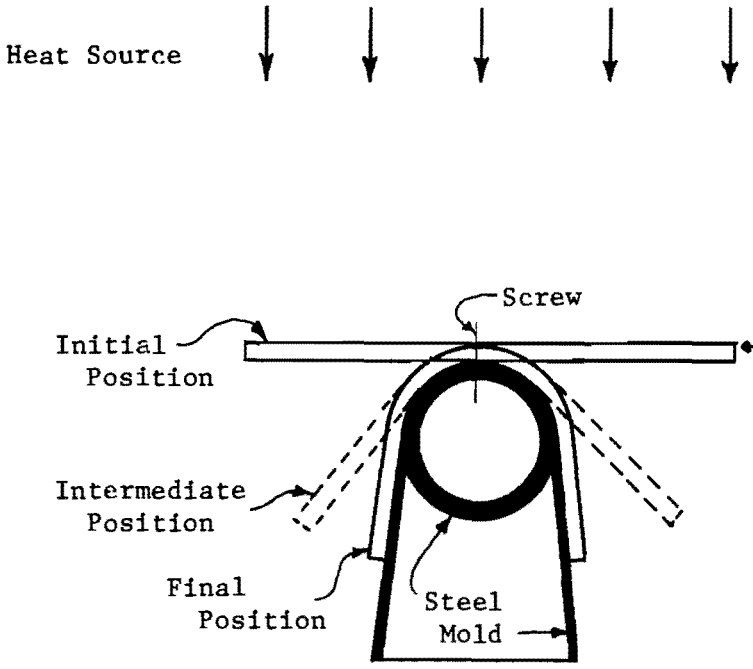

(a) Heating.

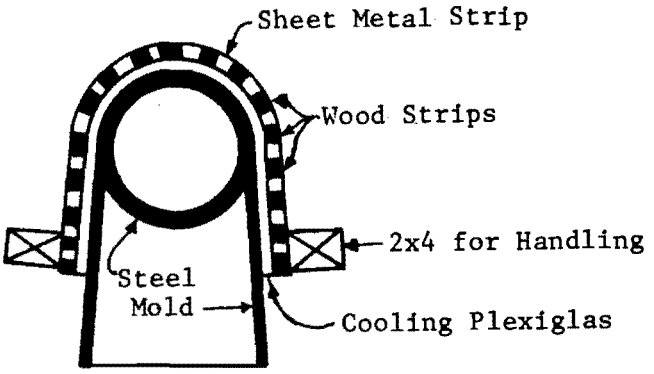

(b) Cooling.

Fig. 3.7. Pan Form Shaping Operations.

from the steel forms. The completed Plexiglas sheet was trimmed to length on a band saw. End plates and interior diaphragms made of Plexiglas were glued in place with ethylene dichloride.

Two completed pan forms are shown in Fig. 3.8. The completed forms were capable of carrying the freshly cast concrete, although additional support at midspan was used to prevent sagging (Plexiglas has a modulus of elasticity on the order of 500,000 psi, compared to 29,000,000 psi for steel).

Pan forms were constructed as individual pans so that they could be used for skewed bridges in the same manner as the prototype pans. Typical end forming details of the pans for 45° skew bridges are also shown in Fig. 3.8.

Footing and bent cap forms were also constructed from 1/8-in. thick Plexiglas stock. Ethylene dichloride was used to "glue" the Plexiglas together. Column forms were constructed from 4-1/2-in. inside diameter Plexiglas tubing with 1/8-in. wall thickness. The tubing was split longitudinally in order to facilitate form stripping. During casting the two halves were held in place with hose clamps. Figure 3.9(d) shows the substructure forms for columns and bents in place during casting.

3.4 Fabrication

All reinforcement cages were fabricated by hand-tieing the steel with "safety wire" having a diameter of 0.028 in. "Reinforcing bars" as small as SWG No. 18 were tied without difficulty.

The substructure was detailed following Texas Highway Department Standard Plans, with each bridge model having the substructure which was usually designed for it. Figure 3.9 shows the reinforcement cages used in a typical substructure as well as the casting of a four-column bent.

Fabrication of a typical girder cage is shown (inverted) in Fig. 3.10(a). Dimensional tolerances were controlled by the liberal

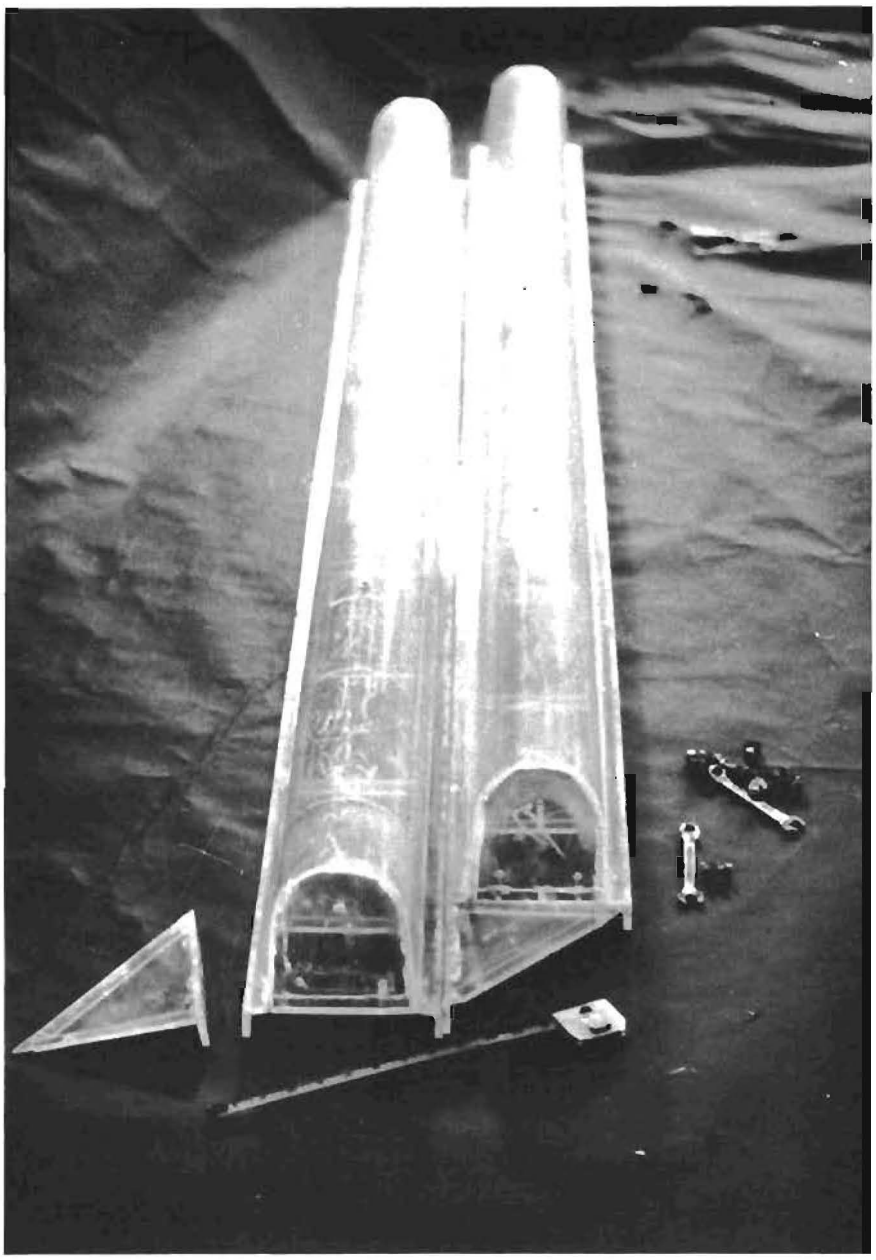

Fig. 3.8. Model Pan Form Details.

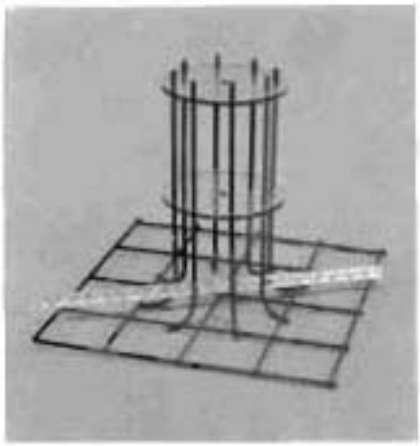

(a) Footing Reinforcement.

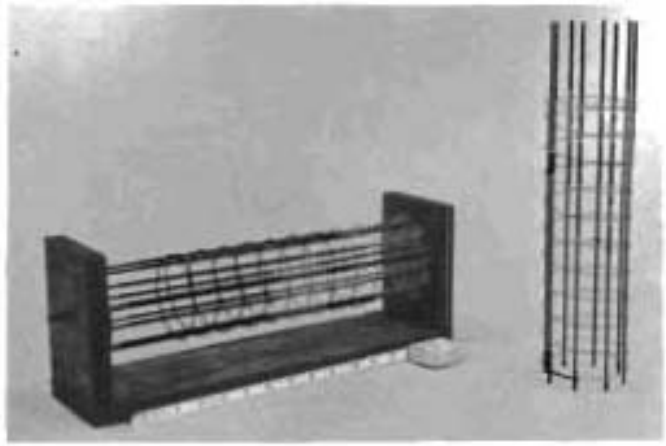

(b) Column Reinforcement.

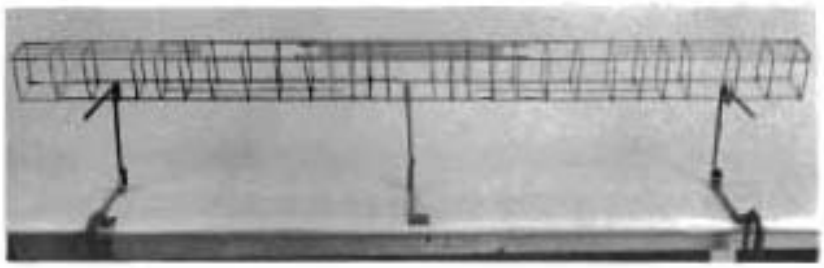

(c) Bent Cap Reinforcement (Three Column Bent).

(d) Casting Bent Cap (Four Column Bent).

Fig. 3.9. Substructure Steel and Casting.

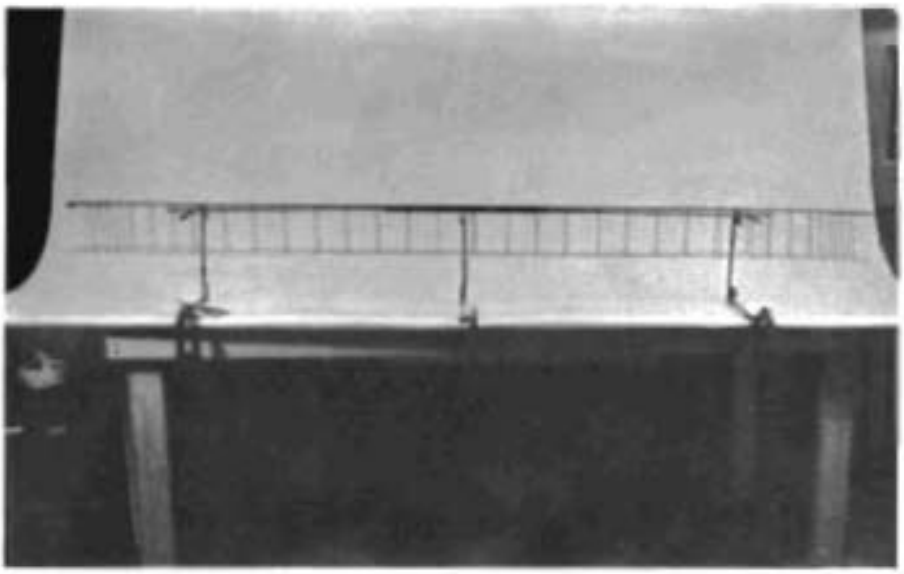

(a) Completed Girder Cage.

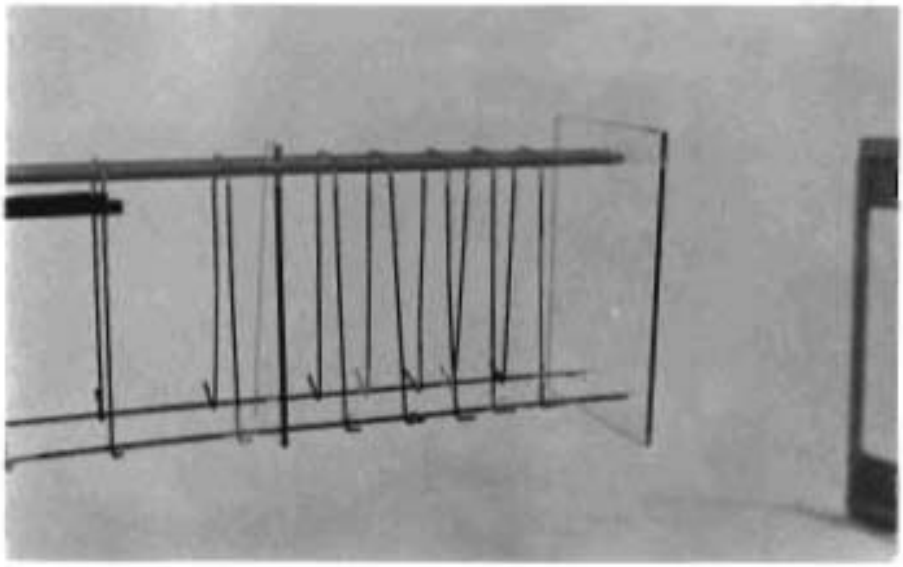

(b) Jigs Used for Control.

Fig. 3.10. Girder Cages.

use of Plexiglas jigs. Two of these jigs near the end of a cage are shown in Fig. 3.10(b). It is absolutely essential to use such jigs to position reinforcement accurately.

Bent caps were positioned in the test frame so that the pan forms could be suspended from them and the slab cast in place. This procedure allowed modeling of the true support boundary conditions of the prototype as shown in Fig. 3.11.

Pan forms were placed one at a time to facilitate placing the girder cages and checking their location and cover. The wires which were later used for hanging dead load compensation weights were placed at this time as shown in Fig. 3.12. After all forms and girder cages were placed, strain gages on the steel were given a final check for circuit continuity. The pretied slab steel was then positioned and tied into place. A 0^{o} skew and a 45^{o} skew model are shown ready for casting in Fig. 3.13(a) and (b).

Figure 3.13 illustrates the ease with which steel placement may be checked when Plexiglas is used as a form material. The procedure for passing strain gage lead wires through the forms is also shown. One of the wires used to support the dead load blocks may be seen to the right of the strain gage lead wire.

Microconcrete was mixed in a 3-cu. ft. capacity rotating drum mortar mixer in 2-1/4 cu. ft. batches. Each bridge superstructure model required from 6 to 8 batches of microconcrete. In order to maintain uniformity and facilitate placement, half of the batches were mixed and placed in a large pan, where they were thoroughly blended. This blended "batch" was placed in the bridge as a first lift. While the first lift was being placed the second and final lift was being mixed and blended.

Each lift was placed uniformly in the forms by hand and compacted with a vibrator. A standard laboratory immersion vibrator with a 3/4-in. head was used to vibrate the concrete both internally and externally. Vibrator power was controlled using a Variac. Microconcrete was usually rather harsh and dry in appearance but was easily

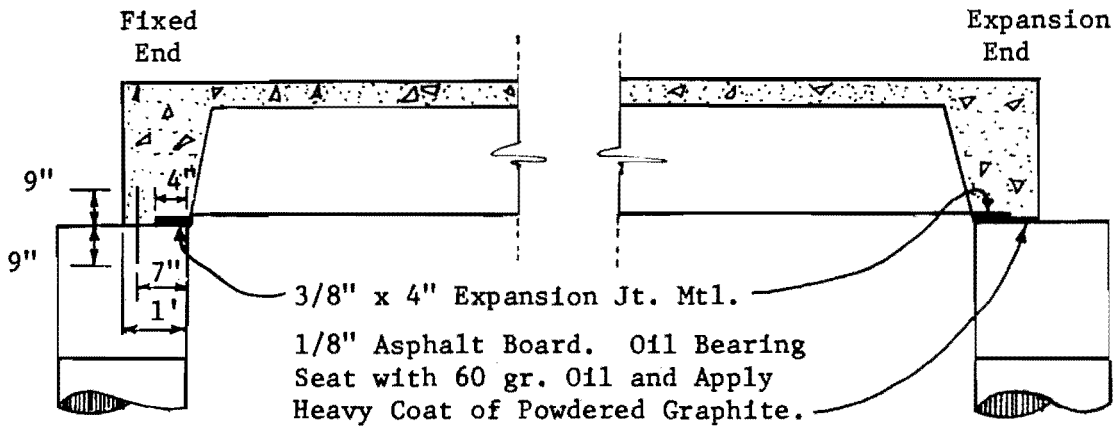

Prototype

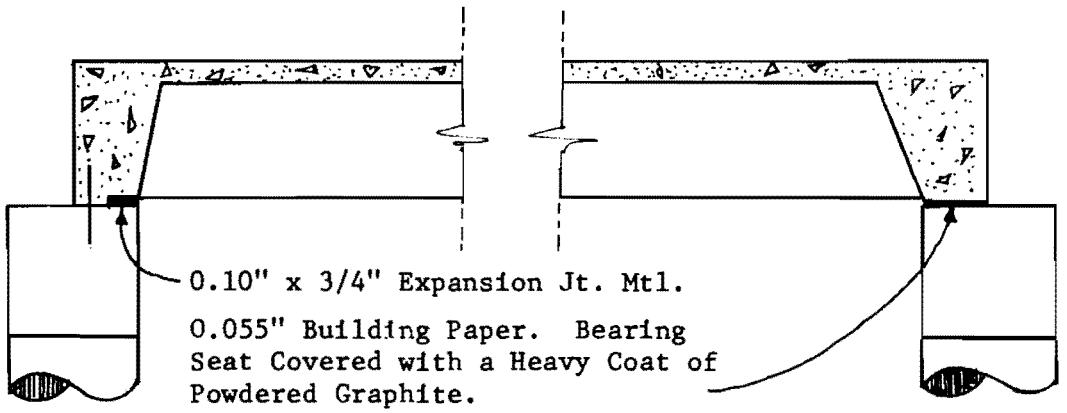

Model
(Scale = 1/5.5)

Fig. 3.11. Support Conditions.

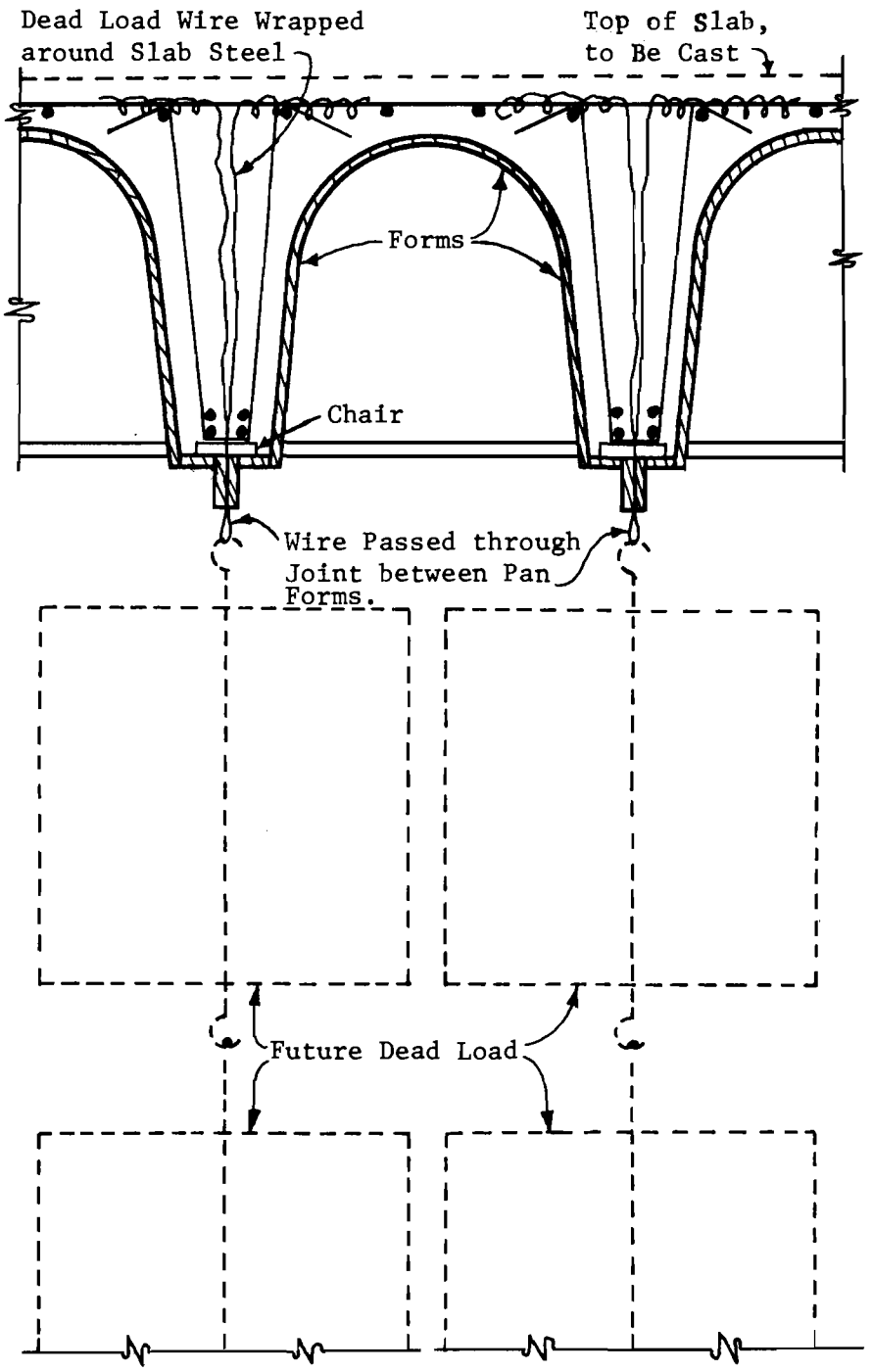

Fig. 3.12. Method of Installing Dead Load Wires.

(a) 0° Skew Bridge.

(b) 45° Skew Bridge.

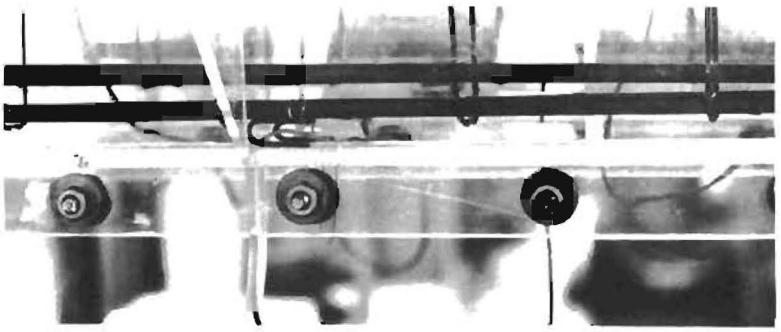

(c) Location of Reinforcement.

Fig. 3.13. Models Ready for Casting.

placed with the aid of the vibrator. Proper placement and compaction was visually inspected through the Plexiglas forms.

After casting and screeding, the surface of the bridge model was allowed to sit before final troweling of the deck. The deck was then sprayed with a membrane curing compound and covered with wet burlap. Forms were left in place as a moisture barrier for about three days, then stripped. Forms were removed by blowing compressed air into threaded couplings which had been fabricated into them.

After the forms were stripped the test span was prepared for testing by marking, setting up dial gages, and completing strain gage circuits.

3.5 Instrumentation

3.5.1 Load Control.--Applied load had to be carefully controlled, since it was one of the prime variables. The loading system used was basically a hydraulic pressure system. However, load control was primarily by use of electronic strain transducers, since pressure gage readings are not accurate enough (particularly at low load levels). In addition, low pressure readings are somewhat suspect in rams with spring return plungers as used in this program. Different pressure-calibration curves are obtained for the same ram at different plunger extensions, due to internal forces required to overcome the spring extension. In this study it was found that service loads could be in error by as much as 10 percent if pressure readings alone were used for load control.

Because of these difficulties, ram loads were controlled by the pancake-type load cell shown in Fig. 3.14 developed by Lee.[11] This load cell has a sensitivity of about three pounds per microinch of strain, with a maximum working capacity of about 8000 lbs.

3.5.2 Structural Response.--Concrete strains were measured with a Demec gage (a mechanical extensometer developed in England) with a gage length of two inches. Due to the small amplitude of concrete strains, the number of these measurements taken was limited.

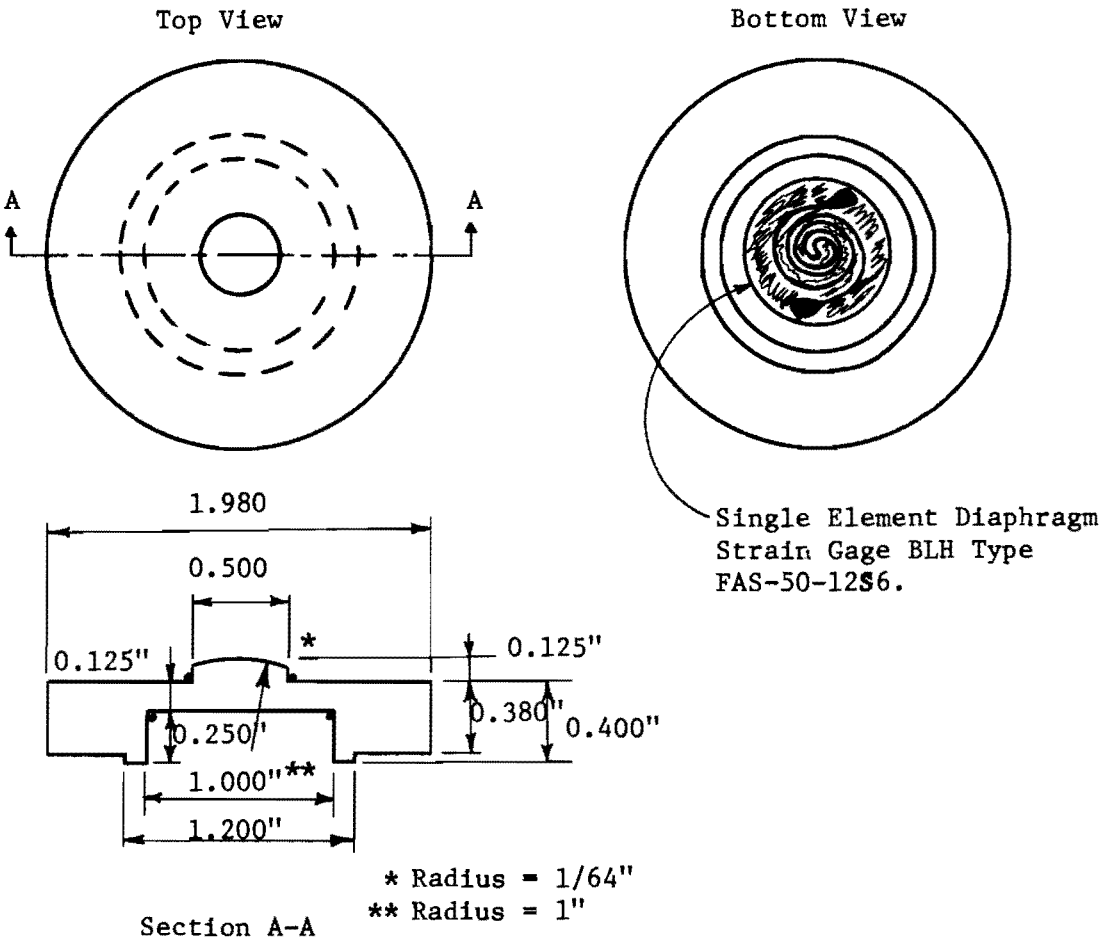

(a) Load Cell Dimensions.

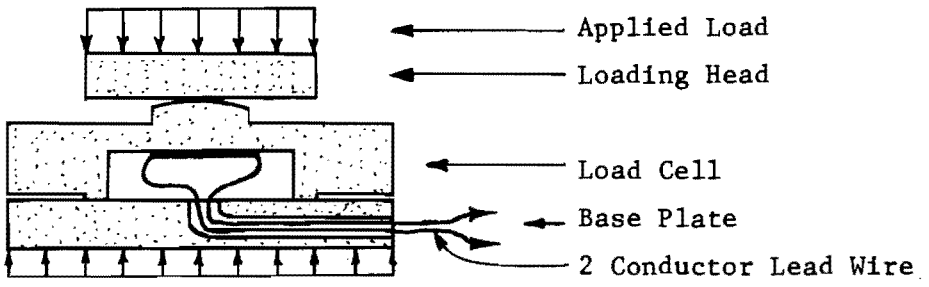

(b) Load Cell Installation.

Fig. 3.14. Pancake Type Load Cell.

A wide variety of reinforcement steel strains were measured with electrical resistance strain gages attached to the reinforcement. The main girder flexural steel had 1/4-in. gage length foil gages while similar gages with a 1/8-in. gage length were applied to the smaller size transverse slab steel. The gages were installed as shown in Fig. 3.15. Strain gages were attached to the reinforcing steel using Budd GA-1 or Eastman 910 contact cement. The coarse lead wires connecting the strain gages to the switch and balance units were connected to the gages with the much finer lead wires shown. During handling, any movement in the coarse leads was absorbed in the flexible fine lead wire rather than damaging the strain gage. Devcon liquid rubber was applied around the complete gage installation. The rubber remained flexible even after setting. This flexibility is important as it dissipates shearing forces between the gage and the surrounding concrete. The hard outer coating of epoxy protects and waterproofs the entire installation during handling and casting. The complete installation extended over less than 3/4-in. of the reinforcing bar. Considerable success was achieved in the laboratory using this system, gage losses remaining below 5 percent. Detailed locations of the gages are shown in the discussion of results for each model.

Deflection measurements with reference to a movable gage base line system were taken using Federal dial gages with a least count of 0.001 in. with estimation to the nearest 0.0001 in. Deflections were taken at the end, 1/8, 1/4, 3/8, and 1/2 span over each girder for a maximum of 108 deflections per load. Frequently, however, only readings in the vicinity of the applied load were taken.

Individual girder reactions were measured at one end of six of the girders as shown in Fig. 3.16. The 1/4-in. plate was designed to be of negligible stiffness when compared to the end diaphragm stiffness; at the same time it provided a smooth bearing surface for the load cells. This method of measuring reactions was not very effective.

The models were divided into a grid system, as shown in Fig. 3.17. Each girder was identified by an alphabetical letter A-M.

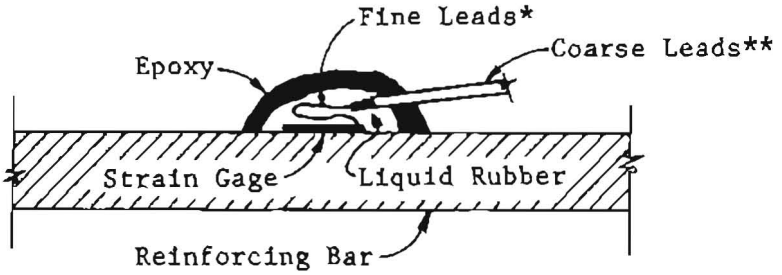

*Fine Leads - No. 32 ga. Single Strand, Enamel Insulated

**Coarse Leads - No. 24 ga. 2 Conductor, Insulated Speaker Wire

(a) Cross Section of Completed Gage Installation.

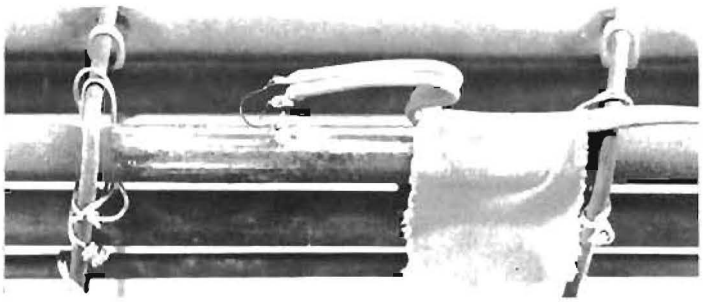

(b) Strain Gage Installation before Waterproofing.

Fig. 3.15. Strain Gage Installation.

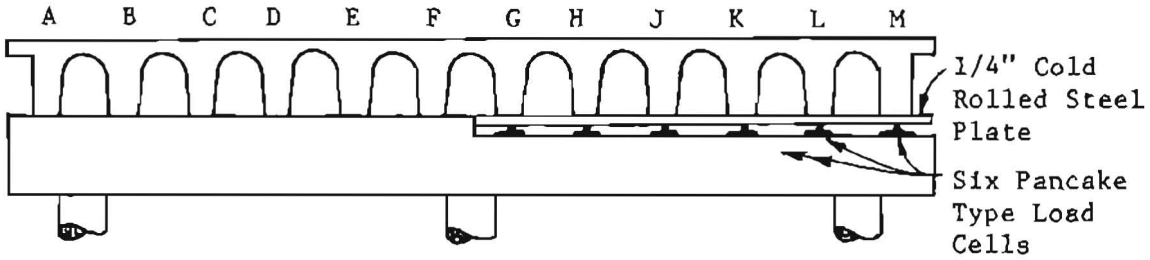

Fig. 3.16. Reaction Measurements.

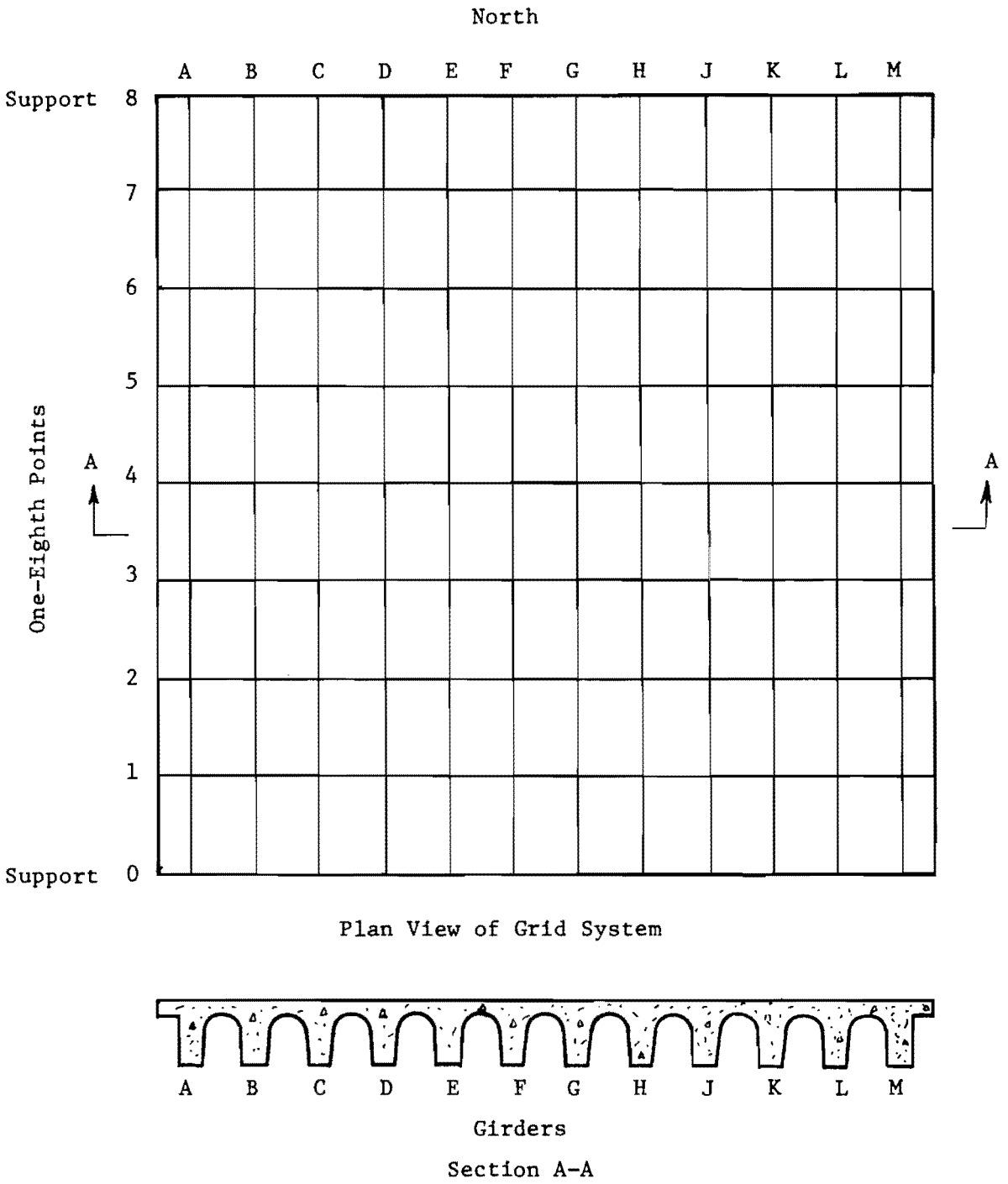

Fig. 3.17. Grid System.

In the span direction the bridge was divided into 1/8 points. Deflections were measured at the intersections of the grids. Steel strains were measured at the midspan on the flexural reinforcement of each girder. In addition, the southwest quadrant was gaged at the 1/10 and 1/4 points, as were the northwest and southeast. Reactions were measured under the diaphragm of the north support where girders G through M framed into it.

3.6 Loading

3.6.1 Gravity Loads.--Prototype self-weight (dead load) stresses are difficult to reproduce in a model, since available model materials do not meet the density similitude requirements (model density = S_ℓ x prototype density). With quasi-static loadings this may be overcome by the application of compensating external uniform load equal to (S_ℓ - 1) times the model weight.

Closely spaced point loads were used to simulate the basic moment envelope due to gravity load. These point loads consisted of dead weights hung below the structure allowing the top surface to remain accessible for live load placement. The basic dead weight used was a 12.5 lb. concrete block with rigid hooks, as shown in Fig. 3.18. A column of blocks could be assembled as required to provide the necessary dead load. Load was transferred from the blocks to the girder by means of steel music wires embedded before casting. Four to five layers of blocks were used, depending on the weight of the prototype bridge. The blocks were freely suspended to prevent binding between columns of blocks. No difficulty was encountered with this load system, even at ultimate loads.

Since the point loads were used to simulate uniform load, it is necessary to examine the errors introduced by this approximation. The accuracy of the approximation is shown in Fig. 3.19 for a simple beam with span length of 85.2 in. (Prototype clear span 39 ft. reduced by the scale factor, S_ℓ = 5.5.) For comparison, the uniform load bending moment of $wL^2/8$ is taken equal to unity. The resulting moment diagrams

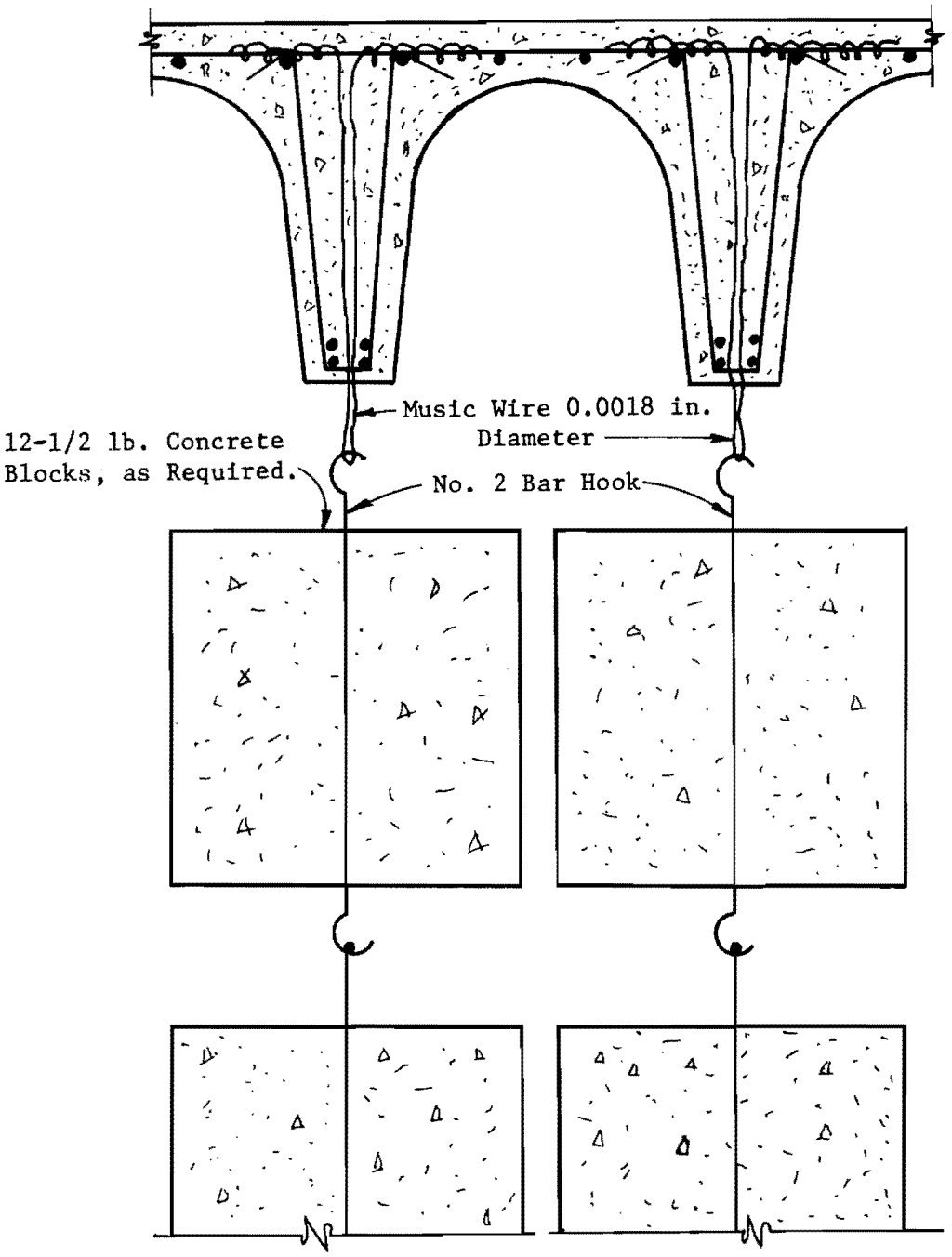

Fig. 3.18. Gravity Load Compensation.

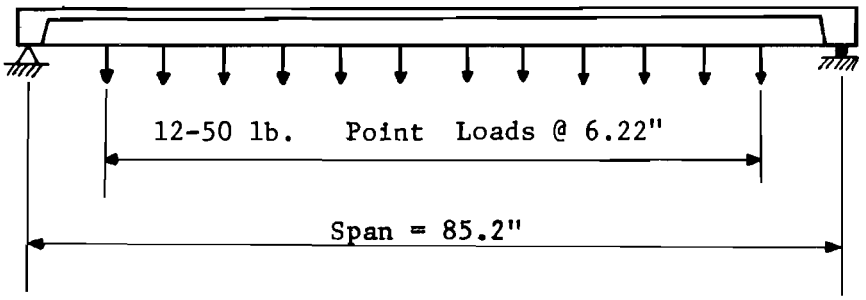

(a) Dead Load Arrangements.

Prototype Dead Load	= 204 lb/sq ft
Desired Model Dead Load	= 204 lb/sq ft
Model Self Weight	= 25 lb/sq ft
Supplementary Weight Required	= 179 lb/sq ft
Actual Weight Provided	$= \frac{50 \text{ lb}}{6.22" \times 6.55"} \times 144$
	= 177 lb/sq ft

(b) Computation of Required Supplementary Weight.

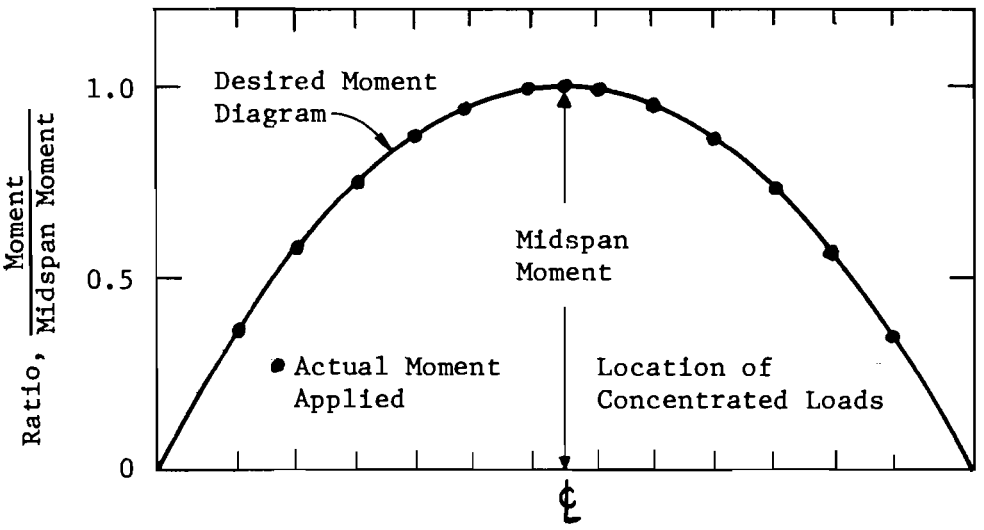

(c) Moment Diagram.

Fig. 3.19. Comparison of Actual and Desired Dead Load Moment Diagrams.

are shown in Fig. 3.19. The agreement between moment diagrams is excellent. The actual moment variation between concentrated loads is linear, due to the concentrated loads plus a parabolic variation, due to the self-weight of the structure.

3.6.2 Live Loads.--Live loading consisted of single wheel loads, axle loads, single truck loads, double truck loads, triple truck loads, a special overload vehicle, and ultimate loads.

The principle of superposition is not necessarily valid for reinforced concrete structures, although its use may not be in serious error at low loads. Hence, a versatile loading system was required to permit the placement of many different loads on the bridges. A yoke type of loading frame was designed, as shown in Fig. 3.20. The two reaction yokes carry the load from the ram reaction beam which may be moved laterally according to truck position. The rams can be placed in any position along the longitudinal axis of the ram reaction beam. Using this system loads could be placed at any coordinate on the test slab.

Two additional spans are shown in Fig. 3.20, one adjacent to each end of the test span. These slabs were used to simulate, as realistically as possible, the boundary conditions of a typical interior span. Their sole purpose was to balance the dead load moment on the bent cap, as would be the actual case in practice. These slabs were approximately equal in weight to the test slab. As the auxiliary dead load was suspended from beneath the test slab, additional weight was placed on the dummy spans. In this fashion a substantial portion of the load response of the test slab due to dead load was able to be measured.

Truck loads were modeled from the AASHO design vehicles.[12] The relation between the full-size H20-S16 truck and the model truck (with a scale factor of $S_{\ell} = 5.5$) is illustrated in Fig. 3.21.

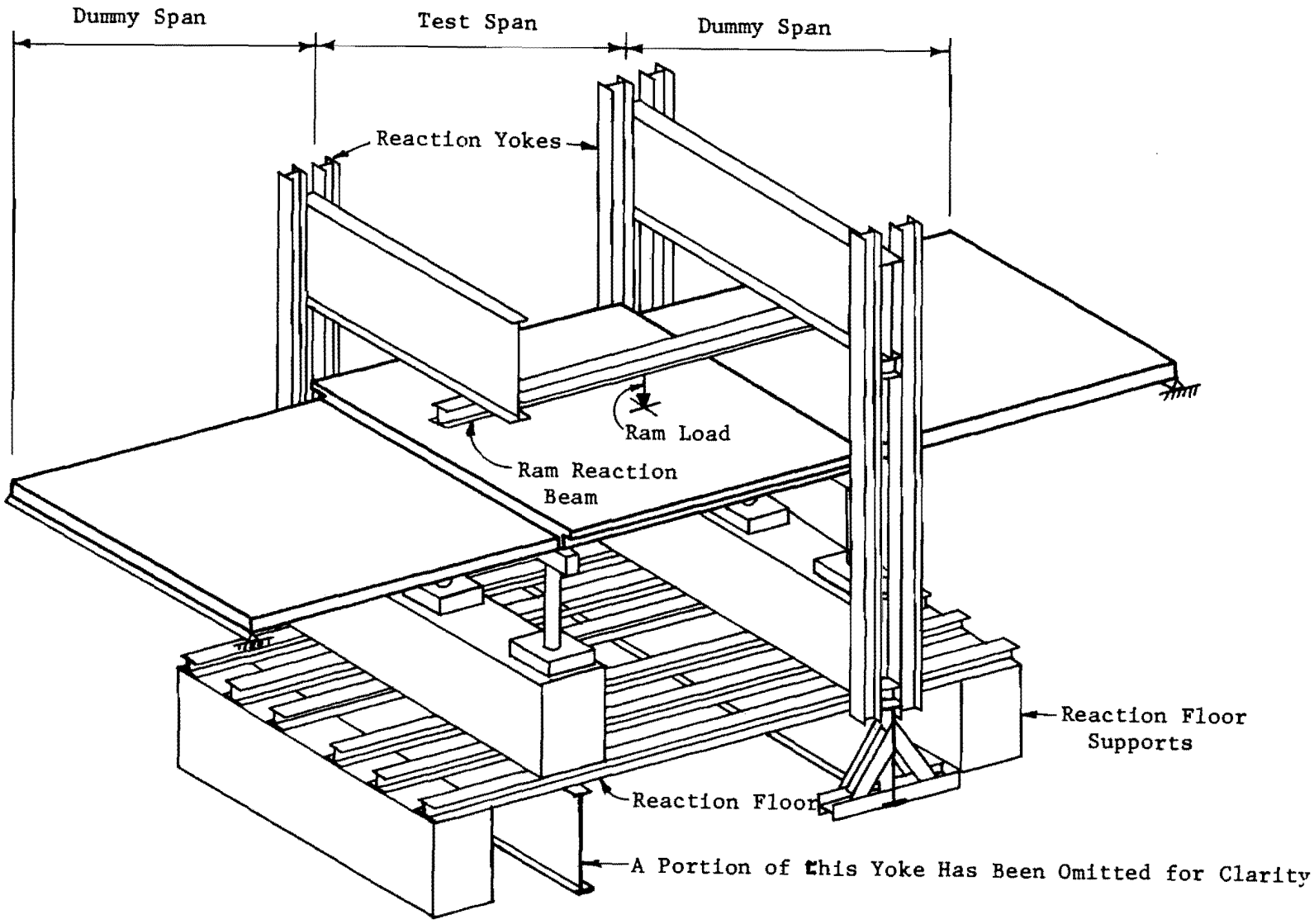

Fig. 3.20. Live Load System.

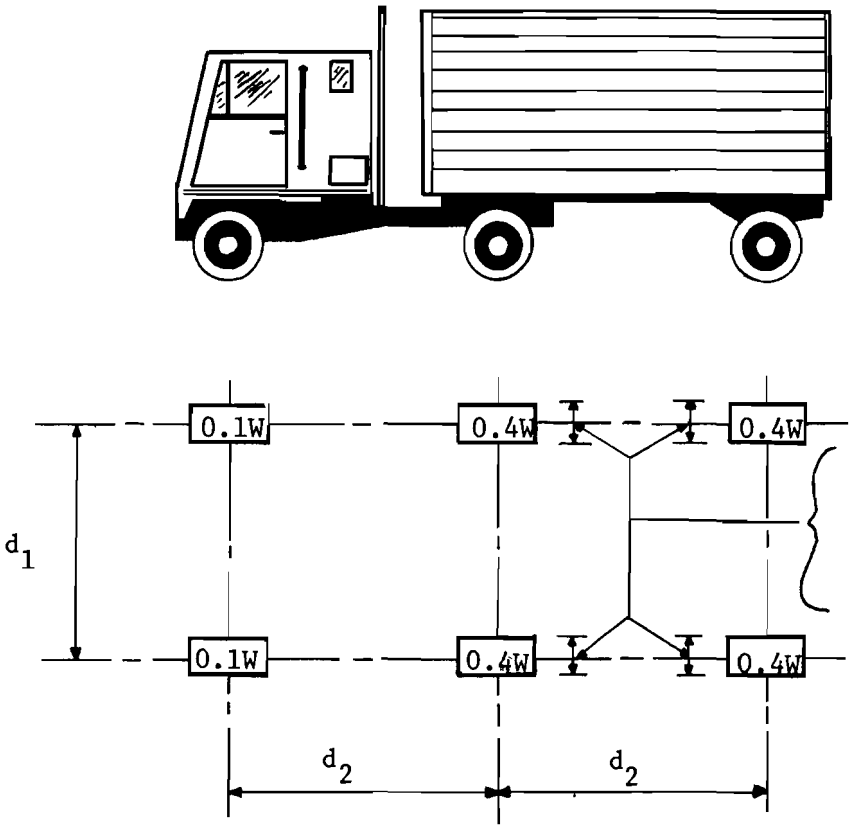

W = Combined Weight on the First Two Axles

Item	Full Size Truck	Model Truck
Truck Type	H20-S16	H20-S16
W, lbs.	40,000	1,322.5
d_1, ft.	6.0	1.091
d_2, ft.	14.0	2.546

Fig. 3.21. Relation between Full Size and Model AASHO H20-S16 Truck.

Single-point loads (equal to one rear wheel from the AASHO truck) were applied by a ram through a loading pad, as illustrated in Fig. 3.22. The dimensions of the loading pad (or "wheel") were determined by using an allowable tire pressure of 80 psi, the total load on the wheel, and a tire width based on the 1965 AASHO specifications[12] as indicated in Fig. 3.21. Axle loads, also shown in Fig. 3.22, were achieved by using a load spreader along with two of the rear tire pads. The rear axle load was equivalent to one rear axle of the AASHO truck. A single AASHO H20-S16 truck loading is also shown in Fig. 3.22. This truck was obtained by using three axles with the front axle load and wheel size reduced as required. Additional truck loads were obtained by adding additional ram reaction beams and axles.

Ultimate loads were carefully selected for each model to yield as much information as possible. These loadings are discussed in a later report.

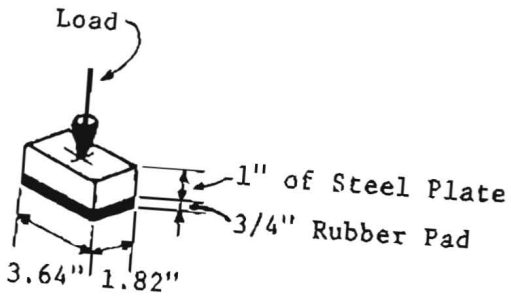

(a) Single Wheel Load.

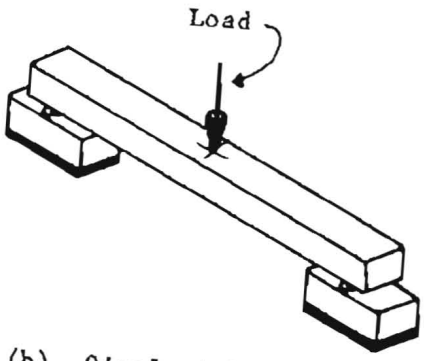

(b) Single Axle Load.

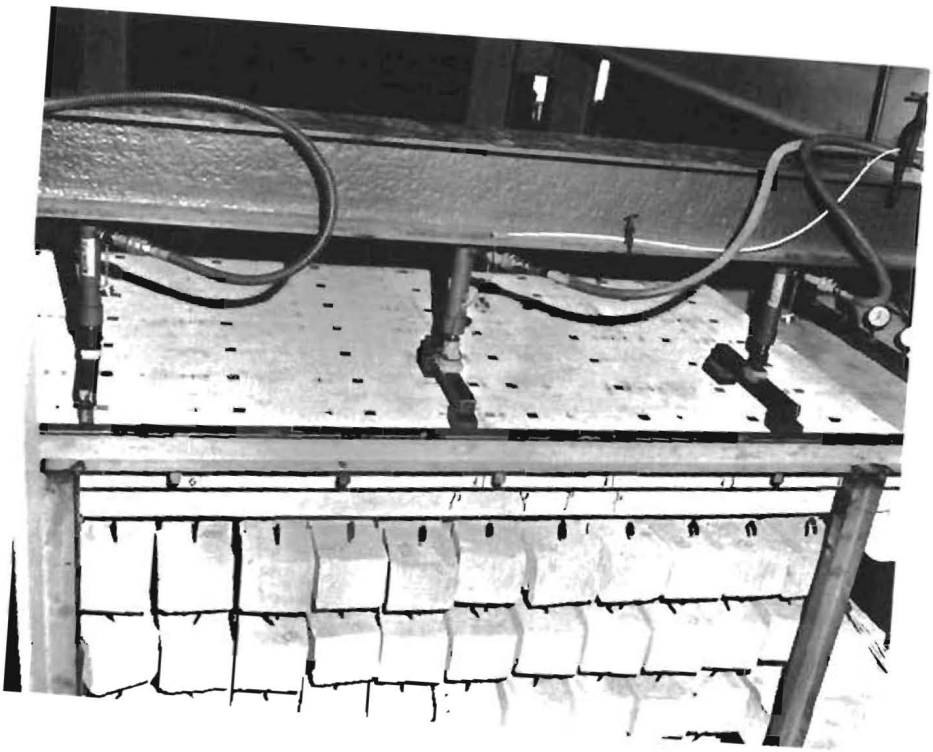

(c) Single AASHO H20-S16 Truck.

Fig. 3.22. Single Wheel, Single Axle, and Single AASHO Truck.

C H A P T E R I V

RELIABILITY

4.1 Introduction

The main objective in the utilization of the direct structural model in this study was to establish the behavioral characteristics of the prototype structure over a wide range of loadings. In order to validate this technique for this type of structure, several studies were r u n to illustrate the credibility and reliability of the techniques utilized.

To assess the general relationship between response characteristics of the model and prototype at service load levels, a prototype bridge being erected on a Central Texas highway was instrumented and load tested at service load levels. A corresponding model was constructed and loaded in the same fashion in the laboratory. A brief comparison of the results is presented in Section 4.2 and indicates good agreement between model and prototype.

Since an ultimate load test of the prototype was not feasible, the accuracy of the model technique at ultimate load levels was established by testing a statically determinate model of a reduced section of the bridge and then comparing the test results to accepted ultimate strength theory. An outline of the results is presented in Section 4.3 and indicates excellent agreement.

4.2 Comparison at Service Load Levels

A prototype bridge, CG-1, and its corresponding model, SG-4, were tested at service load levels (additional loads were placed on the model in keeping with the rest of the model program). The structure had a skew of 26^{o}-34'. The model substructure was an accurate model

of the prototype substructure. Detailed test data are reported in References 13 and 14.

Loading consisted of single, double, and triple truck loads placed on the bridges. The test vehicles were dump trucks with a ten cu. yd. capacity. These trucks were loaded with sand until their total weight was equal to that of the standard AASHO H20 design truck. The major difference between the design vehicle and those actually used was the distribution of the rear axle load, as shown in Fig. 4.1. The H20 design vehicle assumes a single rear axle, while the actual vehicle had two closely spaced rear axles. The two rear axles of the test vehicle carried the same total load as the single rear axle of the H20 truck. The loading applied to the model was a scale representation of the actual vehicles used and not the H20 design vehicle.

In both prototype and model tests corresponding deflections and steel strains were measured, although the strain readings made up the bulk of the data. Prototype deflection measurements were erratic, due to high winds at the test site which interfered with the measuring system.

Typical midspan strain measurements are presented in Figs. 4.2 through 4.7 for two different locations of a single truck, two different locations of double trucks, and one location of triple trucks. In each of these figures axle No. 2 of the test vehicle was placed at midspan. All plots compare the model and prototype data for trucks placed at corresponding locations on the model and prototype structures.

Data are presented in two forms in each figure. The lower plots show the actual strains observed. The upper plots show the strain distribution as a percent of the total midspan strain observed. Because of the relatively low magnitude of the strains, the upper plot based on percent of total midspan strain is probably the better measure of the pattern of load distribution to the individual girders of the cross section.

Strain measurements are in reasonable agreement for the model and prototype under both single and double truck loads. However, the

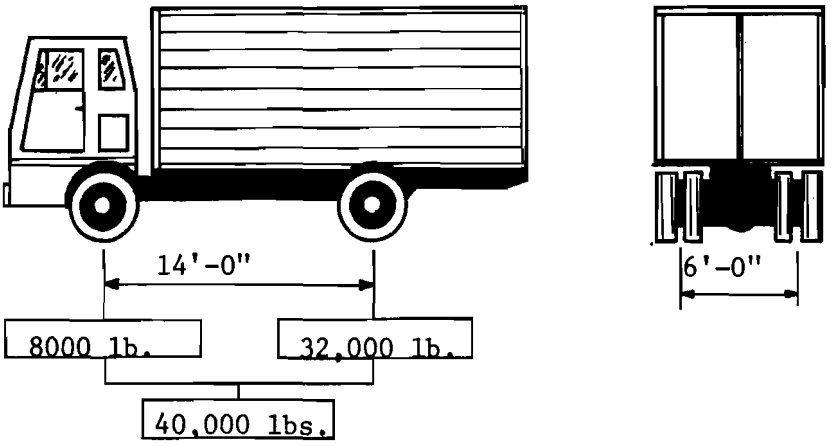

(a) AASHO H20 Design Vehicle.

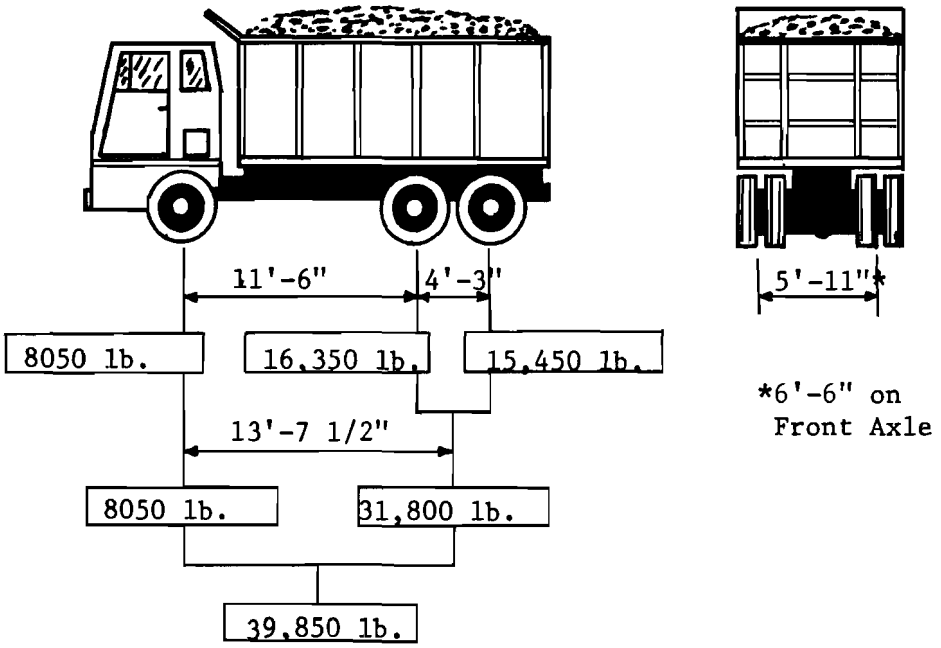

(b) Typical Test Vehicle.

Fig. 4.1. Comparison of AASHO H20 Design Vehicle and Test Vehicle.

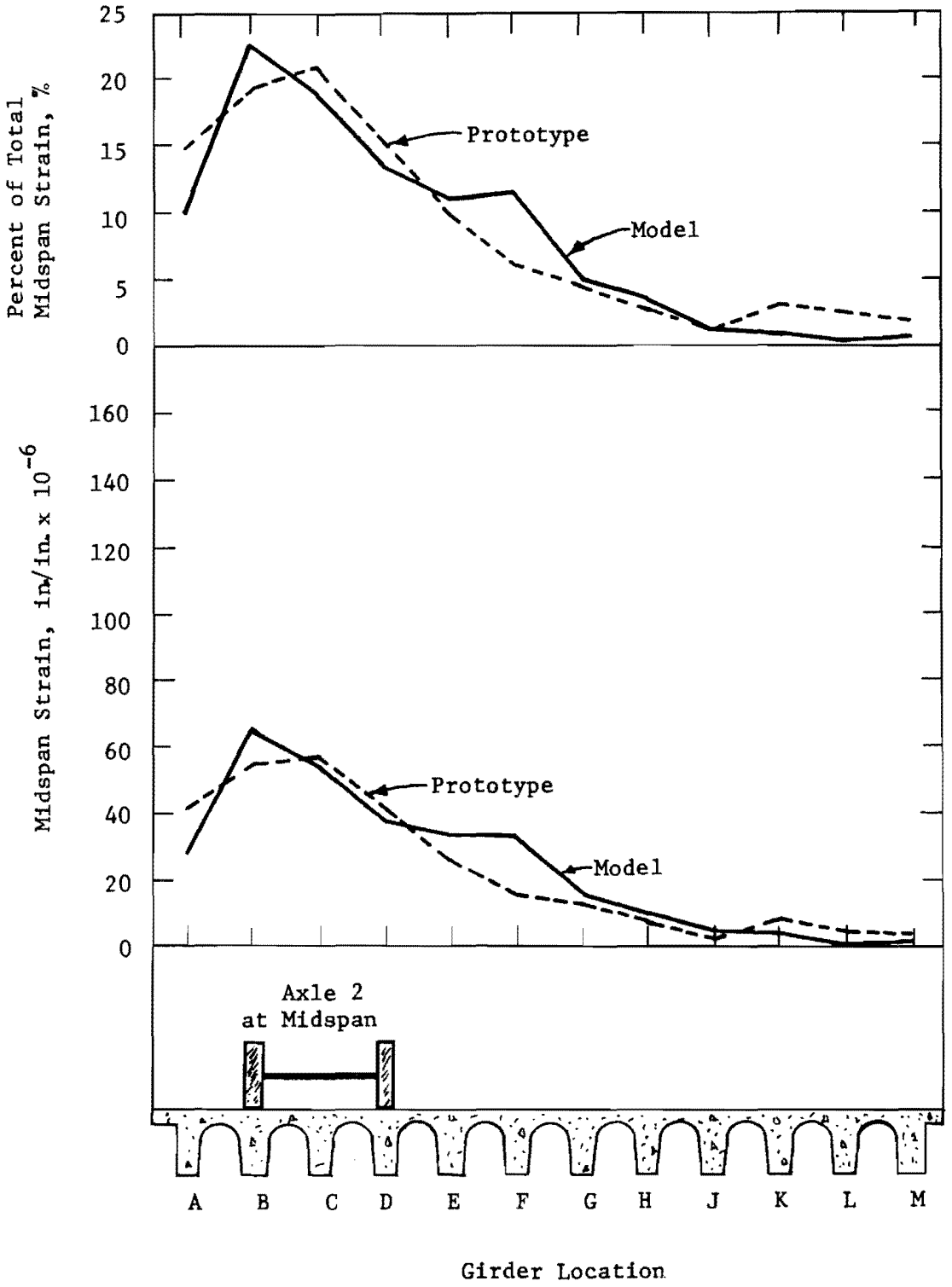

Fig. 4.2. Strain Data for One Truck on Exterior Girders.

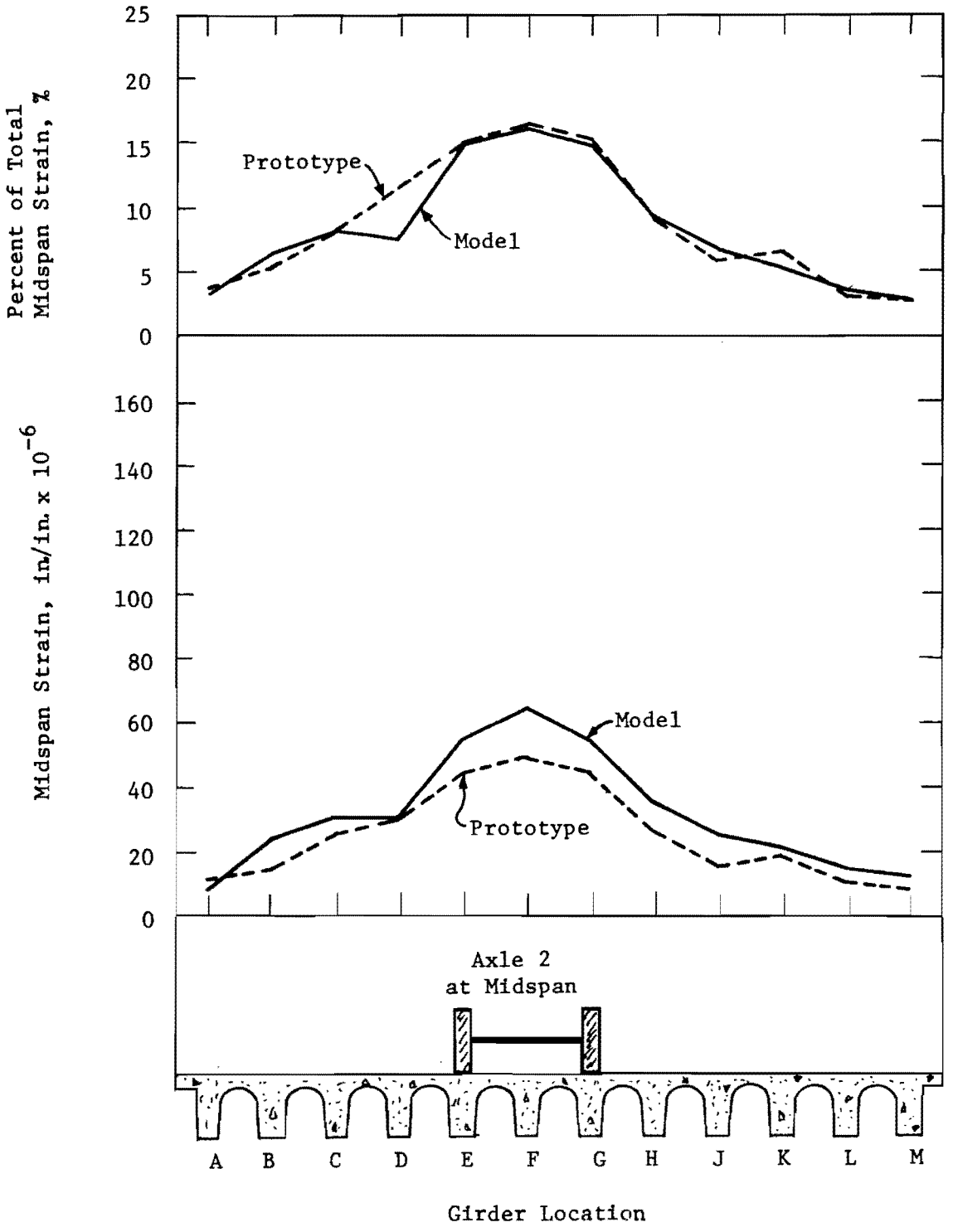

Fig. 4.3. Strain Data for One Truck on Interior Girders.

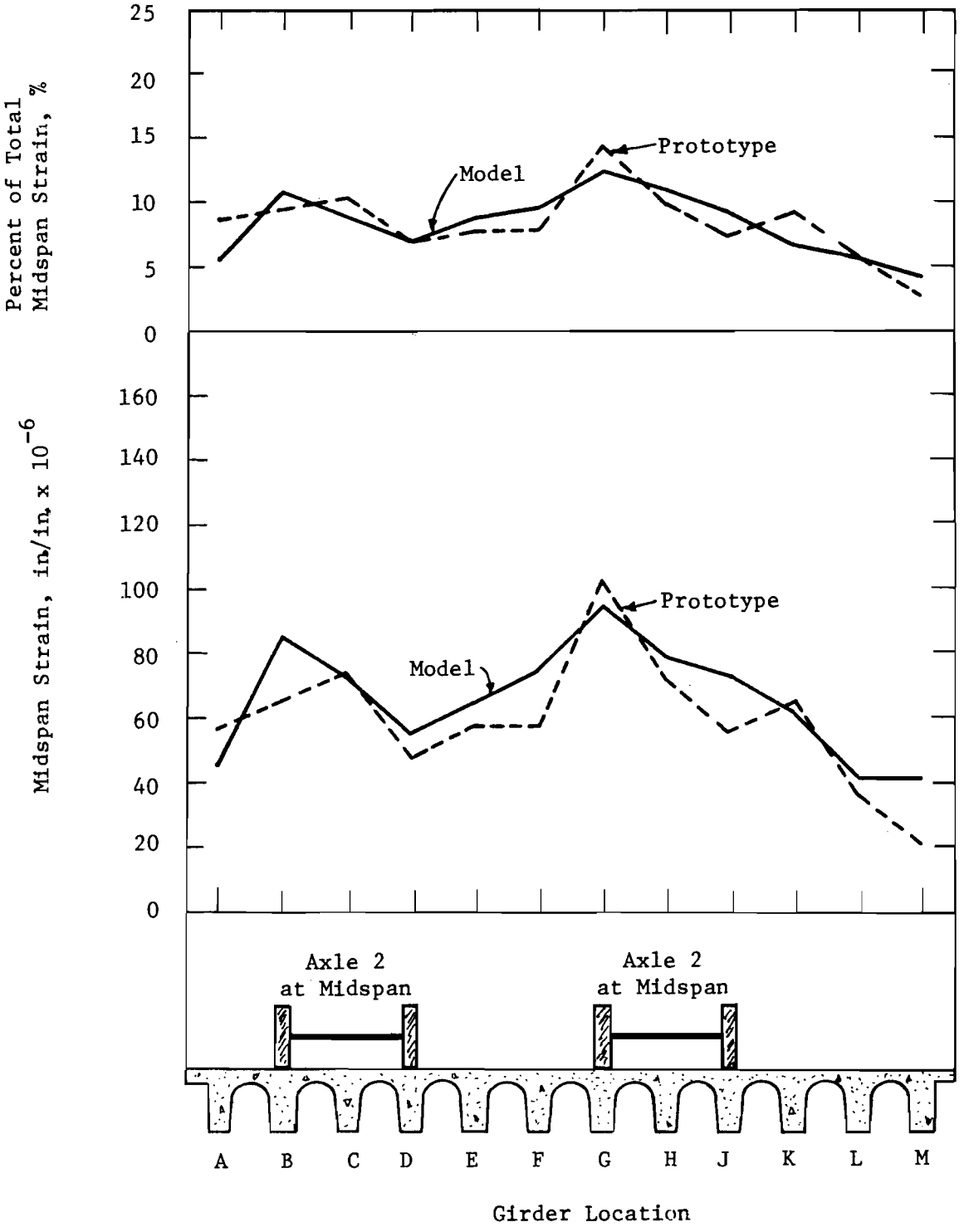

Fig. 4.4. Strain Data for Two Trucks Spaced Apart.

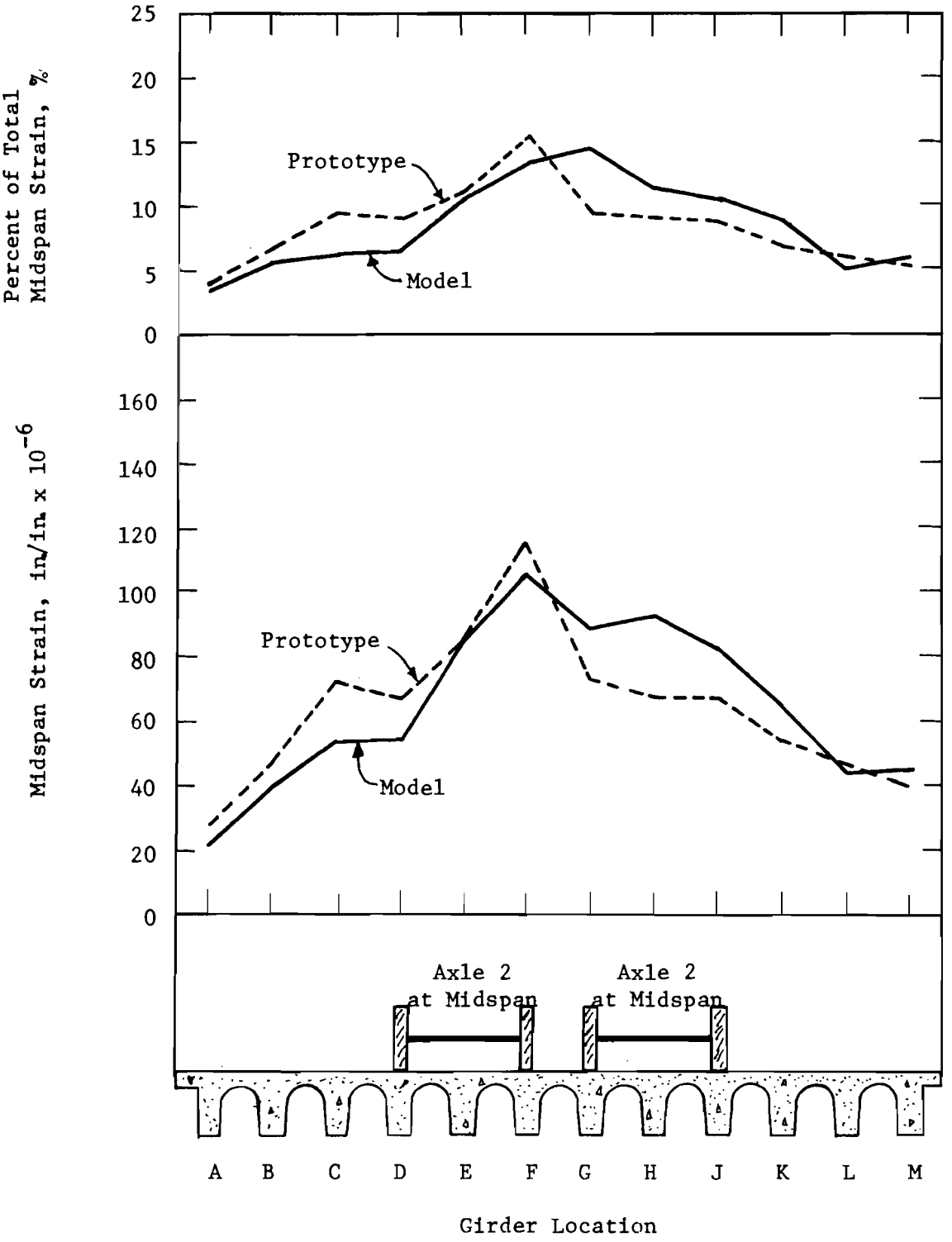

Fig. 4.5. Strain Data for Two Trucks Spaced Close Together.

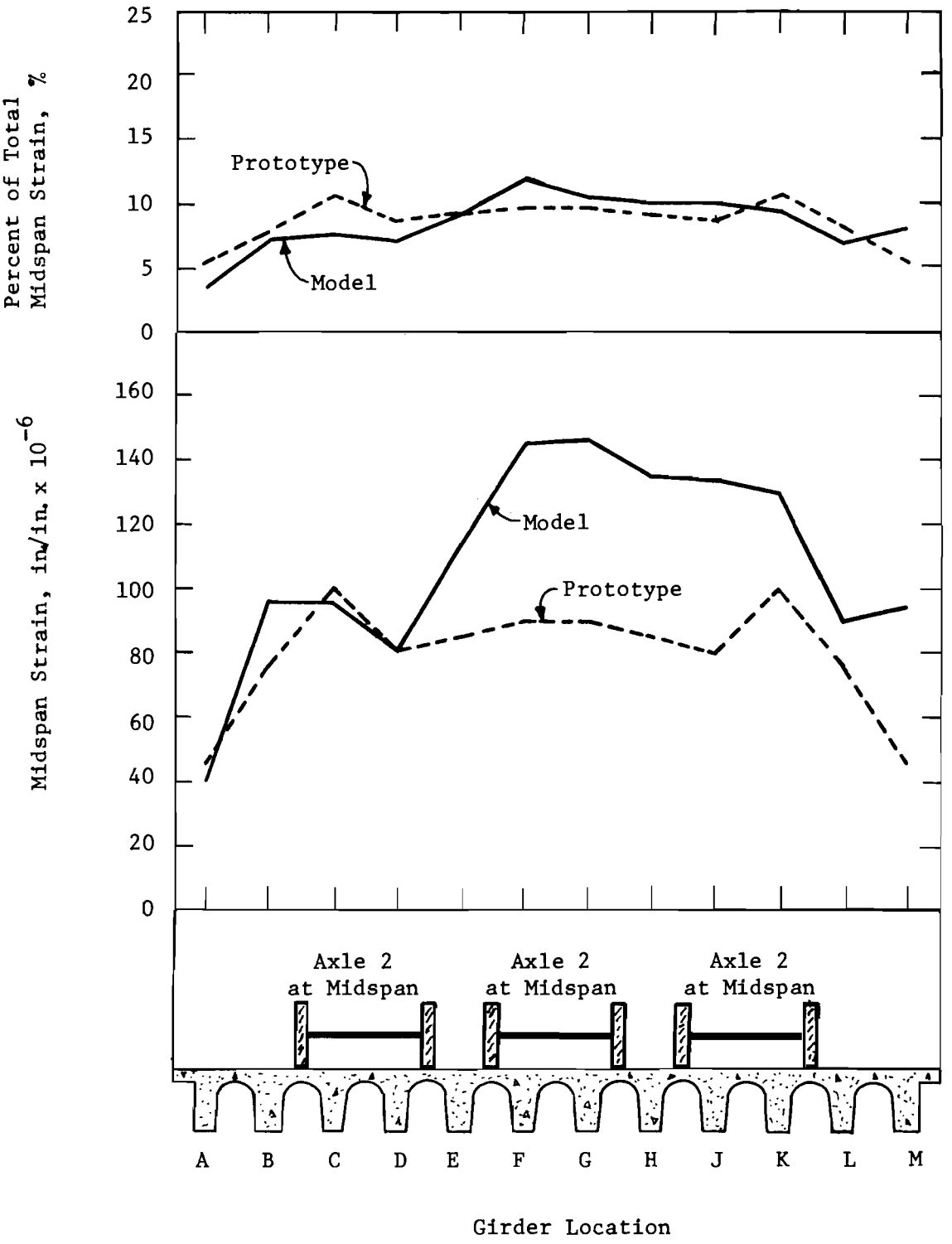

Fig. 4.6. Strain Data for Three Trucks.

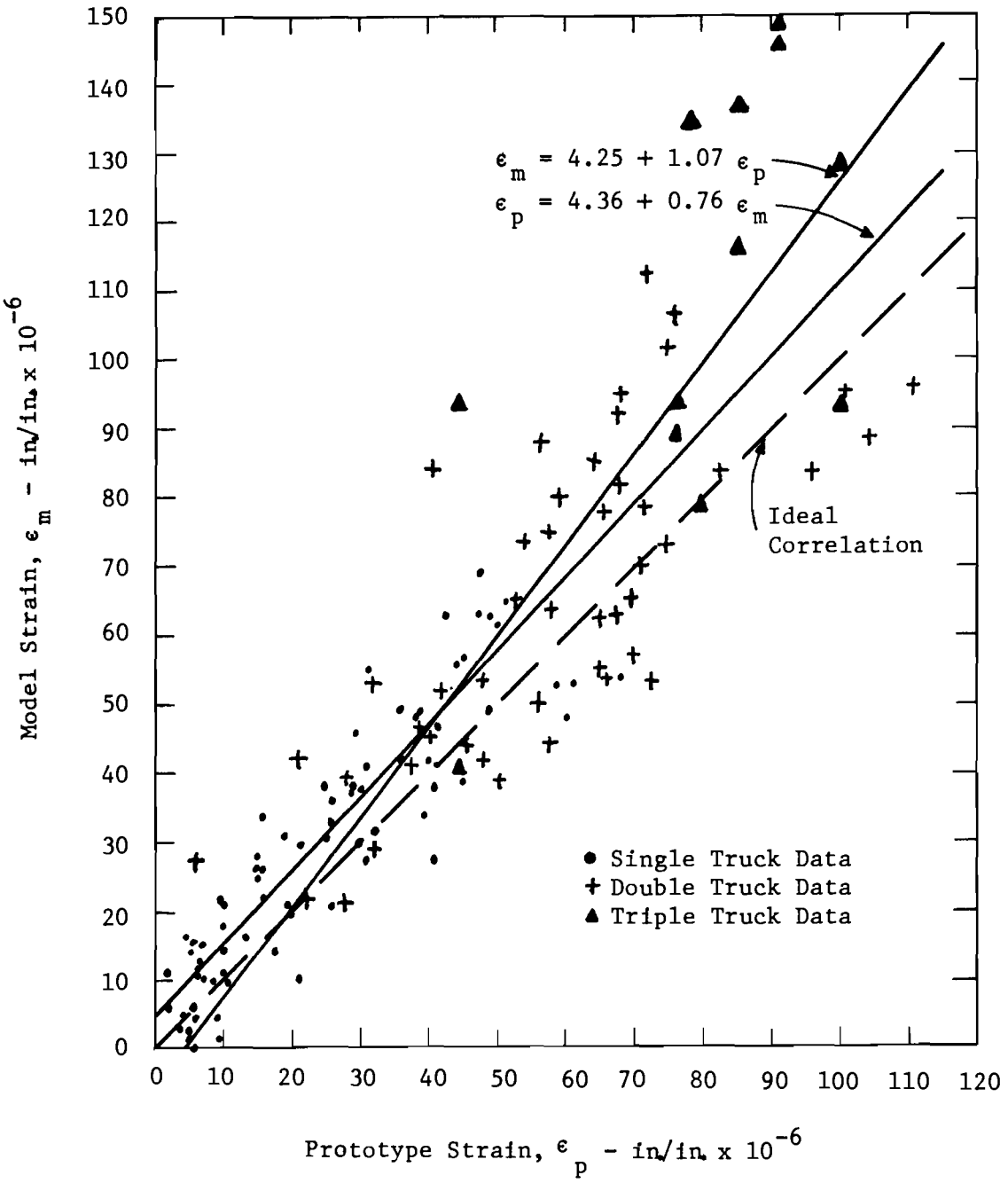

Fig. 4.7. Summary of Model and Prototype Data with Regression Analysis.

model and prototype strains for the triple truck loading differ by relatively large amounts. In most cases the plots based on percent of total observed strain show increased agreement between model and prototype data. This is particularly evident in Figs. 4.3, 4.4, and 4.6.

Midspan strain data have been plotted for twelve widely differing load cases in Fig. 4.7. Each datum point indicates the model strain for a particular location and load versus the prototype strain for the corresponding location and loading. Ideally, these data should fall along the dashed 45^{o} line if perfect similitude was obtained. Two equations are presented on Fig. 4.7 showing the model strain as a function of the prototype strain and vice versa. These regression equations were obtained by applying least squares curve fitting procedure to the data shown. The equations and data show less than a perfect relation between the two structures. The coefficient of linear correlation[15] for the data shown is 0.90. This coefficient is a measure of the linear relation between the model and prototype data. The coefficient varies from -1.0 for negative correlation to 0.0 for no correlation, to 1.0 for perfect correlation. A coefficient of 0.90 indicates relatively good linear correlation.

Certain differences are to be expected between the behavior of the two bridges, due to their history of loading. Due to a tight testing schedule, the model had been subjected to an extensive loading program before the double and triple truck loadings were run. In contrast, the prototype bridge was subjected to very limited loading, other than the test vehicles, since it was not officially open to traffic. This probably caused somewhat different cracking states in the model and prototype, with the model being cracked somewhat more severely due to a more extensive loading history. Examination of model data indicates that girders G through M were cracked early in the loading sequence, while girders A through F were not as severely cracked. This is believed to be a major reason for the large differences in absolute strain values indicated in Fig. 4.6 for the triple

truck loading. However, it should be noted that this does not affect the percentage distribution results to the same degree.

Overall examination of these results indicates that the model technique gives a very reasonable indication of the service load level participation of each girder and can be used to determine overall loading trends in this type of a bridge system.

4.3 Ultimate Strength Reliability

Two statically determinate models of reduced sections of the bridge, consisting of two scaled girders as shown in Fig. 4.8, were tested to failure. The beams were identical except for the main flexural reinforcement properties. Nondeformed No. 2 bars with a yield point of 47.8 ksi were used as the main flexural reinforcement in MSG-1. Deformed No. 2 bars with a yield point of 57.3 ksi were used in MSG-2.

Instrumentation consisted of reinforcement strain gages and dial gages at midspan. Loading consisted of uniformly distributed blocks for dead load compensation, plus two equal concentrated loads at midspan (one load directly over the centerline of each girder). Material properties and beam dimensions are shown in Fig. 4.8, along with the loading.

Relationships between midspan applied moment and observed midspan strains are shown in Fig. 4.9(a). Corresponding moments versus deflection plots are shown in Fig. 4.9(b). Both specimens failed by first indicating yielding of the main flexural reinforcement, with concrete crushing occurring after extensive deflection. Computed ultimate moments, based on conventional ultimate strength theory, are also shown on these figures. The ratio of test to calculated ultimate moment was 0.998 and 0.985, for MSG-1 and MSG-2, respectively. The excellent agreement in these two tests established confidence in the loading system, instrumentation, and modeling techniques.

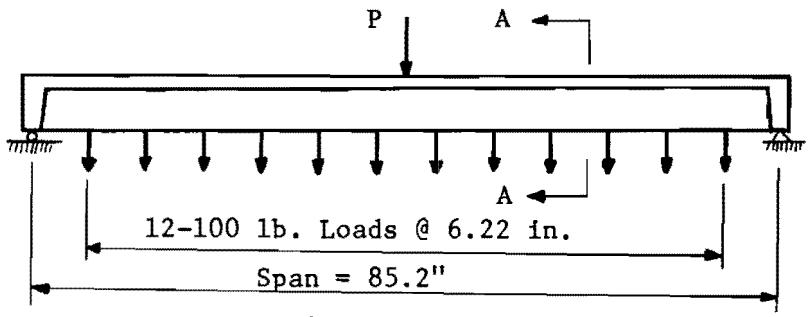

Elevation

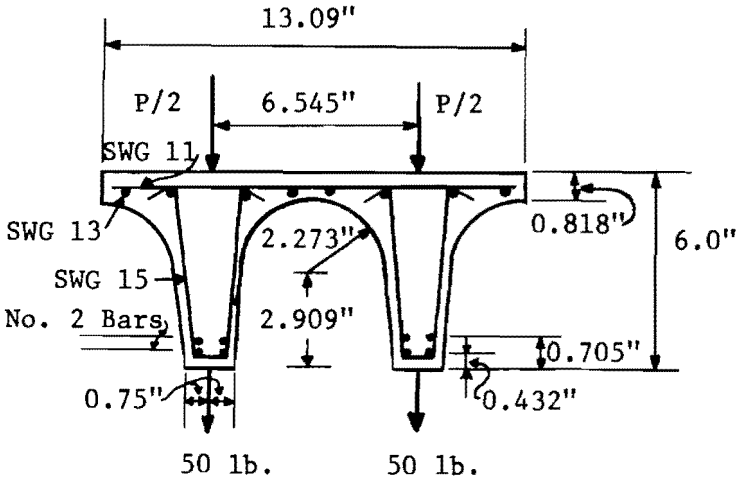

Section A-A

Material Properties								
	MSG-1				MSG-2			
Rein-forcement	No. 2 Smooth	SWG 11 Smooth	SWG 13 Smooth	SWG 15 Smooth	No. 2 Deformed	SWG 11 Smooth	SWG 13 Smooth	SWG 15 Smooth
f_y, ksi	47.8	39.5	37.3	31.9	57.3	39.5	37.3	31.9
f_u, ksi	64.5	48.0	47.1	42.0	76.5	48.0	47.1	42.0
f'_c, psi	3210				4670			

Fig. 4.8. Cross Section and Properties for MSG Series.

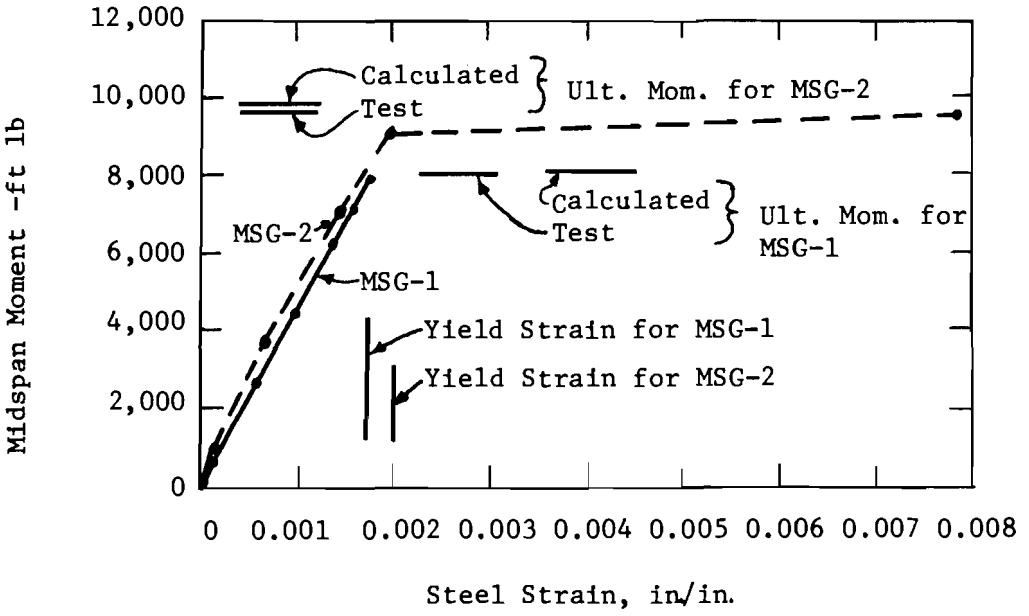

(a) Midspan Moment vs. Midspan Steel Strain.

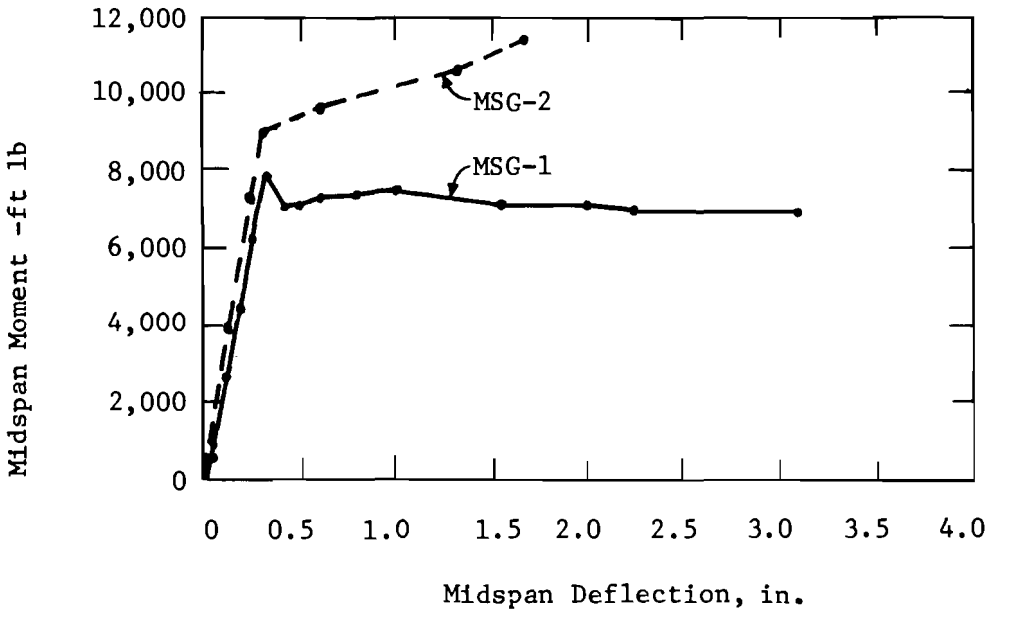

(b) Midspan Moment vs. Midspan Deflection.

Fig. 4.9. Behavior of Beams MSG-1 and MSG-2.

CHAPTER V

CONCLUSIONS AND RECOMMENDATIONS

5.1 Conclusions

The overall research project is a study of the behavior of pan-formed concrete slab and girder bridges. The technology used to fabricate, test, and interpret results of the primary research tool used, the direct structural model, has been covered in detail.

Although the objectives of this report were limited in scope, and the investigation was restricted to a particular bridge system, the following conclusions are warranted:

(1) Fabrication, loading, and instrumentation techniques were developed to realistically model standard Texas Highway Department pan-formed slab and girder bridge spans.

(2) Models of this type may be used to reliably measure load distribution (as indicated by girder longitudinal strain) at service load conditions. This conclusion is based on the comparison of model and prototype midspan strain distributions shown in Figs. 4.2 through 4.7. The patterns of strain distribution are of similar shape with similar magnitudes of strain. The midspan load distributions based on percent of total midspan strain indicate better agreement than the absolute strain values.

(3) The model sections loaded under statically determinate conditions displayed excellent correlation with predicted ultimate strengths and mode of failure. The ratios of observed to calculated ultimate strength were 0.998 and 0.985. Their modes of failure were flexural, with initial

yielding of steel and secondary compression of the concrete. This is the general mode of failure of all specimens in the main investigative series.

5.2 Recommendations

5.2.1 Microconcrete.--Studies indicated that microconcrete is superior to concrete substitutes such as gypsum for use in a structural model of a reinforced concrete structure. Although no comparisons of materials were documented in this report, this conclusions was reached in the early study phase based on literature surveys and discussions. The microconcrete model has been shown to give reliable results at both ultimate load and service load levels. While many of the concrete substitutes give good results at service loads, they generally give less reliable results at ultimate load. This is probably due to the lack of adequate matching of basic failure criteria for concrete. It seems reasonable to assume that if the failure mode of a structure is not known, then it should be modeled with a material with as similar material properties as possible.

Although some concrete substitutes have been recommended because their use may result in faster test times, experience with this program indicates that time required for instrumentation and loading preparations is quite compatible with curing times using Type III cements.

B I B L I O G R A P H Y

1. Guralnick, S. A., and La Fraugh, R. W. "Laboratory Study of a 45-foot Square Flat Plate Structure," Journal of the American Concrete Institute, September 1963, Proc. Vol. 60.

2. Hatcher, D. S., Sozen, M. A., and Siess, C. P. "A Study of Tests on a Flat Plate and a Flat Slab," Structural Research Series #217, Civil Engineering Studies, University of Illinois, July 1961.

3. Lee, S. T. "Small Models of a Multipanel Flat Plate Structure," unpublished Master's thesis, M.I.T., March 1960.

4. Harris, H. G., Sabnis, G. M., and White, R. N. "Small Scale Direct Models of Reinforced and Prestressed Concrete Structures," Report No. 326, Department of Structural Engineering, Cornell University, September 1966.

5. Aldridge, W. W. "Ultimate Strength Tests of Model Reinforced Concrete Folded Plate Structures," unpublished Ph.D. dissertation, The University of Texas, 1966.

6. Pahl, P. J., Soosaar, K., and Hansen, R. J. "Structural Models for Architectural and Engineering Education," R64-3, Department of Civil Engineering, M.I.T., February 1964.

7. Somerville, G., Roll, F., and Caldwell, J. A. D. "Tests on a One-twelfth Scale Model of the Mancunian Way," Technical Report TRA/394, Cement and Concrete Association (London), December 1965.

8. Texas Highway Department. Standard Specification for Road and Bridge Construction (1962), with Item 421, "Concrete for Structures (Natural Aggregate)," amended by "Special Provision to Item 421," issued September 1965.

9. American Concrete Institute. Building Code Requirements for Reinforced Concrete (ACI-318), Detroit, Michigan, June 1963.

10. Breen, J. E. "Fabrication and Tests of Structural Models," Journal of the Structural Division, American Society of Civil Engineers, Vol. 94, ST6, Proc. Paper 5989.

11. Lee, C. E. "A Portable Electronic Scale for Weighing Vehicles in Motion," Paper prepared for presentation at the 45th Annual Meeting of the Highway Research Board, January 17-21, 1966.

12. American Association of State Highway Officials. Standard Specifications for Highway Bridges, Ninth Edition, 1965.

13. Leyendecker, E. V., Armstrong, T. A., and Breen, J. E. "Field Testing of Concrete Slab and Girder Bridges," Research Report 94-2, Center for Highway Research, The University of Texas at Austin, September 1968.

14. Leyendecker, E. V., and Breen, J. E. "Behavior of Concrete Slab and Girder Bridges," Research Report 94-3F, Center for Highway Research, The University of Texas at Austin, September 1968.

15. Spiegel, M. R. Theory and Problem of Statistics. Schaum's Outline Series. New York: McGraw-Hill Book Company, 1961.

A P P E N D I X A

PROTOTYPE BRIDGE PLANS

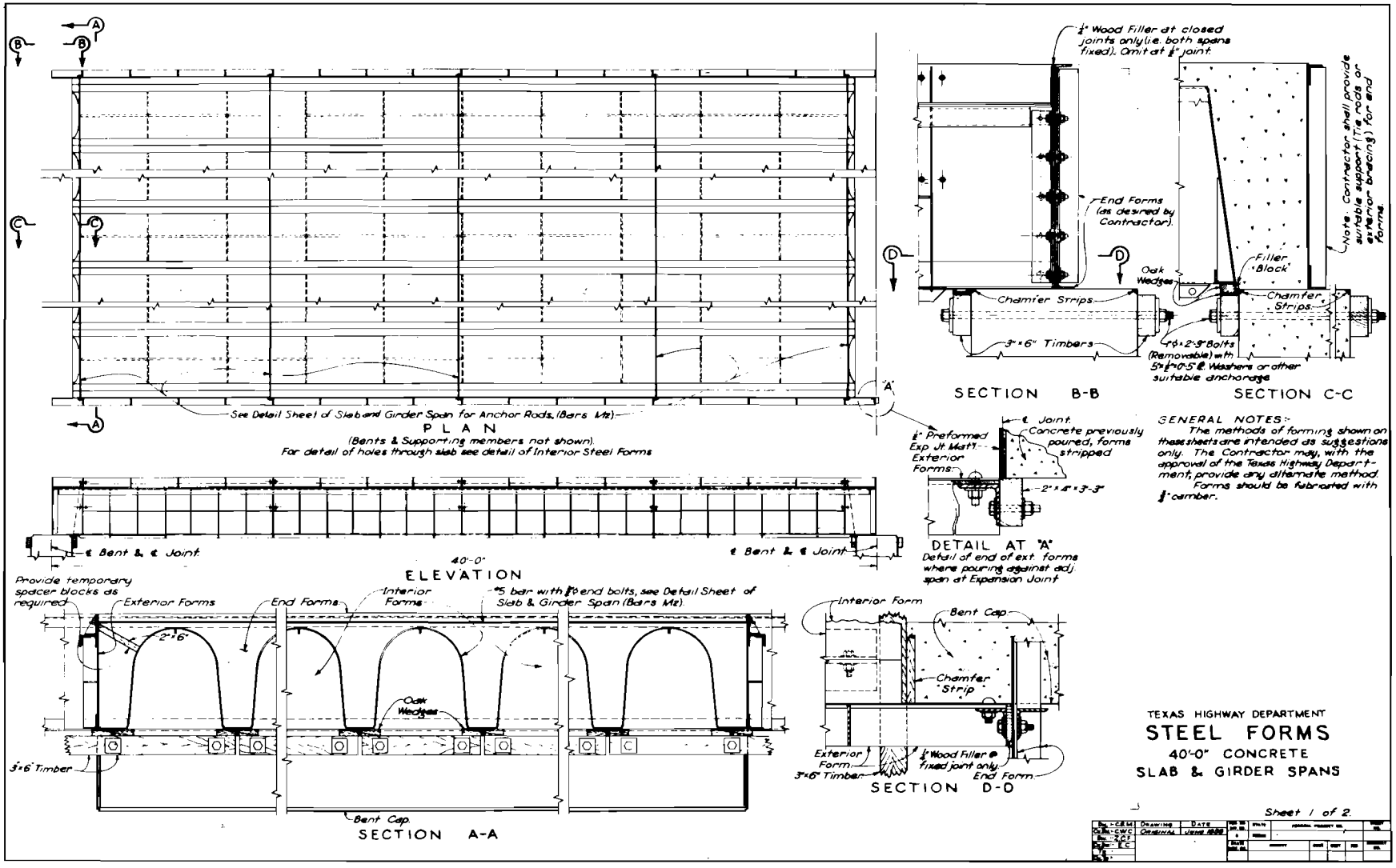

Fig. A.1. Steel Forms for 40'-0" Slab and Girder Spans, Sheet 1 of 2.

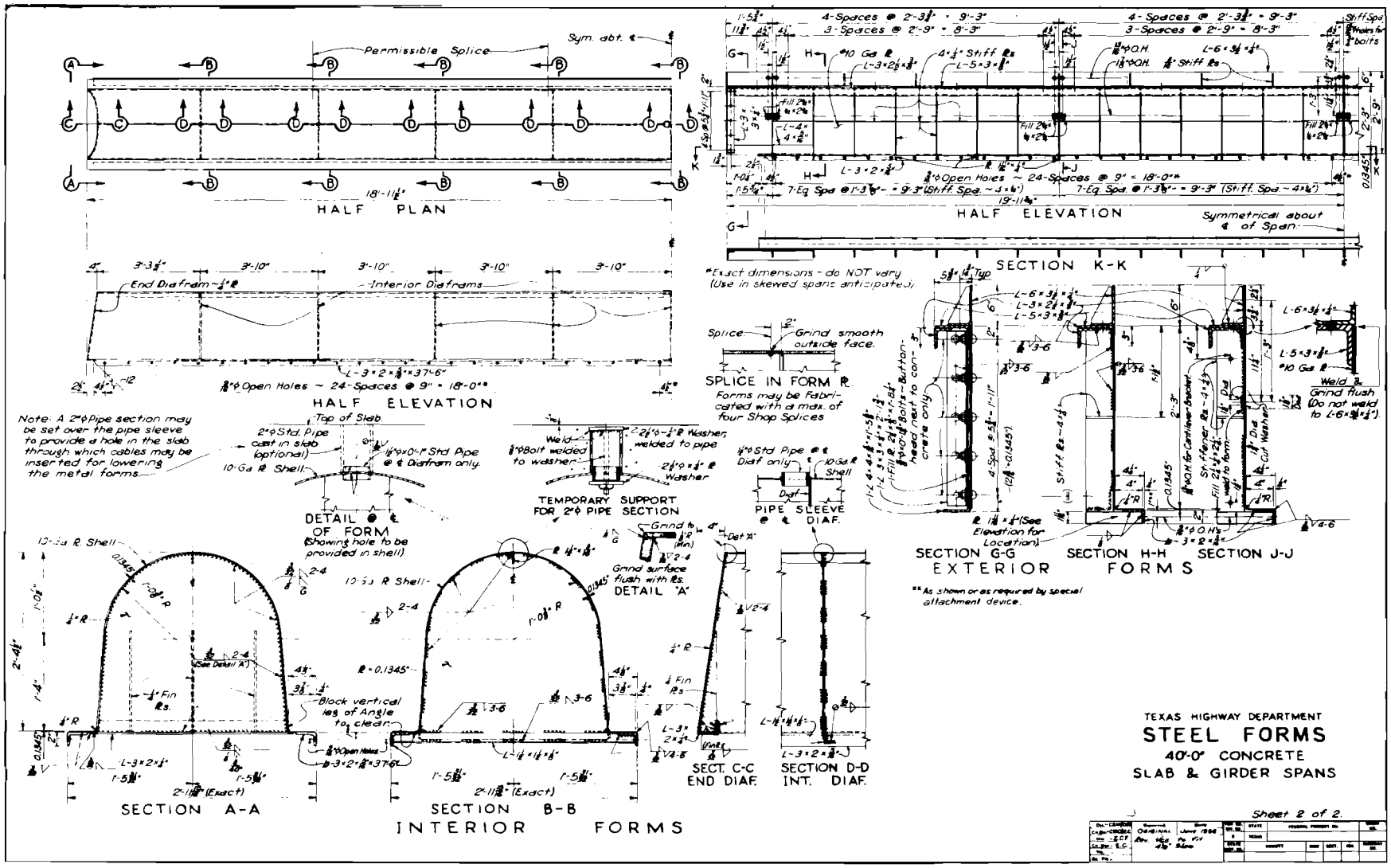

Fig. A.2. Steel Forms for 40'-0" Slab and Girder Spans, Sheet 2 of 2.

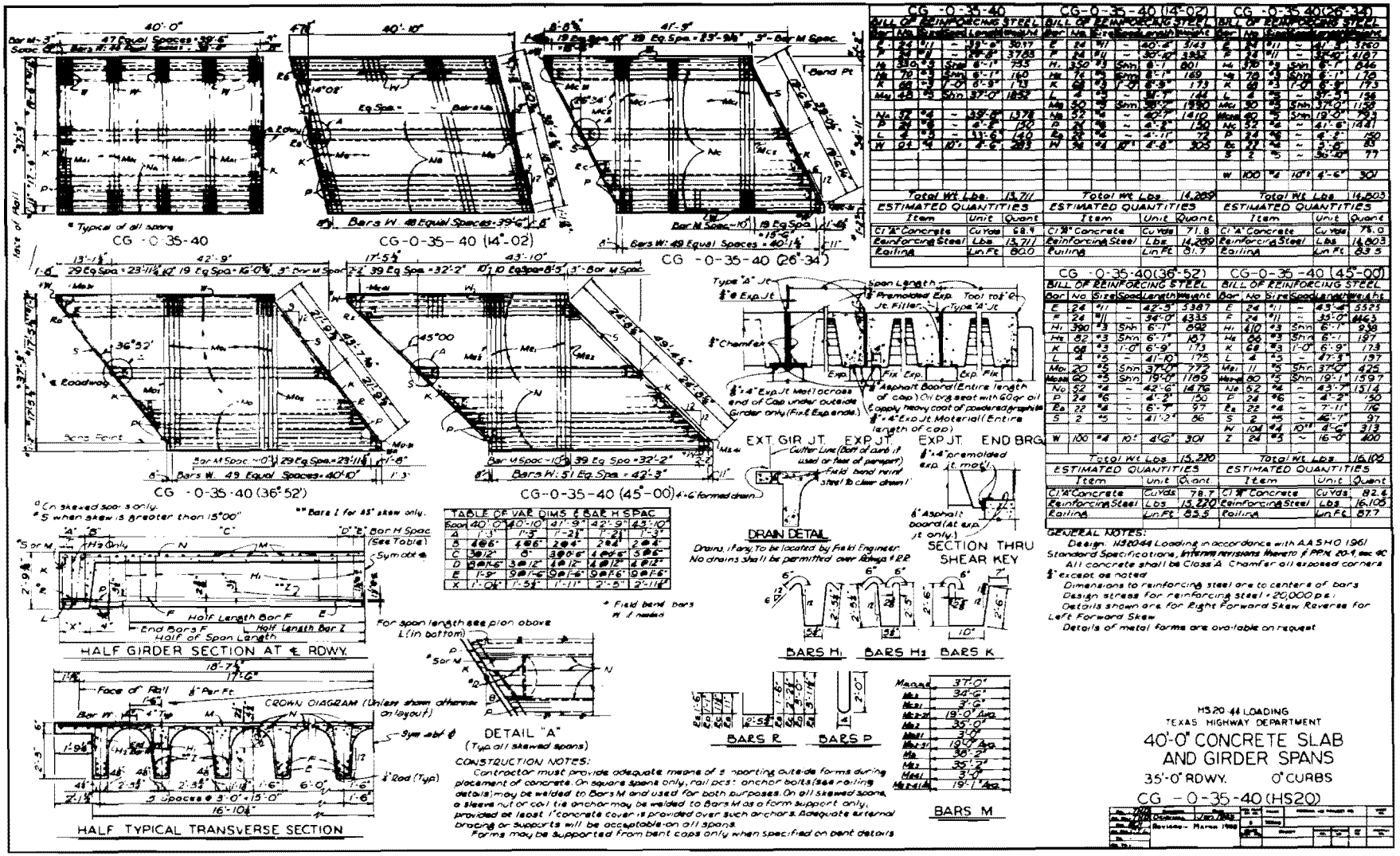

Fig. A.3. Texas Highway Department Plan Sheet, CG-0-35-40.

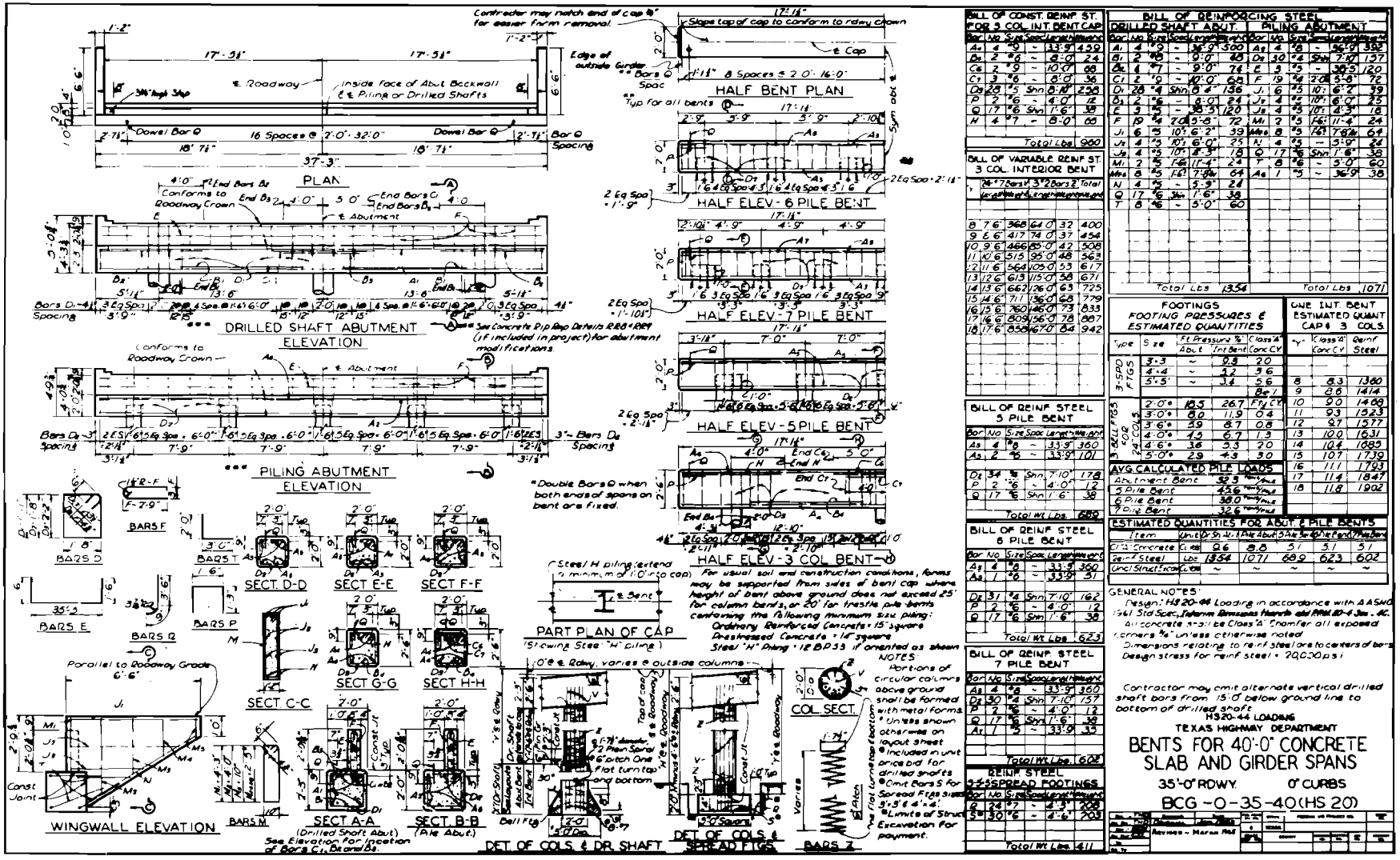

Fig. A.4. Texas Highway Department Plan Sheet, BCG-0-35-40.

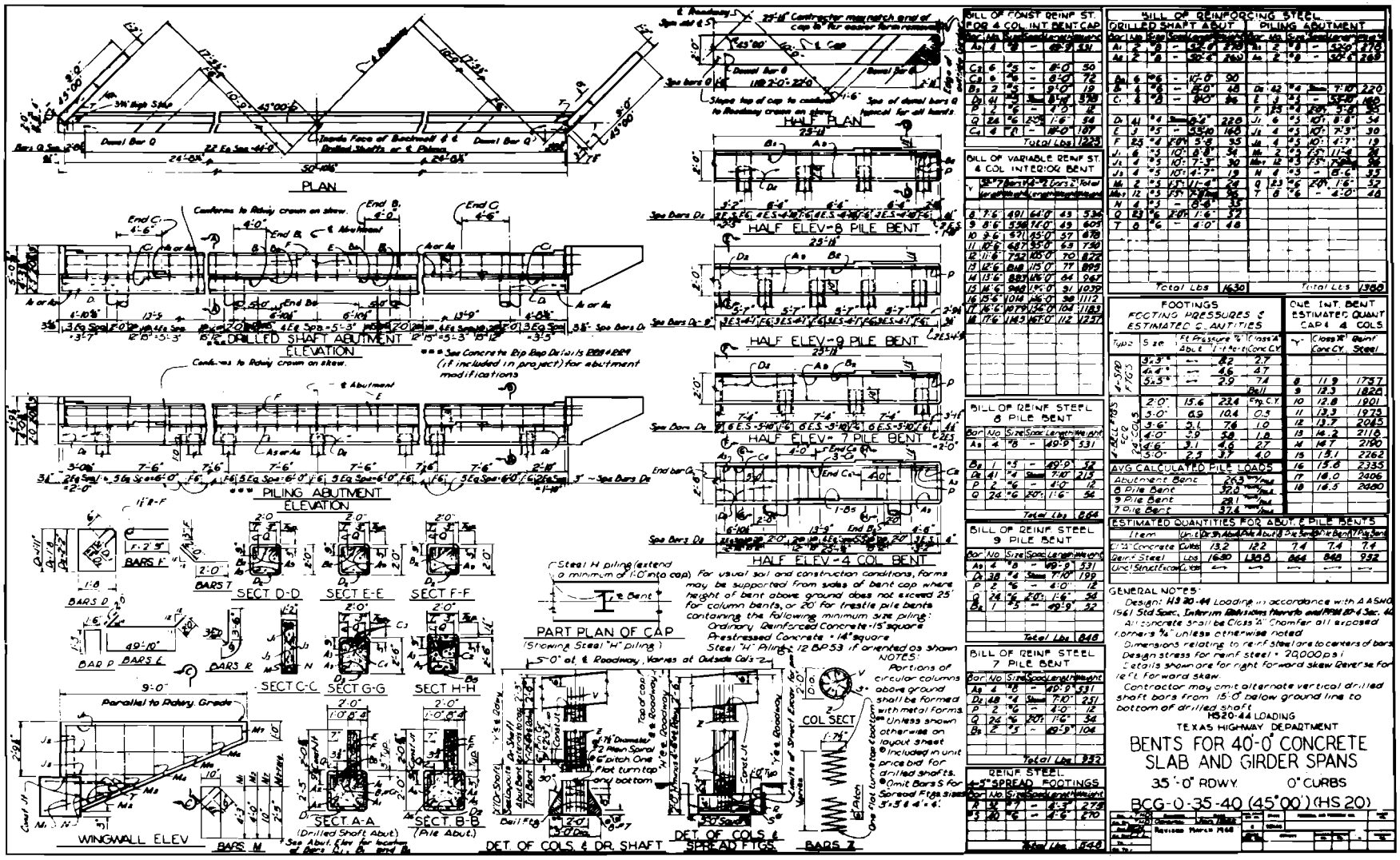

Fig. A.5. Texas Highway Department Plan Sheet, BCG-0-35-40 (45°-00').

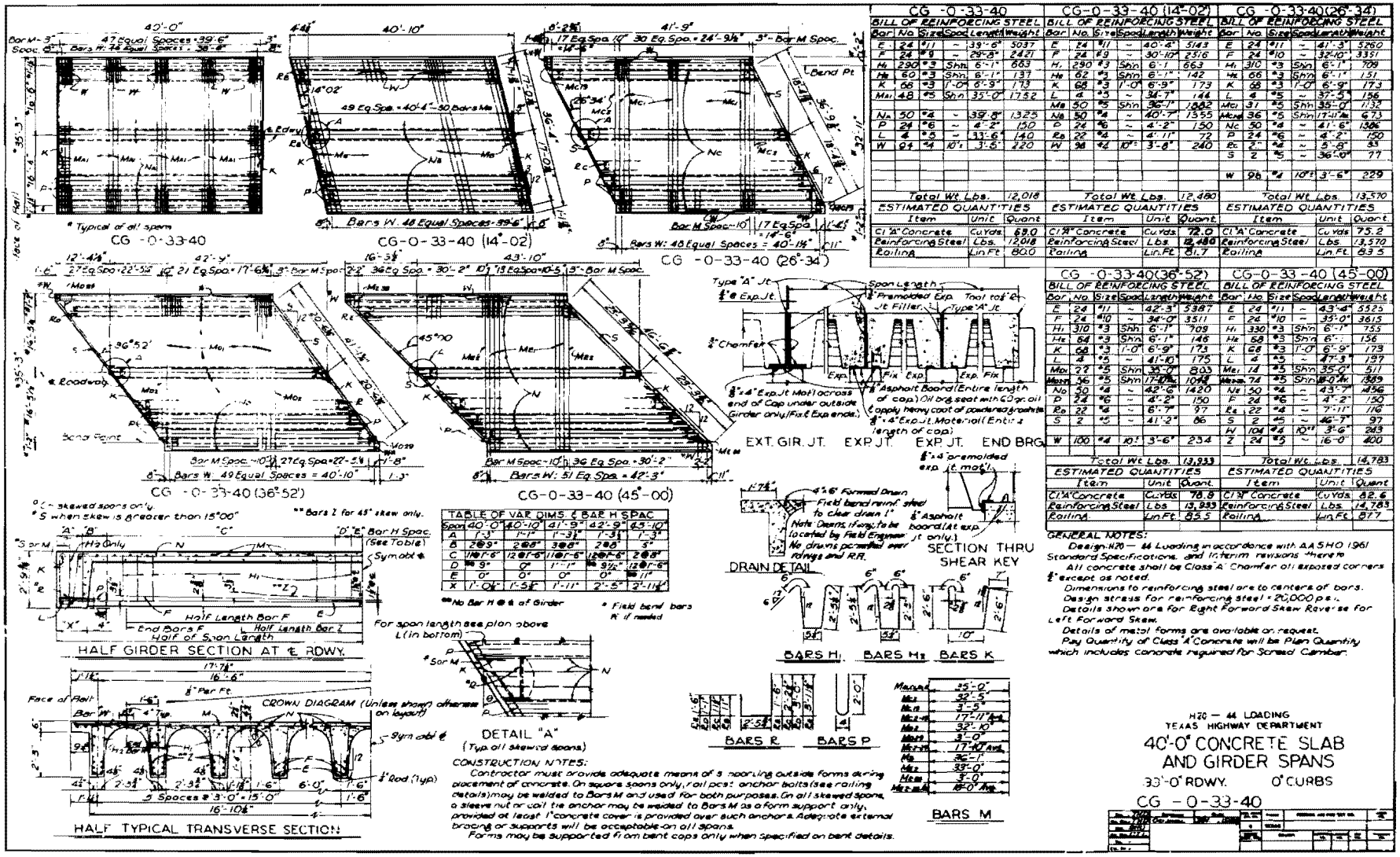

CG -0-33-40 BILL OF REINFORCING STEEL						
Bar	No.	Size	Spac'g	Length	Weight	
E	24	#11	~	39'-6"	5037	
F	24	#9	~	38'-8"	2421	
H1	290	#3	Shn	6'-1"	553	
H2	60	#3	Shn	6'-1"	137	
K	56	#3	1'-0"	6'-9"	173	
Ma1	48	#5	Shn	35'-0"	1752	
Na	50	#4	~	39'-8"	1323	
P	24	#6	~	4'-2"	150	
L	4	#5	~	33'-6"	140	
W	94	#4	10"	3'-8"	220	
Total Wt. Lbs.					12,018	
ESTIMATED QUANTITIES						
Item			Unit		Quant	
Cl "A" Concrete			Cu.Yds.		68.0	
Reinforcing Steel			Lbs.		12,018	
Railing			Lin.Ft.		80.0	

CG -0-33-40 (14°-02') BILL OF REINFORCING STEEL						
Bar	No.	Size	Spac'g	Length	Weight	
E	24	#11	~	40'-4"	5143	
F	24	#9	~	30'-10"	2516	
H1	290	#3	Shn	6'-1"	553	
H2	60	#3	Shn	6'-1"	137	
K	68	#3	1'-0"	6'-9"	173	
L	4	#5	~	34'-7"	144	
Ma	50	#5	Shn	36'-1"	1882	
Na	50	#4	~	40'-7"	1355	
D	24	#6	~	4'-2"	150	
Ec	22	#4	~	4'-11"	72	
W	98	#4	10"	3'-8"	240	
Total Wt. Lbs.					12,480	
ESTIMATED QUANTITIES						
Item			Unit		Quant.	
Cl "A" Concrete			Cu.Yds.		72.0	
Reinforcing Steel			Lbs.		12,480	
Railing			Lin.Ft.		81.7	

CG -0-33-40 (26°-34') BILL OF REINFORCING STEEL						
Bar	No.	Size	Spac'g	Length	Weight	
E	24	#11	~	41'-3"	5260	
F	24	#10	~	32'-10"	3351	
H1	310	#3	Shn	6'-1"	709	
H2	66	#3	Shn	6'-1"	151	
K	68	#3	1'-0"	6'-9"	173	
L	4	#5	~	37'-5"	156	
Mb1	31	#5	Shn	35'-0"	1132	
Mc1	36	#5	Shn	17'-11"	673	
Nc	50	#4	~	41'-6"	1306	
P	24	#6	~	4'-2"	150	
Ec	2	#4	~	5'-8"	83	
S	2	#5	~	36'-0"	77	
W	96	#4	10"	3'-6"	229	
Total Wt. Lbs.					13,510	
ESTIMATED QUANTITIES						
Item			Unit		Quant	
Cl "A" Concrete			Cu.Yds.		75.2	
Reinforcing Steel			Lbs.		13,510	
Railing			Lin.Ft.		83.5	

CG -0-33-40 (36°-52') BILL OF REINFORCING STEEL						
Bar	No.	Size	Spac'g	Length	Weight	
E	24	#11	~	42'-3"	5387	
F	24	#10	~	34'-0"	3511	
H1	310	#3	Shn	6'-1"	709	
H2	64	#3	Shn	6'-1"	146	
K	68	#3	1'-0"	6'-9"	173	
L	4	#5	~	41'-10"	175	
Mb1	27	#5	Shn	35'-0"	803	
Mc1	36	#5	Shn	17'-11"	1049	
Nb	50	#4	~	42'-6"	1420	
D	24	#6	~	4'-2"	150	
Ec	22	#4	~	6'-7"	97	
S	2	#5	~	41'-2"	86	
W	100	#4	10"	3'-6"	234	
Total Wt. Lbs.					13,933	
ESTIMATED QUANTITIES						
Item			Unit		Quant	
Cl "A" Concrete			Cu.Yds.		78.8	
Reinforcing Steel			Lbs.		13,933	
Railing			Lin.Ft.		85.5	

CG -0-33-40 (45°-00') BILL OF REINFORCING STEEL						
Bar	No.	Size	Spac'g	Length	Weight	
E	24	#11	~	43'-4"	5525	
F	24	#10	~	35'-0"	3615	
H1	330	#3	Shn	6'-1"	755	
H2	68	#3	Shn	6'-1"	156	
K	68	#3	1'-0"	6'-9"	173	
L	4	#5	~	47'-3"	197	
Mb1	14	#5	Shn	35'-0"	511	
Mc1	74	#5	Shn	18'-0"	1389	
Nb	50	#4	~	43'-7"	1456	
D	24	#6	~	4'-2"	150	
Ec	22	#4	~	7'-11"	116	
S	2	#5	~	46'-7"	97	
W	104	#4	10"	3'-6"	243	
Z	24	#5	~	16'-0"	400	
Total Wt. Lbs.					14,783	
ESTIMATED QUANTITIES						
Item			Unit		Quant	
Cl "A" Concrete			Cu.Yds.		82.6	
Reinforcing Steel			Lbs.		14,783	
Railing			Lin.Ft.		87.7	

GENERAL NOTES:
Design: H20 — 44 Loading in accordance with AASHO 1961 Standard Specifications, and interim revisions thereto
All concrete shall be Class 'A' Chamfer all exposed corners ¾" except as noted.
Dimensions to reinforcing steel are to centers of bars.
Design stress for reinforcing steel = 20,000 p.s.i.
Details shown are for Right Forward Skew. Reverse for Left Forward Skew.
Details of metal forms are available on request.
Pay Quantity of Class 'A' Concrete will be Plan Quantity which includes concrete required for Screed Camber.

CONSTRUCTION NOTES:
Contractor must provide adequate means of supporting outside forms during placement of concrete. On square spans only, rail post anchor bolts (see railing details) may be welded to Bars M and used for both purposes. On all skewed spans, a sleeve nut or rail tie anchor may be welded to Bars M as a form support only, provided at least 1" concrete cover is provided over such anchors. Adequate external bracing or supports will be acceptable on all spans.
Forms may be supported from bent caps only when specified on bent details.

TABLE OF VAR. DIMS. & BAR H SPAC.					
Span	40'-0"	40'-10"	41'-9"	42'-9"	43'-10"
A	1'-3"	1'-1"	1'-3"	1'-3"	1'-3"
B	2'-9"	2'-8"	3'-8"	2'-8"	5"
C	11@1'-6"	12@1'-6"	11@1'-6"	12@1'-6"	2@8"
D	9"	0"	1'-1"	3½"	12@1'-6"
E	0"	0"	0"	0"	11"
X	1'-0½"	1'-5½"	1'-11"	2'-5"	2'-11½"

Bars M	
Ma1	35'-0"
Mb1	32'-5"
Mc1	3'-5"
Mc1-Mc	17'-11" Avg.
Mb2	32'-10"
Mb3	33'-0"
Mb1-Mb	17'-10" Avg.
Mb	34'-1"
Mb2	33'-0"
Mcm	3'-0"
Mc2-Mc	18'-0" Avg.

Fig. A.6. Texas Highway Department Plan Sheet, CG-0-33-40.

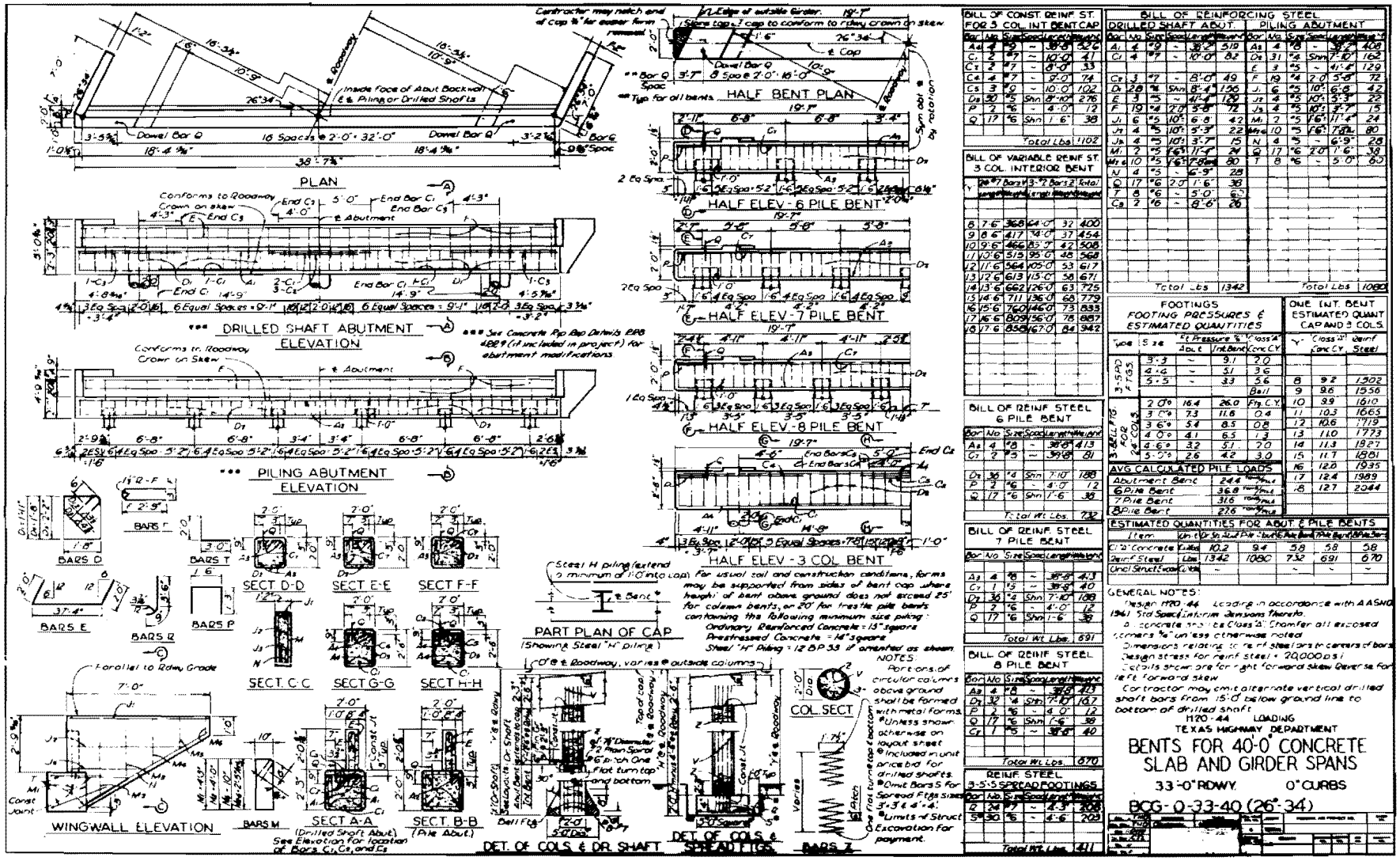

Fig. A.7. Texas Highway Department Plan Sheet, BCG-0-33-40 (26°-34').